Theoretical study of the excited state lifetime by ligand modifications and the vibrational anharmonicity for Fe(II) and Ru(II) complexes

Jianfang Wu

UNIVERSITAT ROVIRA i VIRGILI

Theoretical study of the excited state lifetime by ligand modifications and the vibrational anharmonicity for Fe(II) and Ru(II) complexes

Jianfang Wu

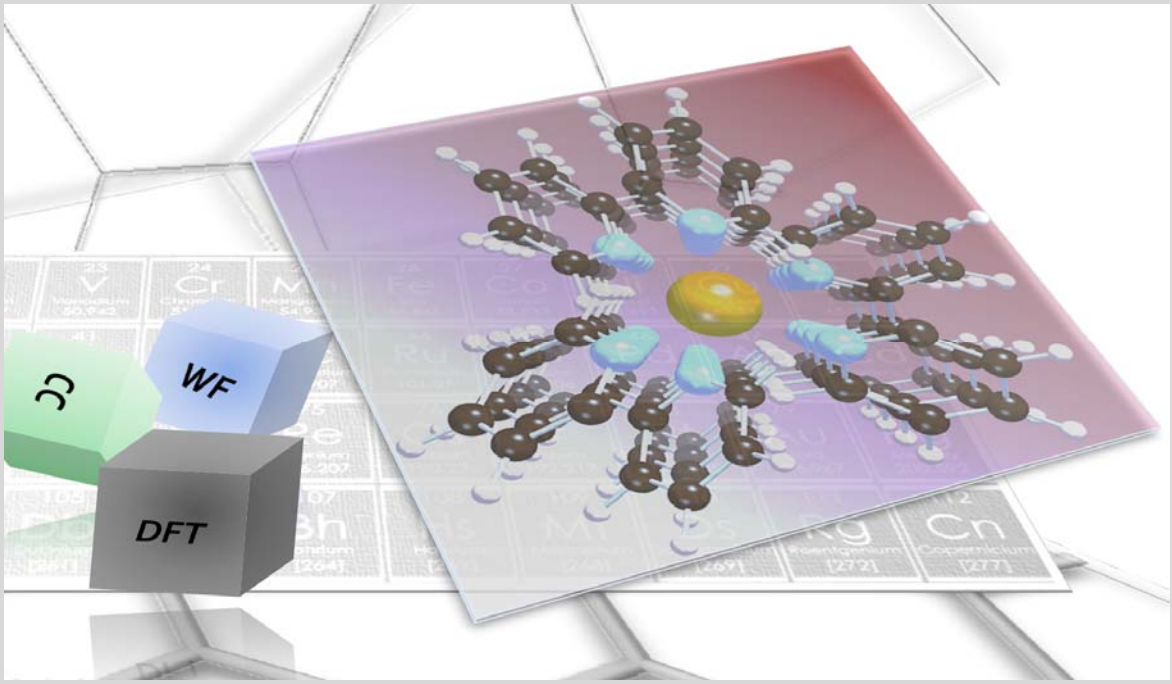

DOCTORAL THESIS
2020

Theoretical study of the excited state lifetime by ligand modifications and the vibrational anharmonicity for Fe(II) and Ru(II) complexes

Jianfang Wu

Theoretical study of the excited state lifetime by ligand modifications and the vibrational anharmonicity for Fe(II) and Ru(II) complexes

Jianfang Wu

Theoretical study of the excited state lifetime by ligand modifications and the vibrational anharmonicity for Fe(II) and Ru(II) complexes

Jianfang Wu

Theoretical study of the excited state lifetime by ligand modifications and the vibrational anharmonicity for Fe(II) and Ru(II) complexes
Jianfang Wu

Jianfang Wu

Theoretical study of the excited state lifetime by ligand modifications and the vibrational anharmonicity for Fe(II) and Ru(II) complexes

---

Doctoral Thesis

Supervised by Dr. Coen de Graaf

Department of Physical and Inorganic Chemistry

Quantum Chemistry Group

UNIVERSITAT
ROVIRA i VIRGILI

Tarragona, Jan.2020

Theoretical study of the excited state lifetime by ligand modifications and the vibrational anharmonicity for Fe(II) and Ru(II) complexes

Jianfang Wu

UNIVERSITAT
ROVIRA i VIRGILI

Department of Physical and Inorganic Chemistry

Dr. Coen de Graaf, ICREA research professor at the Department of Physical and Inorganic Chemistry of the Universitat Rovira i Virgili.

I STATE that the present study, entitled "*Theoretical study of the excited state lifetime by ligand modifications and the vibrational anharmonicity for Fe(II) and Ru(II) complexes*", presented by Jianfang Wu for the award of the degree of Doctor, has been carried out under my supervision at the Department of Physical and Inorganic Chemistry of this university.

Tarragona, the 5th of December 2019

Doctoral Thesis Supervisor

Dr. Coen de Graaf

Theoretical study of the excited state lifetime by ligand modifications and the vibrational anharmonicity for Fe(II) and Ru(II) complexes

Jianfang Wu

List of publications

Related with this thesis

1. Quantum chemical study of the interligand electron transfer in Ru Polypyridyl complexes. G. A. Fortuny, **J. Wu**, R. Caballol and C. de Graaf. J. Phys. Chem. A. **122**, 1114-1123, (2018).
2. The role of vibrational anharmonicity in the computational study of thermal spin crossover. **J. Wu**, C. Sousa and C. de Graaf. Magnetochemistry. **5**, 49, (2019)
3. Controlling the lifetime of excited states by ligand modifications in Fe(II) spin crossover complexes. **J. Wu**, M. Alías and C. de Graaf. (submitted)
4. Benchmarks for HS-LS energy difference by NEVPT2, CASPT2 and DLPNO-CCSD(T) vs TPSSh. **J. Wu** and C. de Graaf. (in preparation)

Theoretical study of the excited state lifetime by ligand modifications and the vibrational anharmonicity for Fe(II) and Ru(II) complexes

Jianfang Wu

Acknowledgements

First I would like to give my deep sincerity thankful to my supervisor Coen de Graaf. During the process of writing the thesis and four years PhD study in Quantum Chemistry Group, you always full of patience to teach me the knowledge, you made a person good from know nothing about chemistry and will get the PhD in this field. You not only pass the knowledge to me, also the attitude about being a researcher. Thanks very much for everything you have taught to me. Thanks a lot for carefully correcting my thesis. Through this process, I learn a lot. I could say that you are a super supervisor.

I want to acknowledge the Spanish ministry for the four years grant to study in Universitat Rovira i Virgili (URV). Great opportunity to study and live in Spain. Thankful to all the members of the whole group for the great scientific environment and some constructive advice for the studying and the enjoyable life in Tarragona. Thanks to the small group members for the weekly discussion. Special thanks to Marc Alías for sharing the idea of the work and nice translation for process of deposit my thesis. Many Thanks to the graduated members Gerard, Sergi, Zhongling for sharing the calculation knowledge to me. Thanks a lot to Roser, Almu, Albert, Toni, Antonio, Yeamin, Khalid, Fei et al. for the great knowledge to share, the kindness help on work and life, and the great party time we spent together. I really treasure these good memories in my life.

Thankful to Jose Carlos Ortiz, Elisenda Mas and Moisés Álvarez for the programs and computer technical support, kindness helping.

Finally, I want to thank to my parents and sister and brother for supporting me four years overseas studying.

Theoretical study of the excited state lifetime by ligand modifications and the vibrational anharmonicity for Fe(II) and Ru(II) complexes

Jianfang Wu

Contents

Theoretical study of the excited state lifetime by ligand modifications and the vibrational anharmonicity for Fe(II) and Ru(II) complexes

Jianfang Wu

"Nothing in life is to be feared, it is only to be understood.
--Marie Curie

Chapter 1

General Introduction

1.1 Transition metal complexes

In the history of technological revolution, the discovery and rapidly evolving technologies constantly asked for the development of new materials. The seemingly unstoppable tendency to smaller devices and higher density data storage has forced materials science to enter the nanoscale some years ago. In this context, transition metal (TM) complexes, also called coordination complexes, have become popular as a class of functional and tuneable nanoscale materials. They are extensively studied and widely used in the fast-developing area of nanotechnology, for example as molecular devices, big data storage, sensors[1] etc., in the multidisciplinary area of research at the intersect of chemistry, physics, electronics and material engineering. These compounds typically consist of one or more transition-metal ions from the third, fourth or fifth row of the periodic table (Fe, Ru, Co etc.) with a certain number of ligands attached to it. These ligands can be single atoms (H, N, O, Cl), small molecular fragments (-CN, -CO, H_2O), or more complex organic structures such as

bipyridine to name one example among the countless different ligands that have been reported.[2] In this thesis, we will focus mainly on the mononuclear systems (one metal centre), which despite their apparent simplicity show a very rich (and sometimes rather complex) scope of interesting properties.

The electronic structure of the transition metal complexes dictates a large part of the properties of these systems, such as the geometry or the reactivity. Analysing the electronic structure of the TM complexes with molecular orbital (MO) theory provides us with a profoundly detailed description and fundamental knowledge about the interaction between metal and ligands and how the interactions affect the properties of these systems in a qualitative predictive way.

The basic ingredients of the MO theory are the shape and the energetic levels of the MOs. In its most basic form, MO theory considers the metal and ligand orbitals separately, and analyses how these atomic (TM) or fragment (polyatomic ligands) orbitals interact based on symmetry arguments and relative orbital energies. For instance, considering the nine valence orbitals of the metal (five d orbitals, one s orbital and three p orbitals), two major types of interaction between metal orbitals and ligands orbitals have to be described: the σ-type interactions and the π-type interactions (see **Fig.** 1.1). The choice of ligand orbitals that should be included in the MO analysis strongly depends on the explicit details of the ligand and cannot be generalized. Because the σ-type interactions are in general stronger than the π-type interactions (axial overlap is more efficient than the sideways overlap), it is in some cases not necessary to take into account the π-type interactions (or treat the interaction only as a small perturbation) to obtain a qualitatively correct picture. But in those cases where one or more π-bonds are present in the TM system, the π-type interaction is important, and cannot be neglected any more.

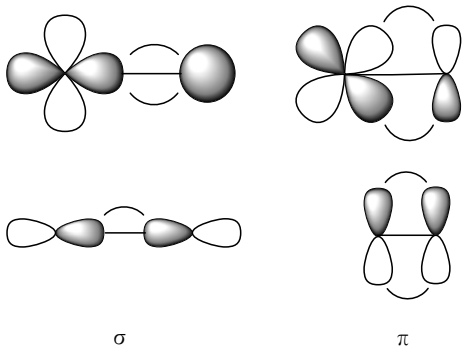

Figure 1.1 *Schematic representations of σ (left) and π (right) interactions. The upper panels show the interaction of a TM-d orbital with s- or p-orbitals on the ligand, the lower panels involve p-orbitals on both centres.*

The final orbitals resulting from the interaction between metal orbitals and ligands orbitals can be classified in three groups: the bonding (stabilizing, constructive interference), the anti-bonding (destabilizing, destructive interference) and the non-bonding (no or very weak interaction) orbitals. In most cases, the highest occupied orbitals on the ligands are more stable than the corresponding ones on the TM. This means that the bonding orbitals are largely located on the ligands and relatively low in energy. The anti-bonding orbitals, higher in energy, are dominated by contributions from the TM-d orbitals as are the non-bonding orbitals, at slightly lower energy (see **Fig.** 1.2). The energy difference Δ_0 between the non-bonding and the anti-bonding orbitals qualifies the TM systems as strong-field or weak-field complexes. The stronger the metal-ligand interaction, the larger the energy difference Δ_0, and vice versa.

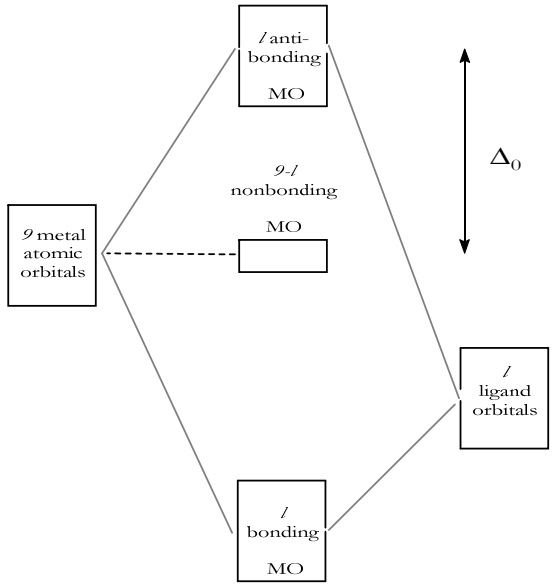

Figure 1.2 *Simplified diagram for the interaction of the atomic orbitals on a metal centre and the l ligands surrounding it (σ interaction only).*

Being largely localized on the metal and having the highest orbital energy, the anti-bonding and non-bonding orbitals largely determine the properties of the system and are sometimes referred to as the 'd-block'. In the case of octahedral ML_6 complexes (see **Fig.** 1.3) which are among the most widely studied complexes until now, the d-block consists of three non-bonding degenerate (t_{2g}) MOs and two anti-bonding degenerate (e_g) MOs (see **Fig.** 1.3). Based on the d-block, there is a direct, intuitive way to understand the strong ligand field and weak ligand field (see **Fig.** 1.4). For an isolated metal ion, the five d orbitals are degenerate, but when the metal is linked to ligands that form an octahedral coordination sphere, the degeneracy is lifted. The σ interaction pushes the d_{x2-y2} and d_{z2} orbitals up in energy to form two anti-bonding orbitals of e_g symmetry (see **Fig.** 1.3). On the other hand, the d_{xy}, d_{xz}, and d_{yz} are subject to the much smaller π interaction and maintain their atomic character. Hence, they form the three non-bonding orbitals of t_{2g} symmetry separated from the anti-bonding e_g orbitals by Δ_0 as shown in **Fig.** 1.4. This energy separation Δ_0 allows us

to distinguish the strong-field (large Δ_0) from weak-field (small Δ_0) complexes in the family of octahedral complexes, and it lays the fundaments for further theoretical analysis of the properties of the TM complexes.

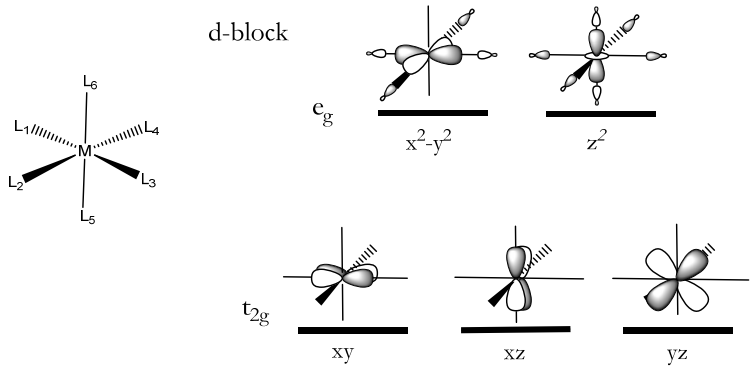

Figure 1.3 *The structure of octahedral ML_6 complex (left), and the d-block (right): the upper panels correspond to the e_g symmetry two degenerate anti-bonding orbitals d_{x2-y2} and d_{z2}, the lower panels correspond to t_{2g} symmetry the three degenerate non-bonding orbitals d_{xy}, d_{xz}, d_{yz}.*

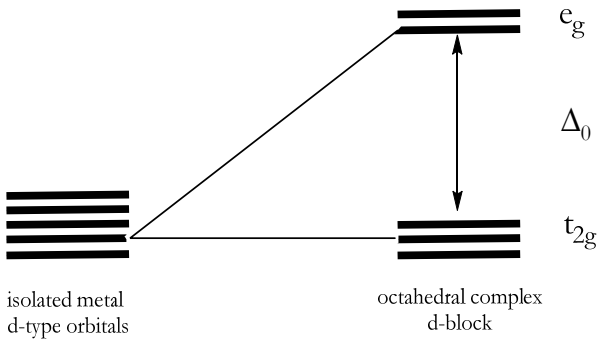

Figure 1.4 *The scheme of ligand interaction on metal centre on an octahedral complex, the forming of the d-block.*

The next step in this basic analysis of the electronic structure concerns the distribution of the electrons over the orbitals of the d-block. Restricting the discussion to (quasi)-octahedral complexes, those with less than 4 electrons or more than 7 will in general have parallel aligned unpaired electrons in the t_{2g} (number of electrons smaller than 4) or in the e_g orbitals. Here, one must keep in mind that for

the complexes with metals from the fourth or fifth row the geometry is distorted in most cases and the degeneracy of the t_{2g} and e_g orbitals is lost, leading to maximal electron pairing. The complexes with 4, 5, 6 or 7 electrons can either maximally occupy the t_{2g} orbitals to minimize the repulsion with the electron density due to the ligands or have the electrons distributed over both t_{2g} and e_g orbitals with parallel spin coupling to maximize the exchange interactions. The subtle balance between minimizing the electron repulsion and maximizing the exchange interactions can give rise to very interesting physical properties as will be discussed in the next section.

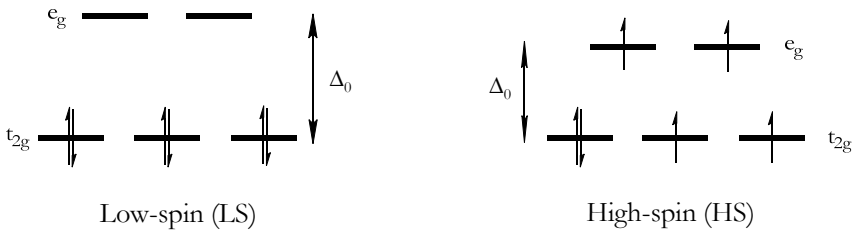

Figure 1.5 *The scheme of most stable electron distributions for a $3d^6$ complex in a (quasi)-octahedral symmetry. The six electrons maximal pairing in the t_{2g} orbitals forming the low-spin (LS) left; and the maximal parallel in both t_{2g} and e_g orbitals forming the high-spin (HS) right. Δ_0 stands for the ligand field splitting, (LS and HS will discuss in next section).*

1.2 Spin-crossover in transition metal complexes

The total spin moment (or "spin" for short) is a main feature of molecular electronic structure. It directly affects the molecular structure, magnetic, reactivity and spectroscopic properties. While in the large majority of the TM complexes, electronic states with different spin moments have very large energy gaps, there are some systems where they are nearly degenerate. Changing the spin in the metal centre of these coordination compounds can be achieved by small external perturbations and is called spin-crossover (SCO) effect. And when both states can be populated in a controlled manner, SCO can be considered as one of the spectacular examples of

molecular bistability, widely studied in the transition metal systems. Switching the spin states can be triggered by variation of the temperature,[3] pressure[4] or light irradiation.[5] The SCO plays a crucial role in the molecule-based magnetic materials applications such as molecular switches, sensors or memories devices. In most cases, the spin state conversion is accompanied by a significant change of structural parameters such as the bond length, angles, volume, magnetism and in some cases also the colour, which makes it easy to recognise by the eye.

The SCO phenomena was first reported by Cambi and co-workers[6] in Fe(III) dithiocarbamate complexes in a study of the temperature dependence of magnetic behaviour in the early of 1930s. They found a spin equilibrium which they described as a situation with one unpaired electron at low temperatures changing to five unpaired electrons at higher temperatures. Van Vleck[7] gave theoretical support based on crystal field theory (CFT) to these observations, indicating that when the energy splitting Δ_0 is smaller than electron pairing energy, that is for a weak ligand field, electrons can populate both the t_{2g} and the e_g orbitals and give a maximum number of unpaired spin; the complex shows a high spin ground state. On the contrary, for strong ligand field electrons tend to pair in the low lying orbitals, favouring a low spin ground state.

1.3 Thermal SCO

As reported in many studies, changing the spin moment of the metal ion from low-spin (LS) to high-spin (HS) can be triggered by the variation of the temperature, and is known as thermal SCO. After the discovery in 1932 by Cambi and co-workers[6] in an Fe(III) complex, it took about 30 years, before thermal SCO was observed in the $Fe(II)N_6$ systems[8] which turned out to be most versatile class of TM complexes concerning SCO. As one of the most typical systems of the $Fe(II)N_6$ family, we mention $[Fe(phen)_2(NCS)_2]$, phen = 1,10-phenantroline (see **Fig.1.6** (a)). Thermal

SCO was observed and as shown in the lower panel of **Fig.** 1.6, it shows an abrupt spin conversion at the transition temperature $T_{1/2}$= 176.5K[10], where $T_{1/2}$ is defined as the temperature for which the HS and LS states are equally populated. In some cases the collective effects are important which leads to different transition temperatures for cooling and heating the sample. For instance, the compound $[Fe(Htrz)_3](ClO_4)_2$, Htrz =1, 2,4-1*H*-triazole, shows abrupt curve both at heating $T_{1/2}$ =313K and a cooling $T_{1/2}$ =296K spanning a hysteresis loop centred around room temperature and also accompanied by a colour change from purple low spin state to white high spin state,[11] which opens the door for practical applications. Depending on the collective effects the system might have other different transition curves:

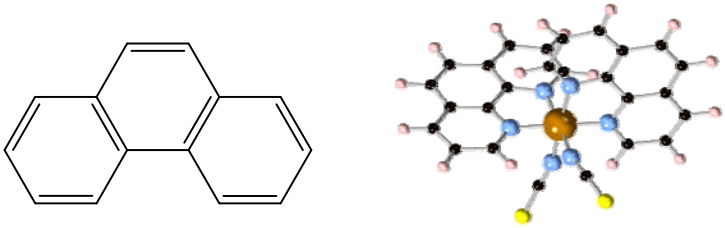

(a) (b)

(c)

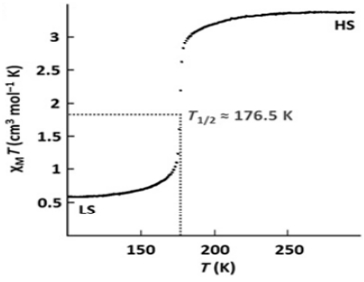

Figure 1.6 *(a) Lewis structure of 1,10-phenantroline (phen) (b) representation of the $[Fe(phen)_2(NCS)_2]$ (color code: Brown for Fe, blue for N, blank for C, pink for H, yellow for S). (c) Temperature dependence of $\chi_M T$ for a polycrystalline sample of $[Fe(phen)_2(NCS)_2]$ (adapted from[9]).*

gradual (in solution), multi-step (two or more steps) and incomplete character.[12] The hysteresis effect is one of the most attractive phenomena for functional switchable materials research such as temperature sensors, memory devices. And recently the research about the SCO phenomena with a large hysteresis loop spanning room temperature has attracted much attention in the functional materials research.[13]

From a theoretical viewpoint, $T_{1/2}$ is the temperature at which the difference in the Gibbs free energy of the HS and the LS state becomes zero

$$\Delta G_{HL}\left(T_{1/2}\right) = \Delta H_{HL}\left(T_{1/2}\right) - T_{1/2}\Delta S\left(T_{1/2}\right) = 0 \qquad 1.1$$

where Δx_{HL} stands for the HS-LS difference of the Gibbs free energy, the enthalpy and the entropy for x = G, H and S, respectively. Under the assumption that the variation of the enthalpy with temperature is negligible with respect to the variations in the entropy, it can be concluded that thermal SCO is an entropy-driven transition. Recalling the analysis of the electronic structure exposed in the previous section, the explanation of an entropy-driven transition is rather straightforward.[14] Upon spin transition two electrons are promoted from the non-bonding t_{2g} orbitals to the anti-bonding e_g orbitals (see **Fig.**1.5). This weakens the Fe-N bonds and increases the bond lengths (typically by 0.2 Å) as illustrated in the schematic potential energy surfaces of the LS and HS as function of the Fe-N distance depicted in **Fig.** 1.7. The weakening of the Fe-N bonds in the HS makes that the vibrational frequencies associated to the FeN_6 core of the complex are softened as can be seen in **Fig.** 1.7 by the wider energy curve for HS state compared to the one representing the LS. Consequently, the vibrational levels of the 15 FeN_6 vibrational modes are significantly closer spaced in the HS than in the LS. Hence, the population of higher vibrational levels becomes more pronounced in the HS state when temperature rises, which makes the entropy rise faster than in the LS. At a certain temperature TΔS becomes as large as ΔH (a necessary condition for thermal SCO is that the LS state

should be the ground state at T=0) and this defines the transition temperature $T_{1/2}$.

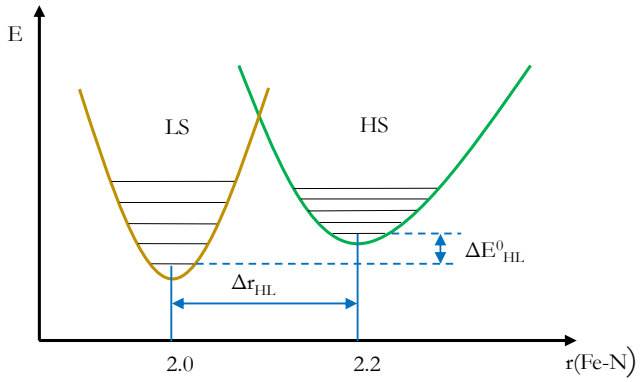

Figure 1.7 *Schematic potential energy surfaces of the LS and HS as function of the Fe-N distance.*

The enthalpy difference ΔH_{HL} can be written to a good approximation as the difference of the adiabatic electronic HS-LS energy difference ΔE_{HL} and the difference in zero-point vibrational energy (ZPVE) of the two spin states

$$\Delta H_{HL} = \Delta E_{HL} + \Delta ZPVE_{HL} \qquad 1.2$$

Typically the entropy of a system is calculated as the sum of four contributions: electronic, vibrational, rotational and translational. Considering the difference in entropy between HS and LS (ΔS_{HL}), the electronic contribution is temperature independent and is directly related to the different spin degeneracy (g = 2S+1) of the two spin states:

$$\Delta S(el)_{HL} = R[\ln(g_{HS}) - \ln(g_{LS})] \qquad 1.3$$

with R the ideal gas constant (8.31 $J \cdot K^{-1} \cdot mol^{-1}$). This usually adds up to a small yet not completely negligible contribution. A much larger contribution can be expected from the vibrational part, which is also strongly temperature dependent. This

contribution is typically calculated within the harmonic approximation for the vibrational modes

$$e_{vib} = \sum_{i=1}^{N} \left(n_i + \frac{1}{2} \right) h\nu_i \qquad 1.4$$

n_i with N the number of normal modes and ν_i the vibrational frequencies. This leads immediately to the vibrational partition function

$$q_{vib} = \prod_{i=1}^{N} \frac{e^{-h\nu_i/2kT}}{1 - e^{-h\nu_i/kT}} \qquad 1.5$$

and from there the entropy can be calculated from standard statistical mechanics equations. Similar reasonings lead to expressions for the rotational and translational contributions, but the differential contribution of these is either very small (rotational) or zero (translational) and can safely be neglected.

1.4 Light-induced excited spin state trapping (LIESST)

The population of the HS and LS states can also be changed by irradiating the sample with light of a suitable frequency, known as light-induced excited spin state trapping (LIESST). Controlling the spin state with light is attractive and easy way to modulate the properties of SCO materials in real-world applications. It was first observed in Fe(II) SCO systems by McGarvey et al[15] in solution at the early 1980s. The experiment was carried out at low temperatures. By shining green light on the complex, the spin state changed from LS ground state to a metastable HS with a lifetime of the order of 100 nanoseconds, but much larger lifetimes (of the order of several days) were measured not long after these pioneering experiments.[16] The inverse process, that is from the light-induced HS state back to the original LS state,

the so called reverse-LIESST, can be achieved by changing the light source (typically red light) as demonstrated by Hauser[17] shortly after the report of McGarvey and co-workers. The mechanism of LIESST is easiest explained using the schematic energy diagram of a typical Fe(II)N_6 system as show in **Fig.** 1.8. Upon irradiating with light, the system is excited from the LS ground state to a singlet excited state, either a metal-centred state (^{1}MC) or a metal-to-ligand (^{1}MLCT) state depending on the wavelength and the specifics of the system under study. The system then decays to the meta-stable HS (^{5}T) via two intersystem crossings, either via ^{3}MLCT or ^{3}MC states, which is still under debate.[18] The reverse process is less well studied, but the **Fig**. 1.8 suggests a similar mechanism.

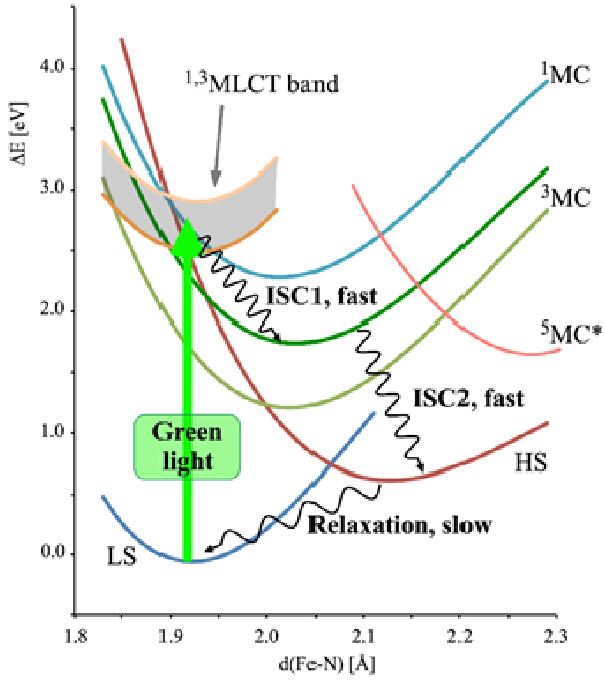

Figure 1.8 *Schematic representation of the potential-energy surfaces of the lowest electronic states of* $[Fe(bpy)_3]^{2+}$ *as function of the Fe-N distance and the main experimental findings on the deactivation dynamics. (Adapted from*[19]*)*

1.5 Objectives

In this thesis, the objectives consist in three parts:

Part1: The $[Ru^{II}(bpy)_3]^{2+}$ is frequently used as electron donor in intermolecular electron transfer reactions. Under light irradiation the $[Ru^{II}(bpy)_3]^{2+}$ complex undergoes ultrafast ISC from the initial populated ^{1}MLCT state to the ^{3}MLCT state and since both the triplet and quintet MC states lie at higher energy there is no relaxation path for SCO and the system is 'stuck' in the ^{3}MLCT state. The overall lifetime for the ^{3}MLCT state is on the order of μs, long enough to let collisions happen with other molecules and induce electron transfer reactions (see **Fig.** 1.9). However, the problem is that Ru(II) is rather rare and hence expensive. For this reason, researchers have been considering to replace Ru(II) by the more common and cheaper Fe(II) without losing the properties of the Ru(II) complex. But the major drawback of Fe(II) complexes is that the ^{3}MLCT state has a very short lifetime because the presence of ^{3}MC and ^{5}MC states at lower energy provide a path for fast SCO.

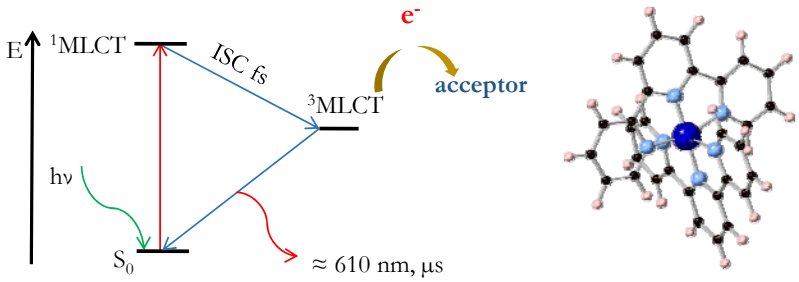

Figure 1.9 *Schematic representation of the absorption and emission processes in* $[Ru^{II}(bpy)_3]^{2+}$.

In this study, we want to increase the ^{3}MLCT state lifetime of $[Fe(bpy)_3]^{2+}$ related complexes to mimic the situation of the $[Ru(bpy)_3]^{2+}$ by ligand modification. Ligand modifications can directly influence the relative energies of the MLCT and MC state. Based on LFT, the stronger the σ donation the stronger the ligand field, which

pushes the anti-bonding e_g orbitals higher energy. This increases the relative energy of the ^{3}MC (and ^{5}MC) states without directly affecting the MLCT states. Eventually, the order of the states is inverted and the situation of the Ru(II) complexes could be reproduced with a low-lying (meta-) stable ^{3}MLCT state.

In this work, we mainly use the cyanide ligand (CN^-) to replace the bipyridine ligand, and study two complexes: $[Fe(bpy)_2(CN)_2]$ where two cyanides replace one bipyridine ligand and $[Fe(bpy)(CN)_4]^{2-}$, four cyanides replace two bipyridine ligands. The correct energy ordering of the state is a necessary but not sufficient condition to mimic the Ru(II) complex. A second condition that needs to be met concerns the oxidation process, which is downhill in the Ru(II) case when oxidation takes place from the excited state. To complete the comparison between Fe(II) and Ru(II) complexes, we will also calculate the oxidation energies in the Fe(II) complexes with two and four CN^- ligands.

Part2: The calculation of accurate enthalpy differences ΔH between different spin-states remains a challenge task for quantum chemical approaches. For SCO system, one usually concentrates on the relative energy of low-spin and high-spin states ΔE_{HL}, because the contribution of the ZPVE to ΔE_{HL} is rather constant for different complexes and in general accurately reproduced by DFT with any of the standard functionals. Many studies of ΔE_{HL} are based on DFT, but the results largely dependent on the functional that is used. CASPT2 (second-order perturbation theory based on a complete active space self-consistent field reference wave function) has been applied in some studies, and gives reasonable good estimates but is rather expensive and the outcomes depend on the value of IPEA shift ε in the zeroth-order Hamiltonian. An alternative wave function based method NEVPT2 (N-Electron Valence State Perturbation Theory) should in principle give more accurate results than CASPT2 because it is based on a more rigorous choice of $\hat{H}_0$. In this work, we employed the NEVPT2 method, and study what NEVPT2 can give us with respect

to the ΔE_{HL}. Except the above mentioned methods, CCSD(T) is considered to be highly accurate but too expensive for any but small systems. DLPNO-CCSD(T) scales much better with the system size (it only correlates electrons that are 'close' together). In this work we also employed the DLPNO-CCSD(T) method and check how it works for the ΔE_{HL}.

Part3: For the SCO systems, the vibrational entropy is always calculated within the harmonic approximation by DFT method, only taking into account the quadratic term of the vibrational modes. In real systems, the experimental $T_{1/2}$ is difficult to reproduce with calculations, and we hypothesize that this discrepancy (or at least part of it) is due to the anharmonic approximation. We introduced anharmonic effects in the description of the vibrational modes to see how this affects zero-point energy and vibrational entropy and via these the transition temperature for SCO.

In summary: The main objectives of this thesis are

(i) Study how ligand modifications affect the lifetime of excited states in Fe(II) complexes.

(ii) Investigation how some relatively new wave function based methods perform in the inherently difficult calculation of the high-spin low-spin energy difference.

(iii) Determine to what extent the neglect of anharmonicity in the description of the vibrational modes affects the theoretical estimates of the critical temperature of spin crossover.

References

[1] a) Olivier Kahn and C. J. Martinez, *Science* **1998**, *279*, 44−48; b) A. Bousseksou, G. Molnár, L. Salmon and W. Nicolazzi, *Chem. Soc. Rev.* **2011**, *40*, 3313-3335; c) O. Sato, *Nat. Chem.* **2016**, *8*; d) P. Gütlich and H. A. Goodwin in Spin crossover – an overall perspective Vol. 233 Eds.: P. Gütlich and H. A. Goodwin), Springer, Berlin, Heidelberg, *Top. Curr. Chem.*, **2004**, pp. 1-47.

[2] a) Y. Liu, T. Harlang, S. E. Canton, P. Chábera, K. Suárez-Alcántara, A. Fleckhaus, D. A. Vithanage, E. Göransson, A. Corani, R. Lomoth, V. Sundström and K. Wärnmark, Chem. Commun. **2013**, *49*, 6412; b) J. Cirera and F. Paesani, *Inorg. Chem.* **2012**, *51*, 8194−8201; c) C. Roux, J. Zarembowitch, B. Gallois, T. Granier and R. Claude, *Inorg. Chem.* **1994**, *33* 12693–12694.

[3] A. Hauser in Spin-Crossover Materials. Properties and Applications, Vol. 52 (Ed. A. H. Malcolm), *Angew. Chem.*, **2013**, p. 10419.

[4] A. H. Ewald, R. L. Martin, E. Sinn and A. H. White, *Inorg. Chem.* **1969**, *8*, 1837-1846.

[5] S. Decurtins, P. Gütlich, C. P. Köhler, H. Spiering and A. Hauser, *Chem. Phys. Lett.* **1984**, *105*, 1-4.

[6] L. Cambi and L. Szego, *Chem. Ber. Dtsch. Ges.* **1931**, *64*, 2591-2598.

[7] J. H. V. Vleck, *J. Chem. Phys.* **1935**, *3*, 807

[8] E. König and K. Madeja, *Inorg. Chem.* **1967**, *6*, 48–55.

[9] B. Gallois, J. A. Real, C. Hauw and J. Zarembowitch, *Inorg. Chem.* **1990**, *29*, 1152–1158.

[10] M. Sorai and S. Seki, *J. Phys. Chem. Solids* **1974**, *35*, 555-570.

[11] J. Krober, E. Codjovi, O. Kahn, F. Groliere and C. Jay, *J. Am. Chem. Soc.* **1993**, *115*, 9810-9811.

[12] J. A. Real, A. B. Gaspar and M. C. Muñoz, *Dalton Trans.* **2005**, *0*, 2062-2079.

[13] E. Tailleur, M. Marchivie, N. Daro, G. Chastanet and P. Guionneau, *Chem. Commun.* **2017**, *53*, 4763-4766

[14] A. Hauser in Ligand field theoretical considerations, Vol. 233 Eds.: P. Gütlich and H. A. Goodwin), Springer, Berlin, Heidelberg, Top. Curr. Chem., **2004**, pp. 49–58.

[15] J. McGarvey and I. Lawthers, *J. Chem. Soc., Chem. Commun.* **1982**, 906–907.

[16] a) J. Jeftic and A. Hauser, *J. Phys. Chem. B* **1997**, *101*, 10262-10270; b) J. Jeftic, R. Hinek, S. C. Capelli and A. Hauser, *Inorg. Chem.* **1997**, *36*, 3080-3087.

[17] A. Hauser, J. Jeftic, H. Romstedt, R. Hinek and H. Spiering, *Coord. Chem. Rev.* **1999**, 190/192:471–491.

[18] C. Sousa, M. Llunell, A. Domingo and C. de Graaf, *Phys. Chem. Chem. Phys.* **2018**, *20*, 2351-2355

[19] C. Sousa, C. de Graaf, A. Rudavskyi, R. Broer, J. Tatchen, M. Etinski and C. M. Marian, *Chem. Eur. J.* **2013**, *19*, 17541 – 17551.

Theoretical study of the excited state lifetime by ligand modifications and the vibrational anharmonicity for Fe(II) and Ru(II) complexes

Jianfang Wu

"If I have seen further, it is by standing on the shoulders of giants."

--Isaac Newton

Chapter 2

Theoretical Background

2.1 Electron structure method

In quantum chemistry calculation, the distribution of electrons in many-body systems can be described by (non-relativistic) quantum mechanics in terms of a wave function Ψ, and the time-independent Schrödinger equation which is given by

$$\hat{H}\Psi = E\Psi \qquad 2.1$$

Here, the Ψ describes distribution of all the electrons around the nuclei, E is the total energy of the whole system and $\hat{H}$ is the Hamiltonian operator which can be described in atomic units form as

$$\hat{H} = -\frac{1}{2}\sum_i \nabla_i^2 + \sum_{i<j}\frac{1}{r_{ij}} - \sum_{i,a}\frac{Z_a}{r_{ia}} - \frac{1}{2}\sum_a \frac{\nabla_a^2}{M_a} + \sum_{a<b}\frac{Z_a Z_b}{R_{ab}} \qquad 2.2$$

where the first three terms correspond to the kinetic energy of electrons (T_e), electron-electron repulsion (V_{ee}) and attraction interaction between electron and

nuclei (V_{ne}), respectively; the last two terms are kinetic energy of nuclei (T_n) and nuclei-nuclei repulsion (V_{nn}).

The Born-Oppenheimer approximation decouples the movement of the electrons and the nuclei. Based on large difference in mass of the two (a proton, the smallest nucleus, is ~1800 times heavier than an electron), it is safe to say (in most cases) that the electrons move in a fixed frame provided by the nuclei.

Then, the Hamiltonian can be written as $\hat{H} = \hat{H}(r;R) + \hat{H}(R)$ with $\hat{H}(r;R)$ the electronic Hamiltonian in a fixed nuclear frame (that is, when electrons and nuclei are decoupled), $\Psi(r;R)$ can be written as $\Phi(r)\Omega(R)$. Then Eq. 2.1 becomes

$$\left(\hat{H}(r;R) + \hat{H}(R)\right)\Phi(r;R)\Omega(R) = (E_{el}(R) + E_{nucl})\Phi(r;R)\Omega(R) \qquad 2.3$$

which reduces to

$$\hat{H}(r;R)\Phi(r;R) = E(R)\Phi(R) \qquad 2.4a$$

for the electrons and

$$\hat{H}(R)\Omega(R) = E\Omega(R) \qquad 2.4b$$

for the nuclei.

Solving Eq. 2.4a (or approximating the solution as accurate as possible) gives the electronic energy and wave function for a certain fixed geometry of the molecule represented by *R*. Repeating the procedure for different geometries that is for different R, will produce a potential energy surface that goes into Eq. 2.4b. By resolving the resulting equation, one obtains the nuclear vibrational wave functions and the corresponding energies. This completes the quantum mechanical treatment of both the electrons and the nuclei of a system under the approximation of decoupling the electrons from the nuclei and neglecting relativistic effects.

Despite this important reduction of the complexity, the electronic problem is still not exactly solvable except for one-electron molecules, and additional simplifications are to be made. The most basic approximate solution to the Schrödinger equation is obtained by writing Φ as a single Slater determinant as is done in Hartree-Fock theory. The Slater determinant is an anti-symmetrized product of one-electron functions ϕ_i, the well-known orbitals

$$\Psi(x_1, y_1, z_1, \sigma_1, x_2, y_2, z_2, \sigma_2, \cdots\cdots, x_N, y_N, Z_N, \sigma_n) = \sqrt{\frac{1}{N!}} det|\phi_1(x_1, y_1, z_1, \sigma_1) \cdot \phi_2(x_2, y_2, z_2, \sigma_2) \cdots\cdots \phi_N(x_N, y_N, z_N, \sigma_N)| \quad 2.5$$

where x, y and z are the Cartesian coordinates and σ is the spin coordinate (α, β; ↑, ↓, etc.) of the electron. This way of writing the N-electron wave function ensures that it fulfils all the formal requirements imposed by quantum mechanics on fermions. Usually, the orbitals are written as a linear combination of the atomic orbitals (LCAO approach), or basis functions.

$$\phi_j^{MO} = \sum_i c_{ij}\chi_i \quad 2.6$$

The minimization of the energy with respect to the orbital expansion coefficients leads to a set of optimal orbitals within the mean-field approximation of the electron-electron interaction, consequence of writing the N-electron wave function as a single Slater determinant. This means that electron correlation is neglected and that the Hartree-Fock can at most be considered as a good starting point for obtaining an accurate description of the electronic structure and more advanced approximations

to the exact N-electron wave function have to be made.

2.1.1 Density Functional methods

A second important effective one-electron description of the electronic structure is given by the Kohn-Sham implementation of density functional theory (DFT). Contrary to Hartree-Fock, correlation is accounted for and in general DFT provides better results. The basic idea of DFT is to determine the energy (and all other electronic properties) from the density ρ instead of the N-electron wave function. This reduces the complexity from a 3N dimensional problem considering the wave function of an N-electron system (4N if the spin is also taken as a variable) to a three dimensional problem when the density is considered. The foundation of DFT is given by the Hohenberg-Kohn (HK) theorems[1] that state that: (i) The electron density $\rho(\mathrm{r})$ of a non-degenerate ground state uniquely defines the Hamiltonian, the energy, and the wave function of the ground state through a certain external potential $\upsilon(\mathrm{r})$. In other words, the $\rho(\mathrm{r})$ determines the number of electrons N and the potential $\upsilon(\mathrm{r})$, which in turn define all properties of the electronic ground state. (ii) The density functional that delivers the ground state energy of the system which correspond to the lowest energy if the density present the true ground state density.

In orbital-free DFT, the energy functional is expressed as a sum of three parts: kinetic energy $T[\rho]$, electron-nucleus attraction $E_{\mathrm{ne}}[\rho]$ and electron-electron repulsion $E_{\mathrm{ee}}[\rho]$. The latter contains the Coulomb $J[\rho]$ and exchange $K[\rho]$ interaction. From these four terms, $E_{\mathrm{ne}}[\rho]$ and $J[\rho]$ have analytical expressions

$$E_{ne}[\rho] = -\sum_{a}^{N_{nuclei}} \int \frac{Z_a(R_a)\rho(r)}{|R_a - r|} dr \qquad 2.7$$

$$J[\rho] = \frac{1}{2}\iint \frac{\rho(r)\rho(r')}{|r-r'|}drdr'$$

2.8

Unfortunately, there are no exact expressions for the other two parts and approximations have to be made. Using the uniform electron gas as a model for more complex systems, the following expressions where derived for $T[\rho]$ and $K[\rho]$

$$T[\rho] = \frac{3}{10}(3\pi^2)^{\frac{2}{3}}\int \rho^{\frac{5}{3}}(r)d(r)$$

2.9

$$K[\rho] = \frac{3}{4}(\frac{3}{\pi})^{1/3}\int \rho^{\frac{4}{3}}(r)dr$$

2.10

This so-called Thomas-Fermi-Dirac DFT is unable to describe bonding between atoms, and even by adding corrections involving the gradient (or higher derivatives) of the density, orbital-free DFT continues to give very poor results.

Kohn and Sham realized that the largest errors in orbital-free DFT arose from the kinetic energy functional and proposed in 1965[2] that the kinetic energy can be obtained from the electron density by introducing a set of auxiliary orbitals ϕ^{KS}.

$$\rho = \sum_{i=1}^{N}\left|\phi_i^{KS}\right|^2$$

2.11

$T[\rho]$ is split into two parts $T[\rho]=T_S[\rho]+T_C[\rho]$, where $T_S[\rho]$ represents the kinetic energy of independent electrons and $T_C[\rho]$ the kinetic energy due to electron correlation. $T_S[\rho]$ can be calculated exactly in terms of the auxiliary orbitals

$$T_S[\rho] = \sum_{i=1}^{N} \left\langle \phi_i^{KS} \middle| -\frac{1}{2}\nabla^2 \middle| \phi_i^{KS} \right\rangle \qquad 2.12$$

and represents approximately 99% of the real kinetic energy. The total density functional can now be written as

$$E[\rho] = T_S[\rho] + E_{ne}[\rho] + J[\rho] + E_{xc}[\rho] \qquad 2.13$$

The first three terms have exact expressions and only the last term, commonly known as the exchange-correlation functional, is unknown and needs to be approximated. The Kohn-Sham implementation of DFT has shown to be very successful, it provides an electronic structure method with approximately the same computational cost of a Hartree-Fock calculation but with the electron correlation taken into account.

The oldest approximation to the exact exchange-correlation functional, the local density approximation (LDA), only contains terms that depend on the density $\rho[\mathrm{r}]$ and finds its origin in the exact solution of the uniform electron gas. This functional has been (and actually still is) quite successful in predicting geometries of molecules and solids and is especially well suited to describe the electronic structure of metals. To improve on this description one should add extra terms that take into account the non-uniformity of the electron density, i.e. terms that also depend on the gradient of the density $\nabla\rho(\mathrm{r})$. One of most popular improvements is the so-called Generalized Gradient Approximation (GGA). Important contributions were made by Becke in 1988[3] by introducing the B88 correction to the LDA exchange functional, ensuring a correct asymptotic behaviour of the energy density. Combined with the LYP functional for the correlation energy of Lee, Yang, and Parr[4] one gets the popular BLYP GGA functional. Other examples of this group of functionals are PW86, PW91 and PBE developed by Perdew and coworkers. Further improvements

can be made by adding terms that depend on the Laplacian of the density ($\nabla^2\rho$) and kinetic energy density, that is the Laplacian of the Kohn-Sham orbitals ($\tau(r) = \frac{1}{2}\sum_i^{occ}\left|\nabla\phi_i^{KS}(r)\right|^2$). Examples of this class of so-called meta-GGA functionals are TPSS and τ-HTCH. This path of continuous improvement of the functionals based on the fulfilment of ever more formal conditions has recently led to the publication of the SCAN functional that is claimed to fulfil not less than 17 formal requirements of the exact functional.[5]

A different path towards better functionals was taken in the early 1990s by Becke with the publication of the B3LYP hybrid functional.[6] This functional combines the above-mentioned BLYP exchange-correlation functional with the exact expression for the exchange interaction. The ratio of GGA and exact exchange was determined by fitting the outcomes with the experimental atomization energies of 56 molecules, leaving behind the path of improvement based on formal considerations. Other popular functionals such as the Minnesota functionals have followed this way of developing new functional. The M06 and M06-2x were constructed by optimizing more than 30 parameters against a very extensive database of diverse experimental data.[7] By now there is a whole range of functionals with different amount of exact exchange mixed in: B3LYP* and TPSSh use 10%, B3LYP 20%, PBE0 has 25% exact exchange, M06 27%, BHandH uses 50% of the exact exchange and M06-2x 54%.

2.1.2 Time-dependent Density Functional theory (TD-DFT)

Time-dependent DFT is an extension of ordinary DFT that is usually applied to deal with excited states, although it can be used to follow the time-evolution of non-stationary electronic states (TD-DFT in its literal meaning). TD-DFT was introduced by Runge and Gross[8] by extending the Hohenberg-Kohn theorems to arbitrary time-dependent systems. This extended HK theorems state that for any fixed initial many-body state Ψ_0, the densities $\rho(\mathrm{r}, \mathrm{t})$ and potentials $\upsilon(\mathrm{r}, \mathrm{t})$ have a one-to-one

correspondence between each other, that means, the time-dependent density is a unique functional of the time-dependent functional and hence determines the time-dependent energy (and other properties) of the system. When time is evolved, the general formalism of ground state DFT and the Kohn-Sham equation becomes

$$\rho(\mathrm{r},\mathrm{t}) = \sum_{i=1}^{N} |\phi_i(\mathrm{r},\mathrm{t})|^2 \qquad 2.14$$

$$\left[-\frac{\nabla^2}{2} + v^{KS}(\mathrm{r},\mathrm{t})\right]\phi_i(\mathrm{r},\mathrm{t}) = i\frac{\partial}{\partial t}\phi_i(\mathrm{r},\mathrm{t}) \qquad 2.15$$

$$v^{KS}(\mathrm{r},\mathrm{t}) = v(\mathrm{r},\mathrm{t}) + \int d^3r' \frac{\rho(r',r)}{r-r'} + v_{XC}(\mathrm{r},\mathrm{t}) \qquad 2.16$$

where ϕ_i are the time-dependent Kohn-Sham orbitals which produce the ρ(r, t), υ_{xc}(r, t) is the time-dependent correlation and exchange potential, the exact υ_{xc} is not known and more complicated than in ground state DFT. Using adiabatic functional in TD-DFT which is an approximation method to predict the properties of the systems.

Time dependent quantum chemical methods can be used to obtain the response of a system to an external (time-dependent) perturbation. A widely used application is the calculation of the dynamic response of the dipole moment of the system to an oscillating electric field[9]

$$\epsilon(t) = \epsilon\cos(\omega t) \qquad 2.17$$

The change in dipole moment at time t > t_0 can be written as

$$\Delta\mu(t) = \int_{t_0}^{t} \alpha(t - t')\epsilon(t')dt' + \text{higer order terms} \quad 2.18$$

with α the dynamic dipole polarizability, the measure of how susceptible the system is to the external perturbation. Hence, the response can be obtained by real-time integration, but it is more common to calculate the absorption spectrum directly. This starts by writing the dynamic response of the dipole in frequency representation, that is, by Fourier transforming eq. 2.18.

$$\Delta\mu(\omega) = \alpha(\omega)\epsilon(\omega) \quad 2.19$$

where is assumed that the electric field is small enough to only consider the linear response, meaning that the higher order terms can be neglected. The electrical absorption may now be calculated as a sum over states

$$\alpha(\omega) = \sum_{i \neq 0} \frac{f_i}{\omega_i^2 - \omega^2} \quad 2.20$$

with ω_i the relative energy of the state i with respect to the ground state. This means that when ω becomes equal to an excitation energy ω_i, the dynamic polarizability goes to infinity, exactly what can be expected when an external electric field is in resonance with an internal electronic transition of the system. f_i defines the oscillator strength and is given by

$$f_i = \frac{2}{3}|\langle 0|\vec{r}|i\rangle|^2 \quad 2.21$$

Now, within the TD-DFT setting, one calculates the response of the density to an external perturbation υ

$$\delta\rho(\mathbf{1}) = \chi(\mathbf{1}, \mathbf{2})\delta v_{ext}(\mathbf{2}) \quad 2.22$$

which can be interpreted as a matrix supposing that the integration is a summation

over a continuous index. After introducing the susceptibility of the non-interacting system

$$\chi_s(\mathbf{1},\mathbf{2}) = \frac{\delta\rho(\mathbf{1})}{\delta\upsilon_S(\mathbf{2})} \tag{2.23}$$

with υ_s the standard one-electron Kohn-Sham potential, the change in the density due to an external perturbation can be written as

$$\delta\boldsymbol{\rho} = \chi\delta\boldsymbol{\upsilon}_{ext} = \chi_s\left(\delta\boldsymbol{\upsilon}_{ext} + \mathbf{f}_{H,xc}\delta\boldsymbol{\rho}\right) \tag{2.24}$$

where $\mathbf{f}_{H,xc}$ is the functional derivative of the Hartree (*H*) plus exchange-correlation (xc) potential $\boldsymbol{\upsilon}_{H,xc}$. This can in principle be resolved iteratively in $\delta\boldsymbol{\rho}$, but solving the following matrix equation is more common

$$(\chi_s^{-1} - \mathbf{f}_{H,xc})\delta\rho = \delta\upsilon_{ext} \tag{2.25}$$

which after some reordering converts into the so-called "Casida[10] equation" for linear-response time-dependent DFT.

$$\begin{bmatrix} \mathbf{A}(\omega) & \mathbf{B}(\omega) \\ \boldsymbol{B}*(\omega) & \boldsymbol{A}*(\omega) \end{bmatrix}\begin{pmatrix} \boldsymbol{X} \\ \boldsymbol{Y} \end{pmatrix} = \omega\begin{bmatrix} \mathbf{1} & \mathbf{0} \\ \mathbf{0}* & \mathbf{1} \end{bmatrix}\begin{pmatrix} \boldsymbol{X} \\ \boldsymbol{Y} \end{pmatrix} \tag{2.26}$$

where the matrix elements of $\mathbf{A}$ and $\mathbf{B}$ are defined as

$$A_{ia,jb}(\omega) = \delta_{ij}\delta_{ab} + \iint \phi_i(1)\phi_a(1)\mathrm{f}_{H,xc}(1,2,\omega)\phi_j(2)\phi_b(2)d1d2 \tag{2.27}$$

$$B_{ia,bj}(\omega) = \iint \phi_i(1)\phi_a(1)\mathrm{f}_{H,xc}(1,2,\omega)\phi_b(2)\phi_j(2)d1d2 \tag{2.28}$$

with i and j indices for occupied and a and b for unoccupied orbitals. The eigenvalues of this matrix equation provide excitation and de-excitation energies, whereas the eigenvectors contain information about the intensity and the character of the transitions. A common simplification of the Casida equation is obtained by

neglecting the **B**-matrix. All information about the de-excitations is lost but a much simpler equation appears

$$\mathbf{AX} = \omega\mathbf{X} \tag{2.29}$$

the Tamm-Dancoff approximation[11](TDA). Experience has shown that TDA provides roughly equal excitation energies as the full TD-DFT approach but does not (or at least is affected much less) by the so-called triplet instability, which means that in some cases spurious triplet states appear with negative excitation energies.

2.1.3 Wave Function-based Method

HF is an independent particle model in which the full electron-electron interaction is replaced by an average interaction. Although it can reach up to 99% of the total (non-relativistic) energy when a sufficiently large basis set is used (or when an extrapolation to the complete basis set limit is made), the remainder causes large differential effects and has to be accounted for to obtain chemically relevant results. The difference between the exact energy and the lowest possible HF energy is defined as the electron correlation energy can be written as

$$E_{corr} = E_{exact} - E_{HF} \tag{2.30}$$

E_{corr} represents the electron correlation energy, E_{exact} represents the exact energy, and E_{HF} represents the lowest possible HF energy (that is, the energy for a complete basis set). There are many different post-HF methods that can take into account the electron correlation and for the discussion of these methods it is convenient to divide the electron correlation in dynamic and a non-dynamic contributions. Dynamic correlation is caused by the instantaneous electron-electron repulsion at short distance. It causes a cusp in the electronic wave function as function of the electron-electron distance, which is absent in Hartree-Fock theory. The non-dynamic correlation is caused by the presence of different electronic configurations

in a small energy interval making it impossible to describe the electronic structure with one (dominant) Slater determinant. The distinction is not 100% waterproof, and it is sometimes difficult to distinguish between the two effects.

The Hartree-Fock determinant for the ground state is obtained by progressively filling the orbitals by increasing orbital energy. However, this is obviously not the only way in which the electrons can be distributed over the MOs. As much as the basis set constitutes a complete basis for the one-electron functions (the orbitals), the Slater determinants are a complete basis for the many-electron space. Hence the exact many-electron wave function for the ground and excited states can be written as a linear combination of all the Slater determinants that can be formed given a certain one-electron basis.

$$\Psi = a_0 \Phi_{HF} + \sum_{i=1}^{N} a_i \, \Phi_i \qquad 2.31$$

Where N is the total number of Slater determinants. There are three different basic approaches to determine the coefficients a_i in front of the Slater determinants. They are Configuration Interaction (CI), Many-body perturbation theory (MBPT) and coupled cluster (CC).

2.1.3.1 CI and MCSCF

The most straightforward way to find the values of a_i in Eq. 2.31 is based on the variational principle. First, the partial derivatives of energy expectation value $\langle \Psi | \hat{H} | \Psi \rangle / \langle \Psi | \Psi \rangle$ are taken with respect to the coefficients. The resulting equations are set equal to zero and solving these so-called secular equations leads to the coefficients a_i that minimize the energy. Using the complete expansion of Eq. 2.31, the exact energy within the one-electron basis is obtained (full CI), but unfortunately

this is only possible for small molecules. In all other cases one has to truncate the expansion, which is most conveniently done by ordering the Slater determinants following the number of electron replacements with respect to the Hartree-Fock determinant.

$$\Psi_{CI} = a_0\Phi_{HF} + \sum_S a_s\,\Phi_s + \sum_D a_D\,\Phi_D + \sum_T a_T\,\Phi_T + \cdots$$

2.32

where Φ_S is a single excitation, Φ_D is a determinant with two changes, etc. Truncating after Φ_D leads to CISD, which can give reasonable results in some cases but suffers from severe size-consistency problems and hence not widely used anymore. Apart from ad-hoc corrections, one can also solve the problem by not only optimizing the CI coefficient a_i but also the orbital expansion coefficients in a double variational procedure giving rise to the multi-configuration self-consistent field (MCSCF) approach. Then the CI expansion has to be reduced drastically to keep the calculation feasible and a popular way of constructing the MCSCF wave function is by the complete active space self-consistent field (CASSCF) method which divides the MO space in three subspaces (see **Fig** 2.1): (i) inactive orbitals, doubly occupied in all configurations; (ii) active orbitals with a variable occupation (occupied in some configurations and unoccupied in others); (iii) the virtual orbitals, empty in all configurations.

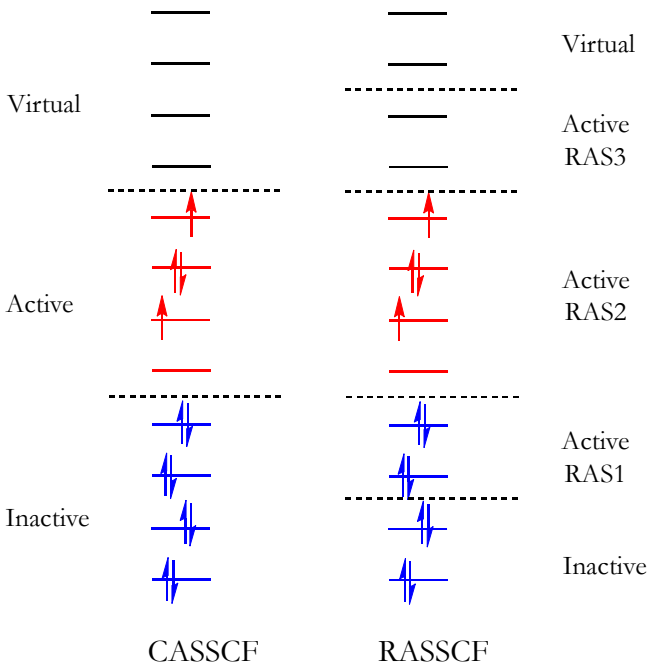

Figure 2.1 *Scheme of MOs classification in the CASSCF and RASSCF spaces.*

In general, the active space is denoted as CAS [m, n] with m the number of active electrons and n the number of active orbitals. The multi-configurational wave function is constructed by distributing the m electrons (typically, the valence electrons) over the n orbitals (typically, the valence orbitals) in all possible ways. In other words, CASSCF can be thought of as a full CI in a limited set of MOs.

The problem with the complete active space approach is that the wave function rapidly becomes intractable, the limit lies around 16 electrons in 16 orbitals with low-spin coupling of the electrons. To stretch the possibilities, a restricted active space self-consistent field wave function can be used instead. Here, the active space is divided into three subsections: RAS1 with doubly occupied orbitals allowing at most a certain number of holes; RAS2 with variable occupations as in the CAS, and RAS3 with empty orbitals allowing a certain number of electrons (see **Fig.** 2.1).

Finally, it should be mentioned that the most delicate part of CASSCF or RASSCF calculations is the choice of the active space, which orbitals should form part of it? There are no general recipes for the best choice of the active space and one should carefully check the choice against results published previously in the literature on similar systems and, preferably, compare results with increasing active spaces. A second important shortcoming of the CASSCF approach is that it can accurately treat the non-dynamic correlation for most systems, but completely lacks dynamic correlation. The inclusion of this effect will be detailed in the next section.

2.1.3.2 Multi-configurational reference perturbation theory

An efficient way of adding dynamic correlation effects to the MCSCF wave functions is based on many-body perturbation theory. There are nowadays basically two widespread implementation of perturbation theory based on a multi-configurational reference wave function, CASPT2 and NEVPT2, but before discussing some of the details of these two methods, we will first spend a few words on the most-common implementation of perturbation theory for a reference wave function with just one configuration (the Hartree-Fock determinant), namely Møller–Plesset perturbation theory (MPn, where n refers to the order of perturbation theory, normally 2). The two things that define the perturbation theory are the choice of the zeroth-order Hamiltonian and the construction of the first-order wave function. In the MP implementation the zeroth-order Hamiltonian is the sum of all the Fock operators and the first-order wave function is defined by all the determinants with two electron replacements. This leads to the following expression for the correction of the energy at second-order.

$$E^{(2)} = \sum_{i \neq 0} \frac{\left\langle \Psi_i^{(0)} \middle| \hat{V}^{(1)} \middle| \Psi_0^{(0)} \right\rangle \left\langle \Psi_0^{(0)} \middle| \hat{V}^{(1)} \middle| \Psi_i^{(0)} \right\rangle}{E_i^{(0)} - E_0^{(0)}} \qquad 2.33$$

Theoretical background

Things get a little more complicated for a multi-configurational reference wave function, but the complete active space second-order perturbation theory (CASPT2) stays as close as possible to MP2. The zeroth-order Hamiltonian is a Fock-like (one-electron) operator

$$\hat{H}^{(0)} = \hat{P}_0\hat{F}\hat{P}_0 + \hat{P}_K\hat{F}\hat{P}_K + \hat{P}_{SD}\hat{F}\hat{P}_{SD} + \hat{P}_X\hat{F}\hat{P}_X \quad 2.34$$

$$\hat{P}_0 = |0\rangle\langle 0| \quad 2.35$$

$$\hat{F} = \sum_{pq\sigma} f_{pq\sigma}\hat{E}_{pq} \quad 2.36$$

$$f_{pq\sigma} = -\left\langle 0\middle|\left[\left[\hat{H}, \hat{a}^{\dagger}_{q\sigma}\right], \hat{a}_{p\sigma}\right]_+\middle|0\right\rangle \quad 2.37$$

where $|0\rangle$ is the zeroth-order wave function, $\hat{F}$ is a Fock-type one electron operator, $\hat{P}_0$ projects on reference wave function, $\hat{P}_k$ projects on other states in the CAS space, $\hat{P}_{SD}$ projects on single and doubles, $\hat{P}_X$ on the rest.

The first-order wave function is generated by applying single and double excitation operators on the CASSCF wave function as a whole.

$$\Psi^{(1)} = \sum_{pqrs} c_{pqrs}\hat{E}_{pq}\hat{E}_{rs}|0\rangle \quad 2.38$$

This so-called contracted expansion largely reduces the computational cost of the perturbation theory without significant loss of accuracy. CASPT2 is considered one of the standard ab initio methods for studying the properties of excited states but it

has one important drawback related to the one-electron nature of the zeroth-order Hamiltonian. This may cause the appearance of intruder states, configurations external to the CAS with expectation values of $\widehat{H}^0$ very close to $\langle \Psi_{CAS} | \widehat{H}^0 | \Psi_{CAS} \rangle$. This leads to very small denominators in the equation of the second-order energy correction and hence to useless results. This can pragmatically remedied by artificially shifting all the expectation values of $\widehat{H}^0$ by an arbitrary amount and later correcting for this level shift.

Otherwise, one may consider to use the n-electron valence second-order perturbation theory (NEVPT2) which has a very similar way of generating the first-order wave function (in its partially contracted version) but uses a zeroth-order Hamiltonian that goes beyond the purely one-electron nature as used in CASPT2. Here, the Dyall Hamiltonian is used for the active space, while standard Fock operators are used for all the inactive electrons

$$\widehat{H}_0 = \sum_{ij} f_{ij} E_{ij} + \sum_{ab} f_{ab} E_{ab} + \sum_{vw} h_{vw} E_{vw} + \frac{1}{2} \sum_{vwxy} g_{vwxy} (E_{vw} E_{xy} - \delta_{wx} E_{vy}) \quad 2.39$$

The subscript ij and ab represent the Fock-operator in inactive and secondary orbitals; the subscript $vwxy$ represent full Hamiltonian in active orbitals. This leads to an intruder state-free multi-configurational reference perturbation theory that rivals in speed and accuracy with CASPT2.

2.1.3.3 CCSD(T) method

The third method to include dynamic correlation in the wave function is the coupled cluster (CC) method. This efficient and accurate technique generate the wave function by an exponential development

$$\Psi_{CC} = e^{\hat{T}}\Phi_0 \quad 2.40$$

$$\hat{T} = \hat{T}_1 + \hat{T}_2 + \hat{T}_3 + \hat{T}_4 + \cdots\cdots \quad 2.41$$

where $\hat{T}_i$ represent the single $(\hat{T}_1 = \sum_{i,a} t_i^a \hat{a}_a^\dagger \hat{a}_i)$, double $(\hat{T}_2 = \sum_{\substack{a<b \\ i<j}} t_{ij}^{ab} \hat{a}_a^\dagger \hat{a}_b^\dagger \hat{a}_i \hat{a}_j)$ and triple etc. excitation operators, where the 't' stands for the cluster amplitudes. By expanding the exponent in a Taylor series

$$e^T = 1 + \hat{T} + \frac{1}{2!}\hat{T}^2 + \frac{1}{3!}\hat{T}^3 + \frac{1}{4!}\hat{T}^4 + \cdots\cdots \quad 2.42$$

And substituting Eq. 2.42 we obtain the following expression for the cluster operator

$$e^{\hat{T}} = 1 + \left(\hat{T}_1 + \hat{T}_2 + \hat{T}_3 + \cdots\right) + \frac{1}{2!}\left(\hat{T}_1 + \hat{T}_2 + \hat{T}_3 + \cdots\right)^2 + \frac{1}{3!}\left(\hat{T}_1 + \hat{T}_2 + \hat{T}_3 + \cdots\right)^3 \cdots\cdots \quad 2.43$$

Ordering the terms by excitation leads to

$$e^{\hat{T}} = 1 + \hat{T}_1 + \left(\hat{T}_2 + \frac{1}{2}\hat{T}_1^2\right) + \left(\hat{T}_3 + \hat{T}_1\hat{T}_2 + \frac{1}{6}\hat{T}_1^3\right) + \left(\hat{T}_4 + \hat{T}_1\hat{T}_3 + \frac{1}{2}\hat{T}_2^2 + \frac{1}{2}\hat{T}_1^2\hat{T}_2 + \frac{1}{24}\hat{T}_1^4\right) + \cdots \quad 2.44$$

To reduce the computational effort, the T operator Eq. 2.41 is truncated after the T_2 term, which converts the cluster operator to

$$e^{\hat{T}_1+\hat{T}_2} = 1 + \hat{T}_1 + \hat{T}_2 + \frac{1}{2}\hat{T}_1^2 + \hat{T}_1\hat{T}_2 + \frac{1}{6}\hat{T}_1^3 + \frac{1}{2}\hat{T}_2^2 + \frac{1}{2}\hat{T}_1^2\hat{T}_2 + \frac{1}{24}\hat{T}_1^4 + \cdots \quad 2.45$$

The CCSD energy is given by

$$E = \left\langle \Psi_0 \middle| \hat{H} \middle| (1 + \hat{T}_1 + \hat{T}_2 + \frac{1}{2}\hat{T}_1^2)\Psi_0 \right\rangle \quad 2.46$$

And the cluster amplitudes by

$$\left\langle \Psi_i^a \middle| \hat{H} \middle| (1 + \hat{T}_1 + \hat{T}_2 + \frac{1}{2}\hat{T}_1^2 + \hat{T}_1\hat{T}_2 + \frac{1}{6}\hat{T}_1^3)\Psi_0 \right\rangle = t_i^a E \quad 2.47$$

$$\left\langle \Psi_i^a \middle| \hat{H} \middle| \left[\begin{matrix} 1 + \hat{T}_1 + \hat{T}_2 + \frac{1}{2}(\hat{T}_1^2 + \hat{T}_2^2 + 2\hat{T}_1\hat{T}_2) \\ + \frac{1}{6}(\hat{T}_1^3 + 3\hat{T}_1^2\hat{T}_2) + \frac{1}{24}\hat{T}_1^4 \end{matrix} \right] \Psi_0 \right\rangle = t_{ij}^{ab} E \quad 2.48$$

Contrary to truncated CI, CCSD is free of size-consistency errors. By adding an perturbative correction for the triples, the CCSD(T) method can be formulated, which is one of the most accurate yet feasible quantum chemistry methods when the electronic structure is reasonably well described with a single Slater determinant. For strong multi-configurational systems, the method is less reliable.

2.2 Effective Hamiltonian Theory

The effective Hamiltonian theory was formulated in 1958 by Bloch [12] and refined by des Cloizeaux[13] ensuring an hermitian form of the effective Hamiltonian. The aim of the effective Hamiltonian is to represent the relevant information of the full N-electron space (of sometimes huge dimension) in a much more compact manner without losing accuracy. For this purpose one first defines an M-dimensional model space $\mathcal{S}_0$, subspace of the full $N \times N$ Hilbert space $\mathcal{S}$. The M eigenvectors (calculated with high quality ab initio methods) with the largest projection on the model space form the $N \times M$ target space $\mathcal{S}_t$.

$$\tilde{\Psi}_k = \hat{P}_{S_0}\Psi_k \qquad 2.49$$

With the projection operator defined as

$$\hat{P}_{S_0} = \sum_{i=1}^{M} |\Phi_i\rangle\langle\Phi_i| \qquad 2.50$$

The projections of the eigenvectors of S on S_0 ($\tilde{\Psi}_\kappa$) are neither orthogonal nor normalized, and hence, do not directly form a basis for S_0. This can be achieved in different ways. Bloch proposed to construct biorthogonal vectors, leading to a non-Hermitian matrix. Although this certainly is the procedure where the maximum of information of S is retained, it is more convenient to work with a Hermitian Hamiltonian. The orthogonalization procedure suggested by des Cloizeaux

$$\tilde{\Psi}_\kappa^{\perp} = S^{-1/2}\tilde{\Psi}_\kappa \qquad 2.51$$

does lead to the desired orthonormal basis of S_0 and makes it possible to construct a Hermitian effective Hamiltonian by applying the Bloch formula (or spectral decomposition)

$$\hat{H}_{eff} = \sum_{\kappa\in S_t} |\tilde{\Psi}_\kappa\rangle E_\kappa \langle\tilde{\Psi}_\kappa^{\dagger}| \qquad 2.52$$

And then calculate the matrix elements

$$\langle\Phi_I|\hat{H}_{eff}|\Phi_J\rangle = \sum_{k\in S_t} \langle\Phi_I|\tilde{\Psi}_k\rangle E_k \langle\tilde{\Psi}_k^{\dagger}|\Phi_J\rangle \qquad 2.53$$

The eigenvalues of this Hamiltonian are by construction the same as the eigenvalues of the eigenvectors of S_t, and the eigenvectors of $\widehat{H}_{eff}$ are equal to the projection of the eigenvectors of S_t on S_0. This illustrates that we have constructed a Hamiltonian of reduced dimension without losing accuracy, neither in the energies nor in the wave function. Analysis of the physics is much easier with this smaller model space.

2.3 Fermi´s golden rule

Over the last few years the theoretical treatment of the dynamics of excited states has received increasing attention.[14] As discussed in the introduction, spin crossover can be induced by irradiating a sample with light. The process implies at least one, but more often two intersystem crossings (ISC), in which the initially populated excited state relaxes to lower-lying states of different spin multiplicity. On the other hand, an excited state can also undergo internal conversion, a change between two electronic states with the same spin multiplicity. These internal conversions are supposed to be faster than the intersystem crossings and we will only focus on the latter. One of the simplest, yet successful methods to calculate the intersystem crossing rates is based on Fermi's Golden rule.

$$k_{ISC} = 2\pi \sum_{k} \left|\left\langle \Psi_{S_a}, \{v_{aj}\} \middle| \widehat{H}_{\mathrm{SO}} \middle| \Psi_{T_b}, \{v_{bk}\} \right\rangle\right|^2 \delta(E_{aj} - E_{bk})$$

2.54

where a, b label electronic states with multiplicity S or T; j and k label vibrational states; Ψ_{S_a} and Ψ_{S_b} are electronic wave functions of the initial and final states; $\widehat{H}_{SO}$ is the spin-orbit coupling operator. Under the assumption that the states are only coupled by spin-orbit coupling (Condon approximation) Eq 2.54 can be rewritten as the product of the electronic part and the vibrational overlap (Franck-Condon factors) of the initial and final state

Theoretical background

$$k_{ISC} = 2\pi\left|\langle\Psi_{S_a}|\widehat{H}_{\mathrm{SO}}|\Psi_{T_b}^{\alpha}\rangle\right|_{q_0}^2 \times \sum_k \left|\langle\{\nu_{aj}\}|\{\nu_{bk}\}\rangle\right|^2 \delta(E_{aj} - E_{bk})$$

2.55

Using this equation many (smaller) organic systems have successfully been studied but the computational cost of the explicit calculation of the Franck-Condon factors is rather elevated. This can be avoided by transforming Fermi´s golden rule from the space domain into the time domain.

$$k_{ISC} = \left|\langle\Psi_S|\widehat{H}_{\mathrm{SO}}|\Psi_T\rangle\right|^2 \int_{-\infty}^{\infty} dt G(t) e^{it\left(\Delta E_{ST}^0 + \frac{1}{2}Tr\Omega_S\right)}$$

2.56

Where the electronic part (the spin-orbit coupling) remains unchanged but the calculation of the Franck-Condon integrals is replaced by a time integral over the generating function $G(t)$ that contains the vibrational frequencies and normal modes of the initial and final states (for the exact expression see ref.[15]), as does the exponent, which also contains the adiabatic energy difference between initial and final state. In this form, the application of Fermi´s golden rule to calculate ISC rates has been quite successful in photorelaxation of nucleobases,[3] photophysics of iridium-based organic light-emitting diods (OLEDs),[16] and SCO in Fe(II) and Fe(III) complexes.[17]

2.4 Beyond the harmonic description of the molecular vibrations

The potential energy curve of a diatomic molecule as function of the interatomic distance x around the equilibrium distance x_0 can be written as a Taylor series

$$E(\mathrm{x}) = E(\mathrm{x}_0) + \frac{dE(\mathrm{x}_0)}{d\mathrm{x}}(\mathrm{x}-\mathrm{x}_0) + \frac{1}{2}\frac{d^2E(\mathrm{x}_0)}{d\mathrm{x}^2}(\mathrm{x}-\mathrm{x}_0)^2 + \frac{1}{6}\frac{d^3E(\mathrm{x}_0)}{d\mathrm{x}^3}(\mathrm{x}-\mathrm{x}_0)^3 + \cdots \quad 2.57$$

The first term is the zero of energy and can be taken equal to zero. The second term is the gradient of the energy in the equilibrium geometry which vanishes. Neglecting the third and higher derivatives ones arrives at the harmonic approximation

$$E(\mathrm{x}) \cong \frac{1}{2}\frac{d^2E}{d\mathrm{x}^2}\Delta\mathrm{x}^2 = \frac{1}{2}k\Delta\mathrm{x}^2 \quad 2.58$$

Where k is the force constant. And the energy levels of this quantum harmonic oscillator are given by

$$\varepsilon_n = \left(\mathrm{n}+\frac{1}{2}\right)\hbar\nu \quad \mathrm{n}=0, 1, 2, 3..... \quad 2.59$$

$$\nu = \frac{1}{2\pi}\sqrt{\frac{k}{\mu}} \quad 2.60$$

$$\mu = \frac{m_1 m_2}{m_1+m_2} \quad 2.61$$

Here, n is the vibrational quantum number and $\nu$is the vibrational frequency related to the force constant by Eq. 2.60. Within this harmonic approximation the energy between two subsequent vibrational energy levels is constant ħν as illustrated in **Fig.** 2.2. The harmonic approximation has shown its power and in most cases adequate to obtain reliable results.

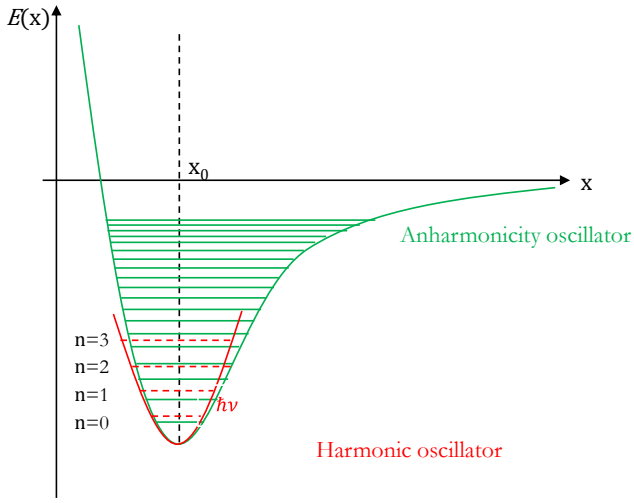

Figure 2.2 *The scheme shows the potential energy curve E(x) of harmonic oscillator and the equally spaced vibrational energy level (in red) and the anharmonic oscillator and unequally vibrational energy level (in blue), n represent the quantum number and x represent the internuclear distances and x_0 is the equilibrium geometry distance.*

Keeping the cubic and quartic term in the Taylor expansion leads to the following expression for the potential energy surface

$$E(\mathrm{x}) = \frac{1}{2}k\Delta\mathrm{x}^2 + \gamma\Delta\mathrm{x}^3 + \delta\Delta\mathrm{x}^4 + \cdots\cdots \qquad 2.62$$

Here γ and δ represent the cubic and quartic anharmonic parameters. The shape of the potential energy surface becomes steeper at small internuclear distances which reflect the repulsion interaction and shallower at larger internuclear distances which corresponds to the process of dissociation. The vibrational energy levels are no longer equally spaced, but get progressively closer together as n increases, see **Fig.** 2.2. This reasoning for a diatomic molecule can be extended to a polynuclear system by replacing x, the internuclear distance, by Q, the normal modes of the molecules. The changes in the spacing of the vibrational levels can have an impact on properties as the entropy as will be studied in Chapter 5

References

[1] P. Hohenberg and W. Kohn, *Phys. Rev.* **1964**, *136*, B864-B871.

[2] W.Kohn and L. J. Sham, *Phys.Rev.* **1965**, *140*, A1133-A1138.

[3] A. D. Becke, *Phys. Rev. A* **1988**, *38*, 3098-3100.

[4] C. Lee, W. Yang and R. G. Parr, *Phys. Rev. B* **1988**, *37*, 785-789.

[5] J. Sun, R. C. Remsing, Y. Zhang, Z. Sun, A. Ruzsinszky, H. Peng, Z. Yang, A. Paul, U. Waghmare, X. Wu, M. L. Klein and J. P. Perdew., *Nat. Chem.* **2016**, *8*, 831-836.

[6] A. D. Becke, *J. Chem. Phys.* **1993**, *98*, 5648-5652.

[7] Y. Zhao and D. G. Truhlar in *Theor Chem Acc.*, *Vol. 120* Springer-Verlag, **2008**, pp. 215-241.

[8] E. Runge and E. K. U. Gross, *Phys.Rev.Lett.* **1984**, *52*, 997-1000.

[9] M. E. Casida and M. Huix-Rotllant in *Many-Body Perturbation Theory (MBPT) and Time-Dependent Density-Functional Theory (TD-DFT): MBPT Insights About What Is Missing In, and Corrections To, the TD-DFT Adiabatic Approximation, Vol. 368* Eds.: N. Ferré, M. Filatov and M. Huix-Rotllant), Springer, **2016**, pp. 1-60.

[10] M. E. Casida in *Recent Advances in Density Functional Methods, Vol.* (Ed. D. E. Chong), World Scientic, **1998**, pp. 152-192.

[11] S. Hirata and M. Head-Gordon, *Chem. Phys. Lett.* **1999**, *314*, 291–299.

[12] C. Bloch, *Nucl. Phys.* **1958**, *6*, 329-347.

[13] J. d. Cloizeaux, *Nucl. Phys.* **1960**, *20*, 321-346.

[14] C. Sousa, M. Alías, A. Domingo and C. de Graaf, *Chem. Eur. J.* **2019**, *25*, 1152 – 1164.

[15] M. Etinski, J. Tatchen and C. M. Marian, *J. Chem. Phys.* **2011**, *134*, 154105.

[16] A. Heil, K. Gollnisch, M. Kleinschmidt and C. M. Marian, *Mol. Phys.* **2016**, *114*, 407-422.

References

[17] a) C. Sousa, C. de Graaf, A. Rudavskyi, R. Broer, J. Tatchen, M. Etinski and C. M. Marian, *Chem. Eur. J.* **2013**, *19*, 17541 – 17551; b) S. Saureu and C. de Graaf, *Phys. Chem. Chem. Phys.* **2016**, *18*, 1233-1244.

"Great works are performed not by strength, but by perseverance"

--Samuel Johnson

Chapter 3

Controlling the lifetime of the excited states by modifying the ligands of Fe(II) and Ru(II) polypyridyl complexes

3.1 Introduction

Fe(II) polypyridyl complexes have received a great deal of attention because they play a central role in the interpretation of the LIESST process. The mechanism of the photocycle was extensively studied both in experiment[1] and by theory.[2] After light irradiation, the system decays from the singlet metal-to-ligand charge transfer (^{1}MLCT) state to the metal-centred (^{5}MC) high-spin (HS) state on a femtosecond time scale, making the Fe(II) complexes less useful for applications such as light-harvesting and photocatalysis, acting as an electron donor for solar energy conversion.[3] Ru(II) complexes have longer excited state lifetimes and do not end up

in a metastable metal-centred quintet state. The drawback of these systems is the scarcity of Ru, making large scale applications extremely expensive. It is therefore desirable to reproduce the properties of the Ru(II) complexes with the much more abundant Fe. Ligand modification have been proposed and studied to increase the MLCT lifetime in Fe(II) complexes.[4] There are mainly two strategies to achieve this goal: one is to create stronger ligands field and push the MC state higher than the MLCT states; another idea is to expand the π-conjugation on the ligand, lowering the MLCT states. Both strategies have been explored here using different ligands coordinated to Fe(II) and Ru(II) ions. We will show that controlling the relative energy of charge transfer and ligand field states becomes an effective way to influence the excited states dynamics. In this work, we will give a detailed investigation of the ligand(s) modification of the parent $[Fe(bpy)_3]^{2+}$ and $[Ru(bpy)_3]^{2+}$ complexes.

3.2 The ligand modifications in FeN_6 system

3.2.1 Replacing N by P atoms

Stronger ligand-fields can be created by using less-electronegative atoms in the first coordination sphere of the metal ion. There are several electronegativity scales for the elements of the periodic table,[5] among which the Pauling scale is the most commonly used. All scales coincide that P is significantly less electronegative than N, and hence, replacing N by P could be a possibility to raise the energy of the excited MC states above the MLCT states. In this part of the work, we mainly focus on the analysis of the vertical excitation energies of these replacements to give a preliminary prediction on interesting candidates to be investigated in more depth. An exhaustive search in the Cambridge Structural Database revealed 14 different complexes with a $FeN_{(6-x)}P_x$ core. The estimation of the vertical excitation energies starts with the optimization of the ground state geometries of these systems. Here, all P-substituted variants systems were optimized with DFT using the OPBE functional with the

def2-TZVP basis set as implemented in ORCA 4.0. Starting from the ground state geometries, TD-DFT calculations were performed to calculate the vertical energies with the same functional and basis set. There are mainly two types of excitations: (i) ligand field or metal-centred (MC) singlet and triplet states; (ii) metal-to-ligand charge transfer transitions (^{1}MLCT or ^{3}MLCT) states. **Fig.**3.1 shows some of the representative P replacement complexes as found in Cambridge Structural Database except the six P replacement. **Table** 3.1 lists the excitation energies of the lowest excited states ^{1}MC, ^{3}MC, ^{1}MLCT and ^{3}MLCT of all the two P, three P, four P and six P atoms replacements, labelled by the acronym used in the database.

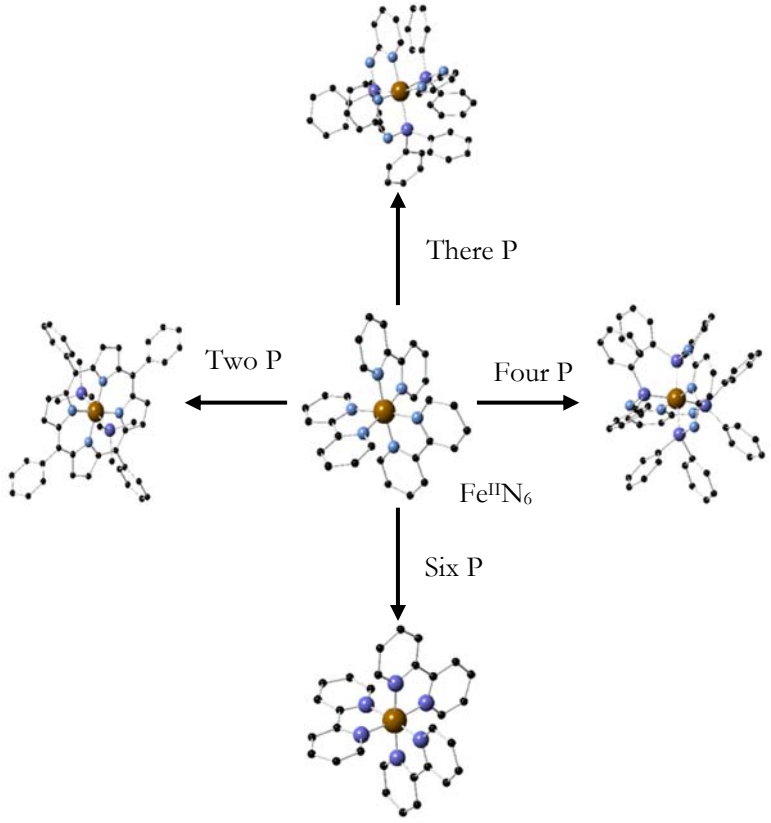

Figure 3.1 *Ball-and-stick representation of the $Fe^{(II)}N_{(6-x)}P_x$ complexes found in the Cambridge Structural Database, with the exception of the FeP_6 complex, for which no entry exist in the database.*

Table 3.1 Vertical TD-DFT energies [eV] of the low-lying electronic states of the FeN_xP_{6-x} system.

Core structure	Crystal name	^{1}MLCT	^{3}MLCT	^{3}MC	^{1}MC
FeN_6	$[Fe(bpy)_3]^{2+}$	2.27	2.08	1.92	2.88
FeN_4P_2	MINWOX	2.31	2.05	1.89	2.66
	JEGRIX	2.33	2.19	2.02	2.72
	GIFJAG	1.75	1.45	1.62	2.28
	KACGIE	1.62	1.31	1.45	2.20
	KACGIE*	1.72	1.42	1.89	2.59
	QOKKAD	1.79	1.51	1.89	2.46
	QOKKEH*	1.78	1.41	1.41	2.22
	SURMAT	1.78	1.49	1.88	2.58
	SURMEX	1.73	1.44	1.91	2.63
FeN_3P_3	YIZMAX	3.70	3.28	1.81	2.54
FeN_2P_4	FOPSOU	3.79	3.32	1.99	2.69
	FOPSUA	3.93	3.28	1.88	2.61
	FOPTAH	4.07	3.29	2.04	2.77
	OWCREA	2.63	2.47	1.92	2.71
FeP_6		2.95	2.36	2.71	3.17

As can be seen in **Table** 3.1, the typical FeN_6 system $[Fe(bpy)_3]^{2+}$ complex has, as expected, the ^{3}MC state below the ^{3}MLCT state. The middle part of **Table** 3.1 lists the different FeN_4P_2 systems, the first two rows MINWOX and JEGRIX have lower ^{3}MC states and show similar feature as the $[Fe(bpy)_3]^{2+}$ complex. In the remaining seven examples the ^{3}MC states appeared a little higher than the ^{3}MLCT states, but

still very close in energy, such as in the case of QOKKEH* the ^{3}MC and ^{3}MLCT states are overlapping with each other. Somewhat surprisingly, the complexes which have FeN_3P_3 and FeN_2P_4 structures show again a larger gap between ^{3}MC and ^{3}MLCT states, with the ^{3}MLCT states located at higher energy. Only the model complex obtained by replacing the six N atoms in $[Fe(bpy)_3]^{2+}$ by P shows a situation comparable to $[Ru(bpy)_3]^{2+}$ with a clearly more stable ^{3}MLCT state. Unfortunately, there are no examples of FeP_6 complexes in the literature, and hence, further studying these complexes is not very useful. For further investigation of the FeN_4P_2 system which show the higher ^{3}MC state, the geometry optimization of the ^{3}MC state has been done in the case of GIFJAG. However this complex turns out to be unstable in the triplet state, since the two PPh(Me)3 ligands dissociate from the complex during the optimization process. So here we conclude that replacing N with P is not a good strategy to invert the relative stability of the ^{3}MC and ^{3}MLCT states in Fe(II) complexes. More strategies will be discussed in the following sections in this chapter.

3.2.2 Replacing bpy by CN^- in $[Fe(bpy)_x(CN)_{6-2x}]^{2x-4}$

Instead of using P to increase the ligand field, one could also replace one or more N atoms by C. As phosphorus, carbon has also a smaller electronegativity than N, and hence, is also a candidate to increase the ligand field strength. In this section we will study the effect of replacing one or two bipyridine ligands by two or four CN^- groups (see **Fig.** 3.2), the one but strongest sigma donor in the spectrochemical series. The same method has been used for ground state optimization and vertical excitation energies calculation as for the $FeN_{(6-x)}P_x$ complexes discussed in the previous section. It is important to note that the vertical excitation energies are only used here to make a preliminary prediction to see if the replacement of bipyidine by CN^- is a good strategy to fulfil our objective of reproducing the properties of Ru complexes with Fe. Further on in this chapter we will discuss the vertical excitation energies in more

detail. As can be seen in **Table** 3.2, the results of the vertical energies for these two complexes indicated that the ^{3}MLCT states are significantly stabilized and the ^{3}MC states destabilized with respect to the $[Fe(bpy)_3]^{2+}$ complex. There exists a significant gap between these two states. The results of the vertical energies indicates that the CN^- ligand is a good candidate for modification of the bipyridine ligands. Experimental work on $[Fe(bpy)(CN)_4]^{2-}$ in dimethyl sulfoxide (DMSO) solvent showed an increased ^{3}MLCT excited state lifetime because of the destabilization of the ^{3}MC excited state suppressing spin crossover.[6] However, the experiments for $[Fe(bpy)_2(CN)_2]$ reveal a similar spin crossover mechanism as observed in $[Fe(bpy)_3]^{2+}$.

Figure 3.2 *Ball-and-stick presentation of the complexes studied in this chapter: $[Fe(bpy)_3]^{2+}$ (left), $[Fe(bpy)_2(CN)_2]$ (middle) and $[Fe(bpy)(CN)_4]^{2-}$ (right). Color code: brown for Fe, blue for N, black for C and all the H not shown here.*

Table 3.2 Vertical TD-DFT energies [eV] of the low-lying electronic states of: $[Fe(bpy)_3]^{2+}$, $[Fe(bpy)_2(CN)_2]$ and $[Fe(bpy)(CN)_4]^{2-}$.

Core structure	complexes	^{1}MLCT	^{3}MLCT	^{3}MC	^{1}MC
FeN_6	$[Fe(bpy)_3]^{2+}$	2.26	2.08	1.92	2.88
$FeN_4(CN)_2$	$[Fe(bpy)_2(CN)_2]$	1.61	1.32	2.33	3.24
$FeN_2(CN)_4$	$[Fe(bpy)(CN)_4]^{2-}$	1.07	0.69	2.80	3.47

3.2.2.1 DFT geometry optimization of the lowest singlet, triplet and quintet states.

The geometries of the $[Fe(bpy)_x(CN)_{6-2x}]^{2x-4}$ system have been optimized for three lowest electronic states with different spin multiplicities: singlet (LS), triplet (intermediate spin: IS) and quintet (HS) using the def2-TZVP basis set and the TPSSh, OPBE, B3LYP, PBE0 and M062x functionals. A comparison of the average Fe-N distance for LS, IS and HS is shown in **Table** 3.3 and the HS-LS energy difference (ΔE_{HS-LS}) is shown in **Table** 3.4. Starting with the $[Fe(bpy)_3]^{2+}$ complex, the Fe-N average distance for LS is 1.99 Å for TPSSh, 1.96 Å for OPBE, and 2.00 Å for PBE0, in good agreement with the experimental value 1.97-1.98 Å. B3LYP and M062x predict an average distance around 2.03 Å slightly overestimating the LS Fe-N distance. The elongation of the Fe-N distance from LS to HS of 0.20 Å found with TPSSh, B3LYP and PBE0 match well with the experimental data from Gawelda et al,[7] but OPBE and M062x gave somewhat larger (0.24 Å) or somewhat smaller (0.16 Å) values. The relative energy without ZPVE correction with the TPSSh functional for $[Fe(bpy)_3]^{2+}$ is in good agreement with the experimental data of around 6000 cm^{-1},[8] OPBE and B3LYP correctly predict that $[Fe(bpy)_3]^{2+}$ is a LS complex. However, the PBE0 and M062x obviously overstabilize the HS for $[Fe(bpy)_3]^{2+}$ complex. The same trends are observed for $[Fe(bpy)_2(CN)_2]$: TPSSh, B3LYP and PBE0 predict similar increases of the Fe-N distance comparing upon changes in the spin state, OPBE slightly smaller and M062x slightly larger. The increased ligand field strength leads to stabilisation of the LS state, that is, larger ΔE_{HS-LS} for all functionals except M062x, which even for $[Fe(bpy)(CN)_4]^{2-}$ predicts a LS ground state. From previous studies it has become very well established that every occupation of an anti-bonding e_g-like orbital is accompanied by an enlargement of about 0.1 Å. Hence by looking at the distances reported in **Table** 3.3 it becomes clear that in all cases the lowest state for each spin coupling corresponds to a standard

d^6 electronic configuration with either 0 (LS), 1 (IS) or 2 (HS) electrons in the anti-bonding orbitals. The situation is obviously different for $[Fe(bpy)(CN)_4]^{2-}$. There we clearly see that the equilibrium distance in the IS state is almost the same as in the LS. Instead of a MC triplet, the lowest state corresponds to a metal-to-ligand charge transfer state and no electrons occupy the anti-bonding e_g-like orbital. This explains the nearly equal equilibrium distance. At first sight, the HS state is again a standard metal centred state, given the ~0.2 Å increase of the average Fe-N distance compared to the LS state. But this is in contradiction with the analysis of the wave function that indicates beyond doubt that we are dealing with an MLCT HS state. The Mulliken spin populations indicate three unpaired electrons on Fe and one on the bpy ligand and the largest weight in CI expansion of the wave function lies on a configuration that can be identified as a MLCT configuration.

Table 3.3 Comparison of the average of Fe-N distances [Å] for different spin multiplicities by DFT method with five different functionals with def2-TZVP basis set for $[Fe(bpy)_x(CN)_{6-2x}]^{2x-4}$ system.

	$[Fe(bpy)_3]^{2+}$			**$[Fe(bpy)_2(CN)_2]$**			**$[Fe(bpy)(CN)_4]^{2-}$**		
	LS	**IS**	**HS**	**LS**	**IS**	**HS**	**LS**	**IS**	**HS**
TPSSh	1.99	2.09	2.19	1.97	2.12	2.26	1.95	2.01	2.22
OPBE	1.96	2.09	2.20	1.95	2.10	2.27	1.93	2.00	2.26
B3LYP	2.03	2.13	2.23	2.01	2.20	2.33	1.99	2.04	2.24
PBE0	2.00	2.10	2.20	1.98	2.16	2.30	1.96	2.01	2.21
M062x	2.03	2.13	2.19	2.04	2.23	2.26	2.08	2.03	2.18

From the more detailed analysis of the Fe-ligand distances reported in **Table** 3.5 it can be seen that only two of the six distances suffer a large increment while the others stay much smaller to the values they adopt in the LS state. The two enlarged distances correspond to ligand that are on opposite sides of the Fe ion as

schematically depicted in **Fig.** 3.3. The increase of the Fe-N distance is much larger than in the quintet MC state of $[Fe(bpy)_3]^{2+}$ since now there is only one Fe-N bond that is weakened and hence the bipyridine does not suffer internal tension but can rotate to accommodate the larger Fe-N distance. Hence, on average the increase is about the same as observed for a MC quintet, but this is due to the larger increase in only two of the six Fe-ligand distances.

Table 3.4 The energy differences between the HS and LS states [cm^{-1}] by using five different functionals with def2-TZVP basis sets for $[Fe(bpy)_x(CN)_{6-2x}]^{2x-4}$ system.

	$[Fe(bpy)_3]^{2+}$	$[Fe(bpy)_2(CN)_2]$	$[Fe(bpy)(CN)_4]^{2-}$
	ΔE_{HS-LS}	ΔE_{HS-LS}	ΔE_{HS-LS}
TPSSh	6044	9646	13755
OPBE	4739	11625	14203
B3LYP	899	3306	6801
PBE0	-461	2258	5899
M062x	-8694	-9395	-1775

As TPSSh gives good geometries and reasonable energy differences (as concluded similarly in previous studies,[9] we will use this functional in the remainder of this chapter. We will only use the PBE0 functional to optimize the geometry of the ^{1}MLCT states since the analytical hessian is not available in ORCA for hybrid meta functionals. Despite several attempts, we have not been able to eliminate the numerical noise in the numerical Hessian using this functional. In all occasions we were facing at least one or two imaginary frequencies, making the results useless for calculating the intersystem crossing rates. We opted for PBE0 as this functional gives geometries (not energies) that are close enough to those calculated with TPSSh.

Table 3.5 The Fe-N and Fe-C distances [Å] of the ground state and the lowest quintet state for three complexes by DFT method (TPSSh functional with def2-tzvp basis set).

	$[Fe(bpy)_3]^{2+}$		$[Fe(bpy)_2(CN)_2]$		$[Fe(bpy)(CN)_4]^{2-}$	
	LS	**HS**	**LS**	**HS**	**LS**	**HS**
Fe-N	1.987	2.182	1.987	2.287	1.948	2.315
Fe-N	1.983	2.186	1.955	2.225	1.946	2.093
Fe-N(C)	1.985	2.203	1.985	2.311	1.969	2.009
Fe-N(C)	1.986	2.187	1.953	2.223	1.967	2.012
Fe-N(C)	1.985	2.182	1.925	2.091	1.935	2.194
Fe-N(C)	1.986	2.205	1.923	2.088	1.934	1.976

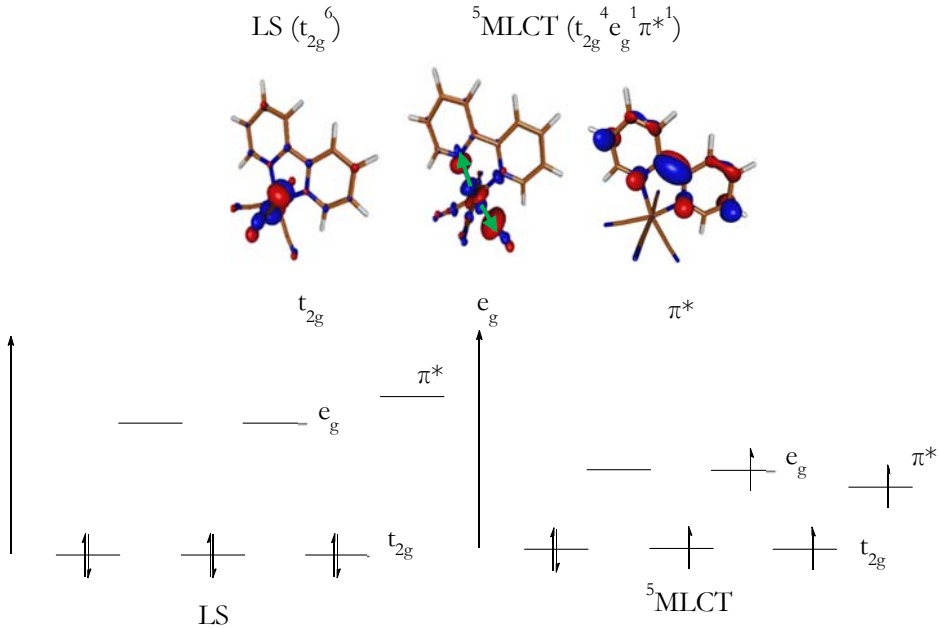

Figure 3.3 *Schematic representation of the one electron occupation causing the enlargement of Fe-N and Fe-C distances (up), t_{2g}, e_g and π^* orbitals; the electronic configurations of the states LS and ^{5}MLCT states (bottom).*

3.2.2.2 The vertical absorption and excitation state optimization

The calculation for vertical excitation energies were starting from the optimized ground state geometries which were performed by DFT method with TPSSh functional. The excited states have been calculated at TD-DFT level, using TPSSh functional and the def2-TZVP basis set for all the atoms. A comparison of the resulting excited state energies reference to ground state is shown in **Table** 3.6. The calculation reproduced the previously calculated vertical energies for $[Fe(bpy)_3]^{2+}$ complex.[2a] The metal-centred (MC) states became higher in energy for the two $[Fe(bpy)_2(CN)_2]$ and $[Fe(bpy)(CN)_4]^{2-}$ complexes. The fact that the ^{3}MC becomes strongly mixed with ^{3}MLCT states makes the ^{3}MC states hard to recognise.

Table 3.6 TD-DFT vertical transition energies [eV] of the lowest electronic states for $[Fe(bpy)_x(CN)_{6-2x}]^{2x-4}$ system with TPSSh functional and def2-TZVP basis set.

state	$[Fe(bpy)_3]^{2+}$	$[Fe(bpy)_2(CN)_2]$	$[Fe(bpy)(CN)_4]^{2-}$
$^1\mathbf{A_1}$	0.00	0.00	0.00
$^1\mathbf{MC}$	2.72	3.05	3.47
$^3\mathbf{T_1}$	1.77	2.13	3.25
$^3\mathbf{T_2}$	2.34	--	--
$^1\mathbf{MLCT}$	2.29	1.59	1.07
$^3\mathbf{MLCT}$	2.09	1.31	0.69
$^5\mathbf{T_2}/^5\mathbf{MLCT}$	2.10	2.69	3.20

However, the metal-to-ligand (MLCT) state became lower and the gap between the ^{1}MLCT and ^{3}MLCT states is nearly the same 0.28 eV in these three complexes. The optimization for triplet and quintet state geometries indicated that ground state of triplet and quintet states still has MC character for $[Fe(bpy)_2(CN)_2]$ (see **Fig.** 3.4), but is MLCT for both triplet and quintet states in $[Fe(bpy)(CN)_4]^{2-}$ complex.

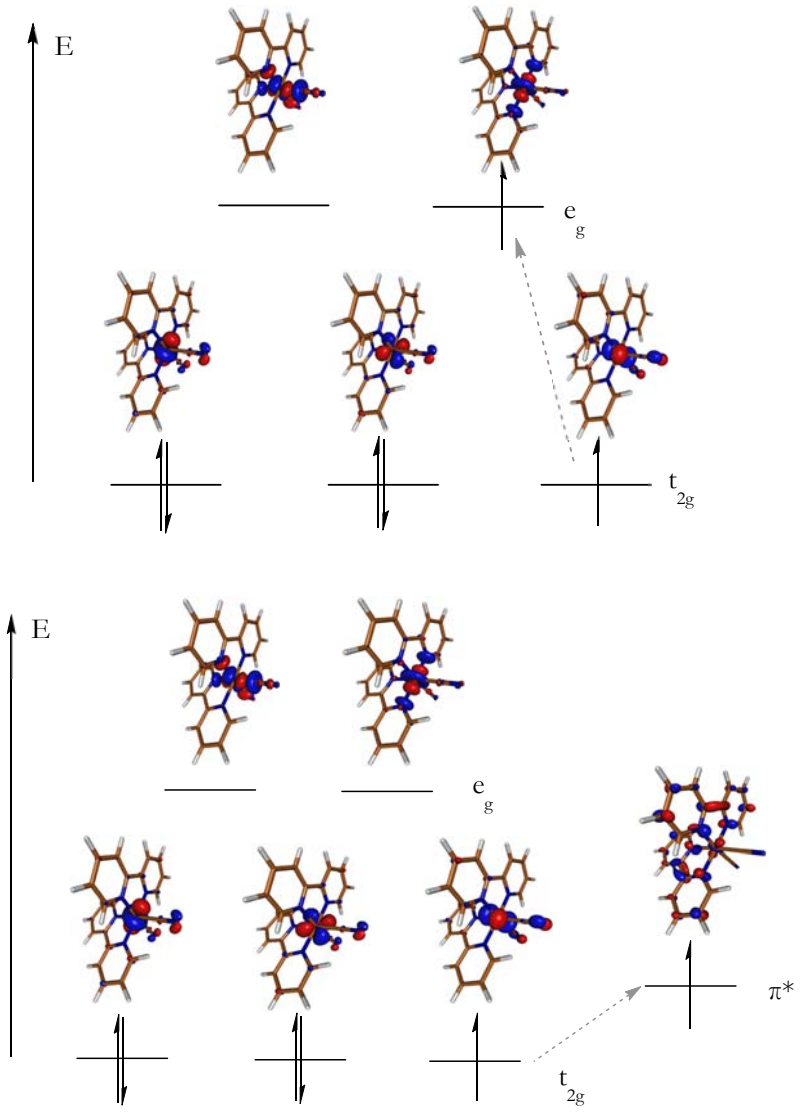

Figure 3.4. *3d orbitals and electronic configuration of the triplet ground state (up) and the lowest vertical excitation state (down) of [Fe(bpy)$_2$(CN)$_2$] complexes.*

The absorption spectrum of the [Fe(bpy)$_2$(CN)$_2$] and [Fe(bpy)(CN)$_4$]$^{2-}$ complexes have been studied by computing the TD-DFT vertical transition energies from the LS equilibrium geometries. The lowest 30 singlet and triplet electronic states have

been studied in gas phase and solvent, respectively. The graphical representation of the absorption spectrum of the complex has been simulated by using Gaussian functions with height proportional to the oscillator strength in each transition and a FWHM (full-width at half maximum) of 20 nm (see **Fig.** 3.5). The upper two graphs in the **Fig.** 3.5 correspond to $[Fe(bpy)_2(CN)_2]$ in gas phase and in methanol (ε=32.613). The solvent was represented with CPCM solvent model.[10] The absorption bands in the region of short wavelengths (300 nm to 460 nm) in the computed spectrum result from the overlap of several transitions, these states include MLCT, LL (CN^- ligand-π to bipyridine ligand-π^*) electron transfer, and states of mixed character. In the region of longer wavelengths (460 nm to 650 nm) pure MLCT absorption bands appear, the most intense at 625 nm. The solvent effect blue-shifts the absorption spectrum. The intense MLCT peak is now centred around 510 nm, in good agreement with the experimental spectrum, which also shows an intense feature in this region and was assigned to a MLCT transition.[11] The peaks in the higher energy range are also shifted by a similar amount, but we also observe a certain redistribution of the intensities among the different absorption peaks. The bottom graph contains the calculated spectra of the $[Fe(bpy)(CN)_4]^{2-}$ complex with and without solvent. As can be seen in **Fig.** 3.5, the absorptions in the short wavelength region around 320 nm to 425 nm are mostly arising from CN^- ligand-π to bipyridine ligand-π^* and metal to bipyridine ligand-π^* transitions, at longer wavelengths there are two MLCT absorption bands, the most intense around 500 nm. Similar solvent effects are observed as in $[Fe(bpy)_2(CN)_2]$. DMSO (ε=46.826) (the solvent used in experiment) blue-shifts the absorption spectrum, the high-energy absorptions appear now around 225 nm to 300 nm, the most intense ones at 235 nm and 275 nm result from CN^- ligand-π to bipyridine ligand-π^* excitations, and the small shoulder appearing at 280 nm is due to MLCT, MC mixed state. The low-energy MLCT absorption bands are shifted to 375 nm and 520 nm, the most intense at 375 nm, coincides with the peak observed in UV-visible difference spectra[6] at 370

nm which was assigned to a MLCT excited state.

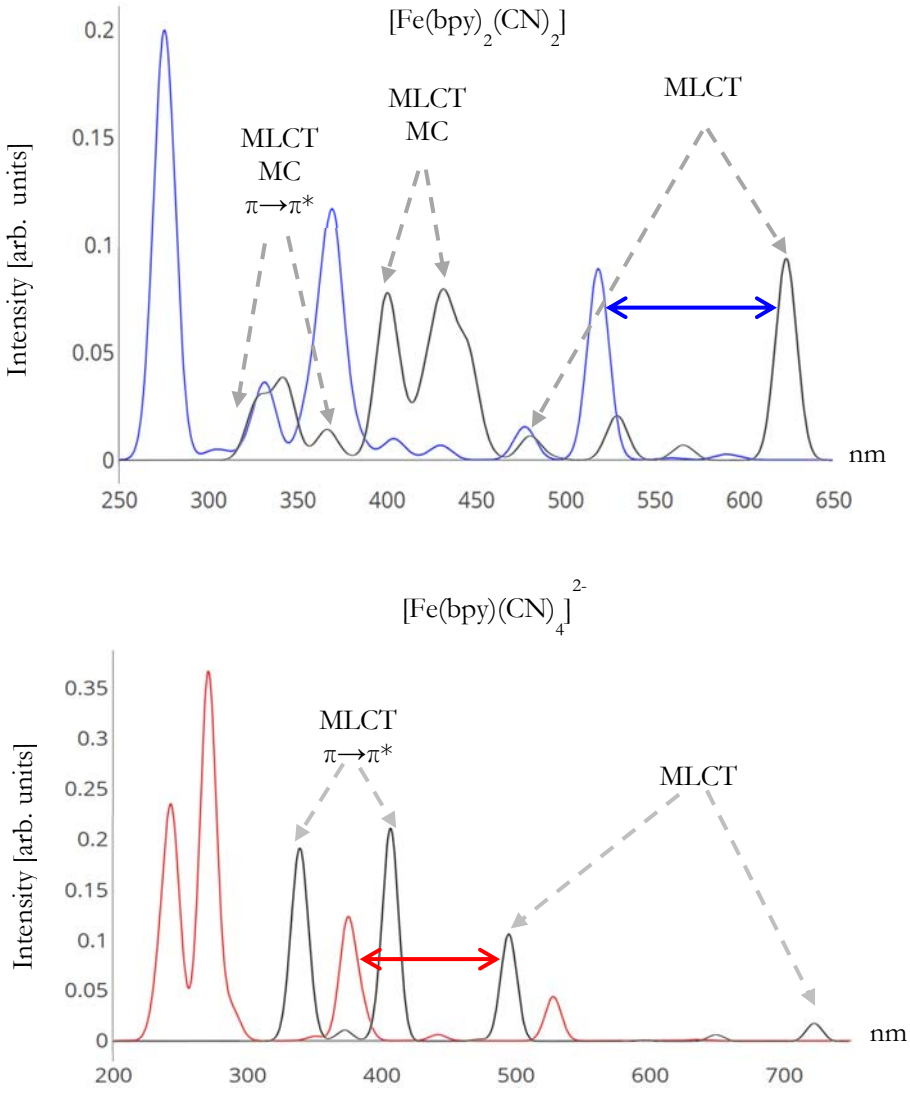

Figure 3.5 *TD-DFT absorption spectrum obtained by adding Gaussian functions to the first 30 singlet transitions for [Fe(bpy)2(CN)2] (top) and [Fe(bpy)(CN)4]2- (bottom). Black lines correspond to the gas phase calculations and the colored lines where obtained with solvent (methanol, blue or DMSO, red).*

In summary, the TD-DFT calculations clearly indicate a tendency of decreasing MLCT energies when bipyridine is replaced with CN^- ligands. The most intense low-

energy peak arising from MLCT transitions changes from 460 nm in $[Fe(bpy)_3]^{2+}$ [12] to 620 nm in $[Fe(bpy)_2(CN)_2]$ and to 725 nm in $[Fe(bpy)(CN)_4]^{2-}$. The same decrease is observed in experimental measurements. Hence, the stronger donating character of CN^- increases the ligand field and the negative charge on the CN^- ligand tends to facilitate the charge transfer from Fe to bipyridine leading to higher-lying MC states and lower MLCT energies.

3.2.2.3 CASPT2 vertical energies and character of the MLCT states.

The vertical excited energies were also calculated with the CASPT2 method as implemented in MOLCAS 8.2 using the ground state OPBE/def2-TZVP optimized geometry. CAS [10, 14] and CAS [10, 13] wave functions need to be employed for $[Fe(bpy)_2(CN)_2]$ and $[Fe(bpy)(CN)_4]^{2-}$ to accurately describe both MC and MLCT states. The active orbitals are depicted in **Fig.** 3.6 and 3.7. The orbitals of the [10, X] active space can be identified as five Fe 3d orbitals, five 3d´ diffuse orbitals that account for the double-shell effect (breathing of the 3d orbitals due to the different radial extension of these orbitals in the $3d^7L^{-1}$, $3d^6$, $3d^5L^1$ electronic configurations), two N σ orbitals that point towards the Fe atoms for a more precise incorporation of the sigma donation, two ligand orbitals of π* character for $[Fe(bpy)_2(CN)_2]$ and one ligand orbital of π* character for $[Fe(bpy)(CN)_4]^{2-}$. The atomic natural orbitals basis set (ANO-RCC) was used for all the atoms. The number of the contracted basis functions is [7s6p5d4f3g2h] for Fe, [4s3p1d] for N and C that coordinate to the metal centre, [3s2p] for other C and [2s] for H.

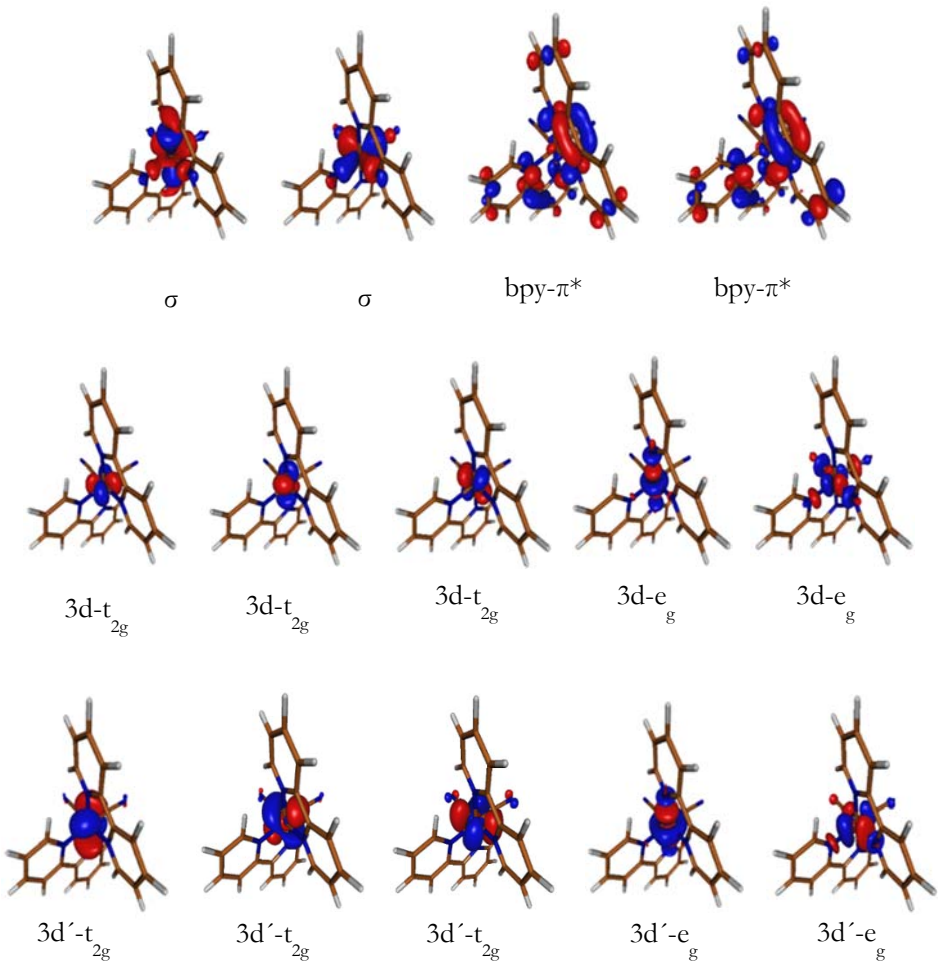

Figure 3.6. *Metal-ligand orbitals included in the [10, 14]-CAS estimation of the vertical excited state energies.*

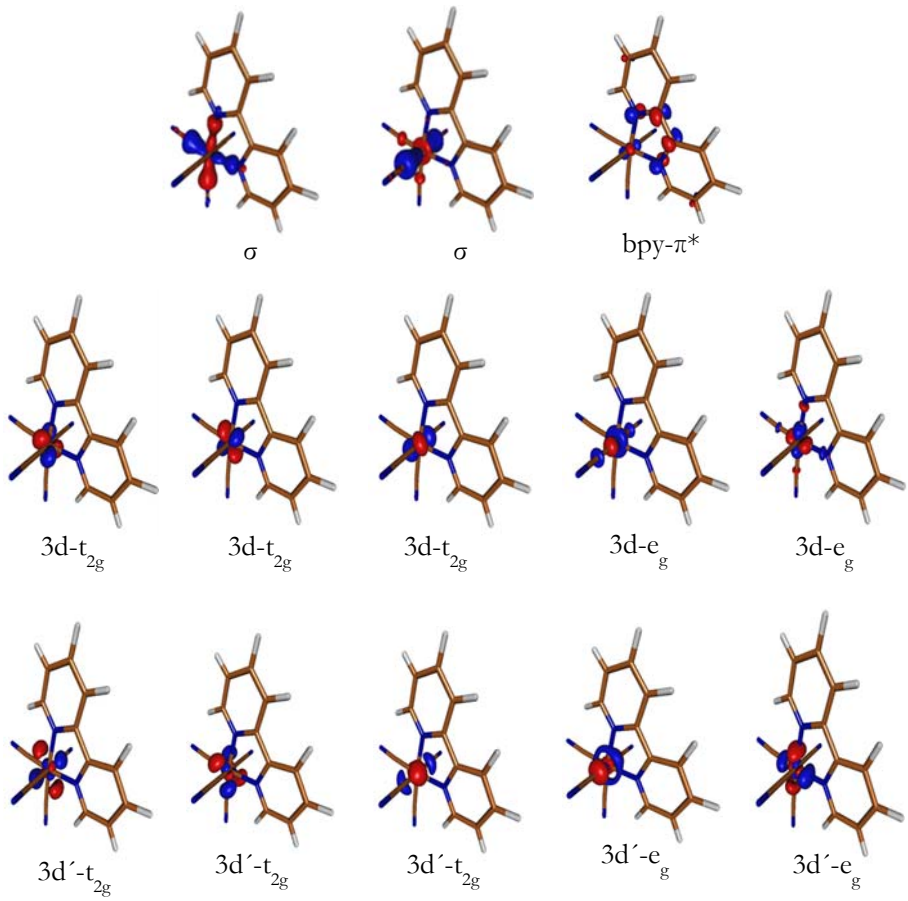

Figure 3.7 *Metal-ligand orbitals included in the [10, 13]-CAS estimation of the vertical excited state energies.*

As can be seen in the **Table** 3.7, the CASPT2 vertical energies are (as expected) different from the TD-DFT ones, but show the same tendencies. The MC states became gradually higher in energy by increasing the number of CN^- ligand from 0 to 2 to 4. The ^{1}MLCT and ^{3}MLCT states indicated opposite trends and became gradually lower in energy with the increasing number of CN^- ligands. In the case of $[Fe(bpy)_2(CN)_2]$, the MLCT and ^{3}MC states are close in energy. The lowest ^{3}MLCT at 2.08 eV has a somewhat higher energy than the lowest ^{1}MLCT at 1.88 eV, different

Table 3.7 CASPT2 vertical excitation energies [eV] for $[Fe(bpy)_3]^{2+}$, $[Fe(bpy)_2(CN)_2]$ and $[Fe(bpy)(CN)_4]^{2-}$ complexes in gas phase.

state	$[Fe(bpy)_3]^{2+}$	$[Fe(bpy)_2(CN)_2]$	$[Fe(bpy)(CN)_4]^{2-}$
GS	0.00	0.00	0.00
^{1}MC	2.23	2.86	3.27
$^3T_1$	1.23	1.60	2.40
$^3T_2$	1.73	1.94	3.55
^{1}MLCT	2.50	1.88	1.21
^{3}MLCT	2.66	2.08	1.29
$^5T_2$/^{5}MLCT	1.74	3.10	3.48

from what was observed in the TD-DFT calculation. The singlet and triplet state have the same electronic configuration (Fe-3d^5 L-π^{*1}), and hence, in a simple reasoning the triplet state is expected to have a slightly lower energy than the singlet due to stabilizing exchange interaction between the two unpaired electrons (as in Hund's rule for atoms). This is indeed what is observed in the TD-DFT calculation but the multiconfigurational results are in contradiction with this reasoning. There is, however, a second mechanism at play. The lowest set of ^{1}MLCT states consists of one A_{1g} and two E_g states in a strictly octahedral symmetry. The symmetry is of course not strictly octahedral here, but still the states maintain approximately the same character. Hence, one of the three low-lying ^{1}MLCT can interact with the ground state, which also has approximate $^1A_{1g}$ symmetry and lower its energy with respect to the lowest ^{3}MLCT state, for which no such interaction exists. This multi configurational effect is most probably not fully accounted for in TD-DFT and explains the discrepancy concerning the relative ordering of singlet and triplet MLCT states. The lowest quintet state has a d^6 electronic configuration (MC) but has a much higher energy than in TD-DFT. In the case of $[Fe(bpy)(CN)_4]^{2-}$, we also observed

strongly mixed ^{3}MC/^{3}MLCT states. The lowest ^{1}MLCT and ^{3}MLCT states are very close in energy. As in TD-DFT the lowest quintet with MLCT character is quite high in energy.

In the outcomes of the CASPT2 vertical excitation states, we observed severely mixed singlet states. **Table** 3.8 lists the natural occupation numbers of the active orbitals of the lowest 6 singlet states. At first sight, the lowest singlet is similar to the standard LS state found in most SCO complexes base on a $Fe^{II}N_6$ core. The electronic structure is completely dominated by the Fe-3d^6 configuration with small contributions from MLCT and $t_{2g}^4e_g^2$ configurations as reflected in the non-zero natural occupations of the active orbitals labelled as bpy-π* and Fe-3d(e_g). Following this reasoning, the next two states are clean MLCT states and state 5 and state 6 are excited MC singlets. However, a problem arises when deciding on the character of singlet 4. The nearly identical natural occupation numbers as those of state 1 leads to the conclusion that it has the same character as the GS, but this is not possible as there can only be one electronic state with a leading Fe-3d (t_{2g}^6) electronic configuration. Hence, the actual shape of the active orbitals should also be taken into account. **Fig**. 3.8 shows the three Fe-3d(t_{2g}) and the bpy-π* active orbitals and it can immediately be seen that one of the orbitals labelled as Fe-3d(t_{2g}) in **Table.** 3.8 is actually a mixture of bpy-π* and Fe-3d(t_{2g}) orbitals. Therefore, both the lowest singlet and singlet 4 are better understood as a mixture of MC and MLCT states.

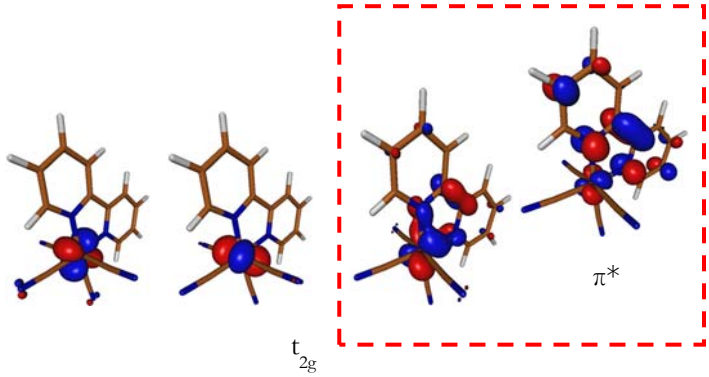

Figure 3.8. *Mixture of MC and MLCT states obtained from the CASPT2 vertical excitation calculation, the occupation number for first two t_{2g} orbitals close to 2, the third one is 1.72, and the π* is 0.26.*

Table 3.8 Natural occupation numbers of the active orbitals of the six lowest singlet states of the $[Fe(bpy)(CN)_4]^{2-}$ complex.

state	σ	3d-(t_{2g})	3d-(e_g)	3d´	π*
1	3.92	5.72	0.10	0.07	0.19
2	3.91	4.91	0.11	0.07	1.00
3	3.92	4.89	0.13	0.07	1.00
4	3.92	5.67	0.12	0.08	0.21
5	3.94	4.78	1.06	0.06	0.16
6	3.94	4.78	1.06	0.06	0.16

3.2.2.4 Intersystem crossing rates

Having analysed the optimal geometries, vertical and adiabatic excitation energies, we now focus on the description of the photocycle of the two modified complexes. The intersystem crossing rate constants, k_{ISC} were calculated with the VIBES program[13] based on Fermi's golden rule. The necessary ingredients include :1) the relative energies of the states involved in the intersystem crossing, 2) a full account

of all vibrational wave functions to calculate the time-dependent correlation function G(t) and the matrix Ω and 3) estimates of spin-orbit (SO) coupling matrix elements. The adiabatic energies and the vibrational information for the lowest state of each multiplicity has already been discussed above, and hence, we only lack the optimal geometry of the excited states and the spin-orbit coupling of all the states. The geometry and frequencies of the lowest ^{1}MLCT state were calculated with TD-DFT as outlined above. In the $[Fe(bpy)_2(CN)_2]$ complex, the ^{3}MLCT state is not the lowest triplet but despite multiple intents, we have not been able to optimize the geometry of this state through TD-DFT because there are several other electronic states close in energy causing changes in ordering of the states, which makes it impossible to follow the ^{3}MLCT during the optimization process.

Following the reasoning used in the previous study of $[Fe(bpy)_3]^{2+}$, we assumed that geometries and frequencies of the ^{3}MLCT are to a very good approximation the same as those of the ^{1}MLCT: both states have the same electronic configuration and the different spin coupling of the two unpaired electrons is not expected to have a major impact on the geometry. The adiabatic energy of the ^{3}MLCT is determined by a single-point TD-DFT calculation at the optimal ^{1}MLCT geometry.

The spin-orbit couplings between the relevant electronic states were calculated as the expectation value of the spin-orbit operator using the CASSCF wave functions. This so-called direct estimate of the SO coupling can be improved by taking into account higher order couplings involving other excited states. It was recently shown that the standard perturbative expression to take into this higher order effects is not very accurate[2b] and instead a variational approach based on the effective Hamiltonian should be used. In the calculation of the effective SO coupling the full interaction space S for both complexes was formed by the nine lowest singlet, nine lowest triplet and five lowest quintet states, a total of 61 eigenfunctions. The model space S_0 for $[Fe(bpy)_2(CN)_2]$ includes the LS ground state, the lowest ^{1,3}MLCT states, the six

triplet MC states and five quintet states giving a total of 48 functions. For $[Fe(bpy)(CN)_4]^{2-}$ S_0 includes the LS ground state, the lowest ^{1}MLCT states, four triplet states (the lowest ^{3}MLCT and three MC states) and one quintet state, leading to 19 functions.

Direct and effective spin-orbit coupling between the spin states that are possibly involved in the deactivation for both complexes are listed in **Table** 3.9 and **Table** 3.10. We only list the maximum values. In the case of $[Fe(bpy)_2(CN)_2]$, the comparison of the direct and effective interaction shows that the spin-orbit coupling between ligand-field states (GS, ^{3}MC and ^{5}MC) is almost not affected by external states, the difference between direct and effective interactions is less than 1 cm^{-1} and a weak effective interaction was observed between the ground state singlet and the ^{5}MC of 3 cm^{-1}. Similar small effects are observed for the interaction between ^{1}MLCT and ligand-field states ^{3}MC and a moderate increased coupling of 19 cm^{-1} was observed for the interaction between ^{1}MLCT and ^{3}MLCT when external states are considered. A moderately decreased coupling was observed for the interaction between ^{3}MLCT and ligand-field states (GS is 15 cm^{-1} and ^{5}MC is 7 cm^{-1}). In the case of the $[Fe(bpy)(CN)_4]^{2-}$ complex, a moderate increase of the coupling was observed for the interaction between GS and ^{3}MLCT by 5 cm^{-1}, ^{1}MLCT and ^{3}MLCT by 2 cm^{-1}, ^{1}MLCT and ^{5}MLCT by 18 cm^{-1}, and a slightly smaller SO coupling was observed at ligand field state GS and ^{3}MC by 3 cm^{-1}. A surprisingly large effective coupling of 125 cm^{-1} was calculated for the ^{5}MLCT and the lowest singlet state.

Table 3.9 Largest direct (H_0^{SO}) and effective (H_{eff}^{SO}) spin-orbit interactions (in cm^{-1}) of the $[Fe(bpy)_2(CN)_2]$ structure among the states that play a role in the photocycle.

Φ_i	Φ_j	H_0^{SO}	H_{eff}^{SO}
^{1}MLCT	**^{3}MLCT**	75.01	94.38
	^{3}MC	45.03	44.61
^{3}MLCT	**GS**	123.52	108.97
	^{5}MC	50.92	44.02
^{3}MC	**GS**	346.58	346.94
	^{5}MC	204.56	205.51
^{5}MC	**GS**	0.00	2.85

Table 3.10 Largest direct (H_0^{SO}) and effective (H_{eff}^{SO}) spin-orbit interactions (in cm^{-1}) of the $[Fe(bpy)(CN)_4]^{2-}$ structure among the states that play a role in the photocycle.

Φ_i	Φ_j	H_0^{SO}	H_{eff}^{SO}
GS	**^{3}MLCT**	134.19	138.82
	^{3}MC	311.33	308.14
	^{5}MLCT	0.00	124.68
^{1}MLCT	**^{3}MLCT**	159.52	161.29
	^{3}MC	15.77	15.98
	^{5}MLCT	0.00	17.95

The next step is to quantify the intersystem crossing rates between these states. **Table** 3.11 and 3.12 reports the inverse of these rates, which can be interpreted as lifetimes of the excited states for both complexes. Apart from the lifetime we also listed the relative energies between these involved states. As reported in **Table** 3.11, the calculated lifetime of the ^{1}MLCT in the decay to the ^{3}MLCT is around 850 fs in

$[Fe(bpy)_2(CN)_2]$, significantly larger than the 200 fs in the parent complex $[Fe(bpy)_3]^{2+}$ caused by the reduction in the SO coupling (200 *vs.* 75 cm^{-1}) and the slightly smaller vibrational overlap ($3.3 \cdot 10^8$ *vs.* $1.4 \cdot 10^8$). The energy difference between ^{1}MLCT (^{3}MLCT) state and ^{3}MC is 0.43 eV (0.23 eV), the decay from ^{1}MLCT to ^{3}MC is reasonably fast 2.40 ps. Being states with the same spin multiplicity, Fermi´s golden rule cannot be used to calculate the timescale of the internal conversion between ^{3}MLCT and ^{3}MC. However, it is assumed to be at least as fast as the ISC between ^{1}MLCT and ^{3}MC. Despite the small energy gap of 0.04 eV between ^{3}MLCT and ^{5}MC state, a very small ISC rate was calculated (lifetime >100 ps) between these two states, the large difference in the average Fe-N distance between ^{3}MLCT and ^{5}MC state makes the vibrational overlap very small and in consequence, the decay from ^{3}MLCT to ^{5}MC less probable. In addition, we also observed almost equal energies for the ^{3}MC and ^{5}MC states and intersystem crossing could take place on a timescale of 15 ps. There is, however, another relaxation path for the ^{3}MC that brings it back to the singlet ground state within 100 fs. So based on the above analyses, we propose the possible decay path for $[Fe(bpy)_2(CN)_2]$ complex.

$$^{1,3}\text{MLCT} \rightarrow {}^3\text{MC} \rightarrow (^5\text{MC}) \rightarrow \text{GS}$$

After initial light irradiation, the system decays by ISC from a ^{1}MLCT state to a ^{3}MLCT of equal character in less than 1 ps. At the same time the ^{1}MLCT can also decay to one of the lower-lying ^{3}MC states. This ISC is, within the uncertainties of Fermi´s golden rule, as efficient as the ^{1}MLCT-^{3}MLCT decay. The ^{3}MC also gets populated by the internal conversion from ^{3}MLCT. From here, the system can either undergo a second ISC and end up in the quintet MC state, similar to what was found in $[Fe(bpy)_3]^{2+}$ or fall back on the singlet GS and return to the initial state. Our computational results favour this last scenario, while experiment has established the existence of a metastable ^{5}MC state, although it is difficult to say with what quantum yield this ^{5}MC is populated. There are several factors in our calculation that may

affect the ISC rates, among which two appear especially relevant. First, the relative energies are calculated with (TD-)DFT in gas phase and although the absorption spectrum was reproduced with reasonable precision, the energies listed in the **Table** 3.11 are subject to a certain degree of uncertainty. The 0.15 eV higher energy of the ^{5}MC with respect to the ^{3}MC actually makes highly improbable the conversion from ^{3}MC to ^{5}MC, but small changes in the relative energy (for example by applying multi-configurational perturbation theory and including solvent effects) could have a substantial influence on the ISC rate. The second point of uncertainty is the rather crude description of the excited state dynamics by Fermi´s golden rule. The calculated ISC rates should be considered only as an indication of the order of magnitude. More precise descriptions can be obtained with explicit time evolutions either by quantum molecular dynamics (QMD) with surface hopping or a full quantum description (not only of the electrons as in QMD, but also of the nuclei) with the multi-configurational time-dependent Hartree (MCTDH) method.

Table 3.11 Intersystem-crossing rates of the involved states of $[Fe(bpy)_2(CN)_2]$. The relative energies, the spin-orbit and vibrational contributions are given separately.

Φ_I	Φ_F	ΔE (eV)	SO term [cm^{-2}]	Vibrational term [cm^2s^{-1}]	k_{ISC}[s^{-1}]	t[ps]
^{1}MLCT	**^{3}MLCT**	0.20	$8.65\cdot10^3$	$1.37\cdot10^8$	$1.18\cdot10^{12}$	0.85
^{1}MLCT	**^{3}MC**	0.43	$5.64\cdot10^3$	$7.4\cdot10^7$	$4.2\cdot10^{11}$	2.4
^{3}MLCT	**^{3}MC**	0.23	--	--	--	--
^{3}MLCT	**^{5}MC**	0.04	$3.37\cdot10^3$	$8.13\cdot10^{-1}$	$2.74\cdot10^3$	>100
^{3}MLCT	**GS**	1.24	$6.05\cdot10^3$	$6.42\cdot10^5$	$3.89\cdot10^9$	257
^{3}MC	**^{5}MC**	-0.19	$4.0\cdot10^4$	$1.82\cdot10^6$	$6.56\cdot10^{10}$	15
^{3}MC	**GS**	1.00	$8.0\cdot10^4$	$1.37\cdot10^8$	$1.1\cdot10^{13}$	0.09
^{5}MC	**GS**	1.20	0	$6.62\cdot10^4$	0	--

In the case of the complex $[Fe(bpy)(CN)_4]^{2-}$ (see **Table** 3.12), ^{3}MC and quintet states, do not take part in the decay relaxation because of their high relative energy. This simplifies the relaxation of the excited state and the only reasonable path corresponds to the ^{1}MLCT→^{3}MLCT→GS decay. The ISC from ^{1}MLCT to ^{3}MLCT takes place on a time scale of around 130 fs, then directly from ^{3}MLCT go back to the nonmagnetic ground state, the overall lifetime approximately 1ps which matched reasonably well with 20 ps at experimental observation.[6]

Table 3.12 Intersystem-crossing rates of the ^{3}MLCT state to other electronic states of $[Fe(bpy)(CN)_4]^{2-}$. The relative energies, the spin-orbit and vibrational contributions are given separately.

Φ_I	Φ_F	ΔE (eV)	SO term [cm^{-2}]	Vibrational term [cm^2s^{-1}]	k_{ISC}[s^{-1}]	t[ps]
^{3}MLCT	**^{1}MLCT**	0.36	$1.73\cdot10^4$	$1.52\cdot10^8$	$7.87\cdot10^{12}$	0.13
^{3}MLCT	**GS**	0.48	$1.24\cdot10^4$	$1.35\cdot10^8$	$1.67\cdot10^{12}$	0.60

3.2.2.5 Reduction potentials for the ground and excited states

Not only the lifetime of the excited ^{3}MLCT state but also the energy that has to be inverted to oxidise the system is an important ingredient to determine the suitability of the modified complexes to serve as replacement for the $[Ru(bpy)_3]^{2+}$.

Eq. 3.1 and 3.2 represent the process of the ground state and the ^{3}MLCT state one electron transfer to acceptor molecule labelled by 'a', respectively.

$$[Fe(bpy)_x(CN)_{6-2x}]^{2x-4}(S=0) + a \rightarrow [Fe(bpy)_x(CN)_{6-2x}]^{(2x-4)+1}(S=1/2) + a^- \quad (3.1)$$

$$[\mathrm{Fe(bpy)_x(CN)_{6-2x}}]^{2x-4}(\mathrm{S}=1)+\mathrm{a} \rightarrow [\mathrm{Fe(bpy)_x(CN)_{6-2x}}]^{(2x-4)+1}\,(\mathrm{S}=1/2)+a^{-} \quad 3.2$$

Where $[Fe(bpy)_x(CN)_{6-2x}]^{2x-4}$ (x=1-3) is written in a general way. And this two equations represent the oxidation process respectively. In our case, the Gibbs free energy associated to the inverse process

$$[\mathrm{Fe(bpy)_x(CN)_{6-2x}}]^{(2x-4)+1}+1e^{-} \rightarrow [\mathrm{Fe(bpy)_x(CN)_{6-2x}}]^{2x-4} \quad 3.3$$

can be used to estimate the reduction potential of the system in ground and excited state.

The redox potential (E in V) and the Gibbs free energy related by the equation as following

$$\Delta G = -nFE \quad 3.4$$

Where F is the Faraday constant, and the n is the number of the electrons in the half-reaction. Using as reference the reduction potential of Normal Hydrogen Electrode (NHE) that has been estimated as 4.43 V[14] we can compare our calculated estimates to the experimental values.

Here, we calculated the reduction potential in gas phase, water and the solvents corresponding to the experiment [1, 6, 11] for example the reduction potentials for $[Fe(bpy)_3]^{2+}$ have been calculated in gas phase and water, $[Fe(bpy)_2(CN)_2]$ have been calculated in gas phase, water and methanol; $[Fe(bpy)(CN)_4]^{2-}$ have been calculated in gas phase, water and DMSO. All the calculation are performed with PBE0 applying a CPCM solvent model. The Gibbs free energy have been calculated from

the numerical frequencies of the ground state and ^{3}MLCT state of $[Fe(bpy)_x(CN)_{6-2x}]^{2x-4}$ and the doublet state $[Fe(bpy)_x(CN)_{6-2x}]^{2x-4}$ optimized geometry.

As the geometry optimization of the lowest ^{1}MLCT (used to calculate the ΔG of the ^{3}MLCT as explained before) in water leads to the dissociation of one of the bpy ligands, we only report the result in gas phase. Our goal in this work is to mimic the $[Ru(bpy)_3]^{2+}$ situation, so we can take the $[Ru(bpy)_3]^{2+}$ reduction potential both in theoretical[15] and experiment[16] in acetonitrile at 298K as reference. As can be seen in **Table** 3.13, the ^{3}MLCT state with negative reduction potential energy indicated that the ^{3}MLCT state releases more easily an electron than ground state. The calculated reduction potentials for the $[Fe(bpy)_3]^{2+}$ indicate that the complex is not easily oxidised, neither in the ground state nor in the MLCT state.

On the other hand, the replacement of one bpy ligand by two CN groups greatly reduces the energy needed to remove one electron from the complex. The reduction potential becomes negative in the MLCT state as was observed for $[Ru(bpy)_3]^{2+}$. Although this seems to validate $[Fe(bpy)_2(CN)_2]$ as substitute of the $[Ru(bpy)_3]^{2+}$, we should not forget that the ^{3}MLCT is very short-lived in this compound. The situation seems more favorable for the $[Fe(bpy)(CN)_4]^{2-}$ complex. The somewhat longer-lived ^{3}MLCT state has a reduction potential that is similar to the one calculated for the Ru complex. The (small) negative value for the ground state indicates that at this level of calculation the complex is not stable and would spontaneously loose an electron, but one has to keep in mind that the calculation of the energies of anions is a rather delicate matter and for a more precise determination of the reduction potential the computational parameters (basis set, solvent model, electronic structure method) should be carefully checked and probably be improved.

Table 3.13 PBE0 computed Gibbs free energy variation (in eV) and reduction potentials (in V) for the ground and ^{3}MLCT states of the studied complexes and the reference $[Ru(bpy)_3]^{2+}$ complex[15].

	$[Fe(bpy)_3]^{2+}$		**$[Ru(bpy)_3]^{2+}$**	
	gas phase		acetonitrile	
	ΔG	*E*	*E*	*E*(exp.)
Doublet+1e$^-$→GS	-7.62	7.62	1.07	1.29
Doublet+1e$^-$→^{3}MLCT	-4.86	4.86	-0.84	-0.81

$[Fe(bpy)_2(CN)_2]$			
	gas phase	methanol	water
	E	*E*	*E*
Doublet+1e$^-$→GS	1.46	0.36	0.32
Doublet+1e$^-$→^{3}MLCT	-0.27	-1.17	-1.19

$[Fe(bpy)(CN)_4]^{2-}$			
	gas phase	DMSO	water
	E	*E*	*E*
Doublet+1e$^-$→GS	-5.12	-0.16	-0.09
Doublet+1e$^-$→^{3}MLCT	-5.09	-1.30	-1.27

3.3 Increasing the π-conjugation system

A second strategy to alternate the MC and MLCT state is to increase the π-conjugation on the ligand directly lowering the MLCT state. In general, the increased π-conjugation system will lower the overall energy and increases stability of the system. Here we choose six isolated π-conjugation ligands (a) pyridine, (b) bipyridine, (c) terpyridine, (d) phenantroline, (e) 2-(2-pyridyl)-1,10-phenanathroline, (f)

dipyrido-[4,3-b;5,6-b] acridine which have the increased tendency of π-conjugation systems (see **Fig.**3.9). The geometries of all isolated ligands were optimized by OPBE functional with def2-tzvp basis set and the energy calculation of the lowest π*-orbital ε was carried out by TPSSh functional with the same basis set, the obtained energies have the tendency that

$$\varepsilon_a > \varepsilon_b \approx \varepsilon_c \approx \varepsilon_d > \varepsilon_e > \varepsilon_f$$

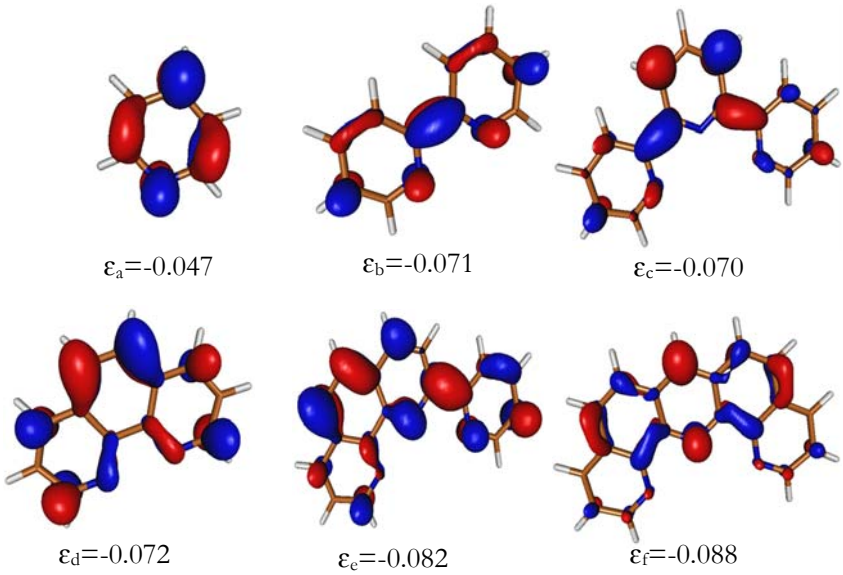

Figure.3.9 *Lowest lying unoccupied π-orbital of the six ligands (isosurface=0.05e⁻/Å²) and orbital energy in Eh.*

Not unexpected, the smallest ligand (a) gives the highest orbital energy of π*-orbitals (-0.047 Eh). The isolated ligands (b), (c) and (d) have very similar π*-orbital energies of -0.071 Eh, -0.070 Eh and -0.072Eh, respectively. The last two isolated ligands (e) and (f) with larger π-conjugation system have the lowest energies -0.082 Eh and -0.088 Eh, respectively. Obviously, we found that the lowest π*-orbital energies significantly decrease by the enlarged π-conjugation system. Therefore, we supposed

that the energies of lowest charge transfer states of the Fe(II) complexes (see **Fig.**3.10) with the above six ligands should have the same tendency.

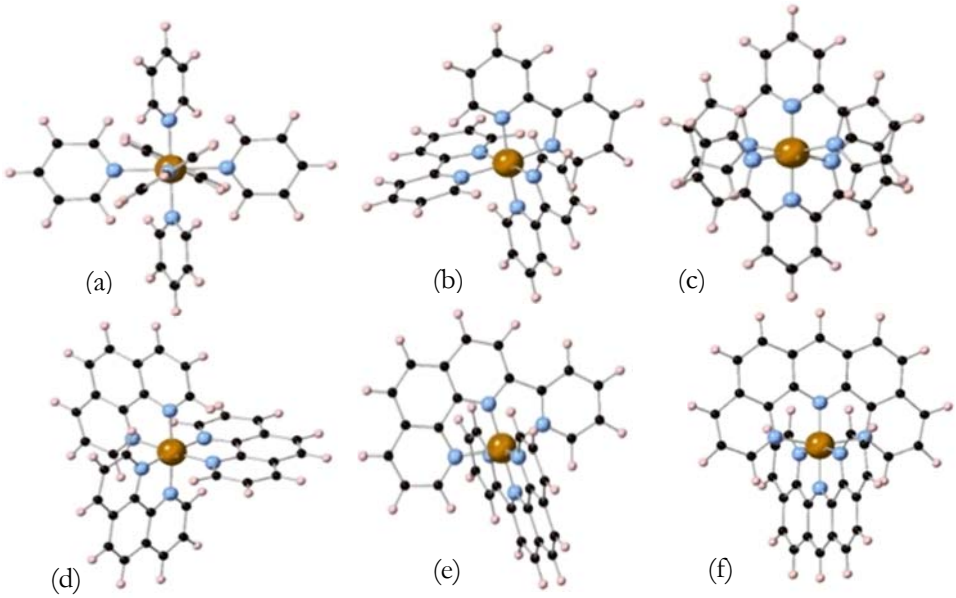

Figure 3.10 *The six complexes with increasing π-conjugation on the ligand. (a)*$[Fe(py)_6]^{2+}$*, (b)*$[Fe(bpy)_3]^{2+}$*, (c)*$[Fe(terpy)_2]^{2+}$*, (d)*$[Fe(phen)_3]^{2+}$*, (e)*$[Fe(bphen)_2]^{2+}$*, (f)*$[Fe(acridine)_2]^{2+}$*. py = pyridine; bpy = 2,2´-bipyridine; terpy = 2,2´:6´,2´´-terpyridine; phen = 1,10-phenantroline; bphen = 2-(2-pyridyl)-1,10-phenanathroline; acridine = dipyrido-[4,3-b;5,6-b] acridine.*

In the next step, the vertical excitation energies were calculated as the preliminary prediction discussed in section 3.2 to compare the relative energies of MLCT and MC states of these complexes. The same functional OPBE with def2-TZVP basis set has been used for geometry optimization and TPSSh functional was used for vertical excitation energies. **Table** 3.14 lists the lowest excited states energies of these six complexes. As can be seen in **Table** 3.14, the ^{3}MC states lie at lower energy respect to the ^{3}MLCT states in all cases except $[Fe(terpy)_2]^{2+}$ ^{3}MLCT and ^{3}MC are nearly degenerate. The influence of the enlargement of the π-conjugation system on the ^{3}MLCT states can be summarized as follows

$$E_a > E_d > E_b > E_c > E_e > E_f$$

which approximately the tendency of the lowest energies of the π*-orbital on isolated ligands. Complex (a) has the highest MLCT states both for singlet and triplet, and the lowest MC states. The lowering of the relative energy of the ^{3}MC state is in line with the fact that pyridine is a weaker sigma donor than bipyridine, and as a matter of fact, the relative energy of the ^{3}MC state of 1.11 eV is right in between the relative energy of 1.92 eV calculated for the ^{3}MC state in $[Fe(bpy)_3]^{2+}$ (stronger sigma donor) and the 0.54 eV calculated for $[Fe(H_2O)_6]^{2+}$, an Fe(II) complex with a very weak sigma donating ligand. The relatively high MLCT energy and the low MC transition energy leads to a 1.70 eV gap between these two states, the largest observed in the series. The group of complexes with the bidentate bipyridine and phenantroline ligands and the tridentate terpyridine ligand (all three with approximately the same orbital energy for the lowest unoccupied ligand π-orbital) have significantly lower MLCT energies. Actually the vertical excitation energy is very close to the ^{3}MC energy, but one should keep in mind that the geometry relaxation of the MC state has a much larger stabilizing effect than in the MLCT state (the optimal geometry of the MLCT state is nearly identical to the one of the ground state, while the Fe-ligand distance is significantly larger in the ^{3}MC state). Therefore, these complexes do not fulfil the requirement of inversion of MLCT and MC states as observed in $[Ru(bpy)_3]^{2+}$. The two complexes with the largest conjugated π system (complexes e and f) have indeed the lowest MLCT transition energies, 0.2 eV lower than in the complexes b, c and d, but unfortunately, these larger ligands turn out to be weaker sigma donors, and hence, also give rise to a lowering in the MC excitation energy. In conclusion, enlarging the π-conjugation on the ligand does indeed lower the MLCT energy but does not lead to the desired stability inversion of MC and MLCT states.

Table 3.14. TD-DFT vertical energies [eV] of the low-lying electronic states of studied systems.

names	^{1}MLCT	^{3}MLCT	^{3}MC	^{1}MC
a	2.96	2.81	1.11	2.02
b	2.26	2.08	1.92	2.88
c	2.29	1.98	1.99	2.76
d	2.35	2.11	1.93	2.81
e	2.18	1.88	1.80	2.61
f	2.15	1.74	1.54	2.37

3.4 Computational study of the methyl substituted $[Ru(bpy)_3]^{2+}$ complexes

The photochemistry properties of Ru(II) polypyridyl complexes have been studied for a long time, because they are fairly easily oxidized in the excited state and therefore can play a role in photoinduced electron and energy transfer reactions. This makes the Ru(II) complex a good electron donor for real world application. The photocycle mechanism of the Ru(II) complexes have been discussed in many publications. Essential for the possibility of electron transfer to an acceptor is the existence of a long-living ^{3}MLCT state at lower energy than the ^{3}MC state. It has been proven that addition of the methyl groups on the outside of the bipyridine ligands have an important impact on the relative energies of the excited states and it can make the ^{3}MC state comparable or even lower in energy than the ^{3}MLCT state, opening the path to the initial closed-shell $4d^6$ singlet state via the triplet ligand field states as occurs in the corresponding Fe(II) complex. The description of the deactivation from the vertically excited ^{1}MLCT state via ISC to the relaxed ^{3}MLCT

is an central issue of the Ru(II) polypyridyl complexes. It is supposed to take place on a very short time scale, and depending on the spectroscopic technique, estimates have been obtained in the range of 100-300, 40±15 or 15±10 fs. The ISC rate is determined to a large extent by the spin-orbit coupling between singlet and triplet states, but it has been shown that this is not the only determining factor and structural feature are also expected to play an important role. The lowest ^{3}MC state lie at 0.5 eV slightly higher than the ^{3}MLCT state. They are not expected to play a role in the deactivation of the initially excited ^{1}MLCT state but have been invoked to explain the thermally assisted quenching of the luminescence. By adding the methyl groups on the outside of the bipyridine ligands has been shown to affect the ligand field exerted by the ligands in such a way that the ^{3}MC states become more stable than the ^{3}MLCT state. This completely eliminates the luminescence signal ascribed to a fast ^{3}MLCT to ^{3}MC internal conversion followed by an ISC with the initial closed-shell $4d^6$ singlet.

This work concentrates on the ab initio calculation the methyl substitution on different positions of the bipyridine ligand (see **Fig.**3.11) of the $[Ru(bpy)_3]^{2+}$ complexes. We provide a detailed theoretical explanation of the changes in the electronic structure of the different substitutions by investigating the changes of the average distance of the Ru-N, the absorption spectrum and the distorted dihedral angle.

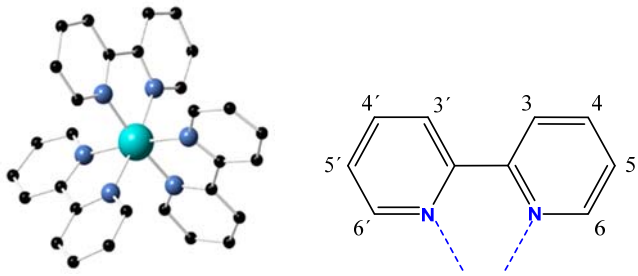

Figure 3.11 *Schematic of $[Ru(bpy)_3]^{2+}$ complex (left). The middle large green sphere is Ru; the smaller blue spheres are N; and dark spheres represent C and H atoms not show here. The enumeration of the substitution sites of the bipyridine ligand are shown on the right.*

3.4.1 Geometry optimization

The structures of methyl group(s) substituted complexes includes: one methyl group on the 5 or 6 position; two methyl groups on the 5, 5´ or 6, 6´ positions; and four methyl groups on the 3, 3´, 5, 5´ or 4, 4´, 6, 6´ positions as illustrated in **Fig.** 3.11 (right). The geometries optimization have been done with DFT using different functionals PBE0, TPSSh, B3LYP and OPBE with def2-TZVP basis set for all the atoms, the dispersion interactions are included through the D3 correction in all calculations. The calculations were performed in ORCA 4.0.

The average Ru-N distance calculated with the different functionals are collected in **Table** 3.15 with available experimental data in parentheses. While PBE0 and TPSSh the optimized distances of 2.055 Å and 2.059Å are in good agreement with the experimental distance of 2.056Å for $[Ru(bpy)_3]^{2+}$, the average distance of 2.075 Å produced by the functional B3LYP indicates an overestimation and the 2.010 Å obtained by the functional OPBE an underestimation of the experimental value. The same tendency appeared in the 5´-Me, 6-Me, 6, 6´-Me complexes. Analysing the remaining complexes with no experimental data the same tendency can be expected, apparently.

In all of these cases, we concluded that the functionals PBE0 and TPSSh can reproduce the geometries in good agreement with experiment. For those complexes without experimental data, we expect that these two functionals also produce rather accurate geometries.

Table 3.15. The Ru-N average distance [Å] obtained by different functionals, and the experimental Ru-N distance is given in parentheses.

	Ru-N distance (exp.)			
Complexes	**PBE0**	**TPSSh**	**B3LYP**	**OPBE**
$[Ru(bpy)_3]^{2+}$	2.055 (2.056)	2.059	2.075	2.010
5-Me	2.056 (2.059)	2.059	2.076	2.009
5,5´-Me	2.056	2.058	2.076	2.009
3,3´,5,5´-Me	2.064	2.064	2.085	2.011
6-Me	2.090 (2.091)	2.087	2.111	2.028
6,6´-Me	2.120 (2.117)	2.118	2.144	2.050
4,4´,6,6´-Me	2.121	2.110	2.151	2.049

In addition, we also observed that the methyl substitution on the 6 position leads to important steric hindrance and causes an expansion of the first coordination sphere of the Ru ion. Taking into account the changes of the dihedral angle shifted around ±10° will not affect the properties of the structure. In the 6-Me complex, the bipyridine ligands stay nearly flat, but in the 6,6´-Me and 4,4´,6,6´-Me, the expansion is accompanied by a significant rotation of the two pyridine rings around the central C-C bond. The two rings have a dihedral angle of the approximately 21° (see **Table** 3.16). The substitutions on the 5 position do not cause important changes in the geometry, except for the 3, 3´, 5, 5-Me case. The closeness of the methyl groups on the 3 and 3´ position induce large distortions of the two pyridine rings to release the

steric hindrance; the dihedral angles along the C-C bond that connects the two rings is 27° for NCCN and 39° for $C_3CCC_{3'}$.

Table 3.16. Comparison of the dihedral angles (degree) along the C-C bond.

	N-C-C-N			**C_3-C-C-$C_{3'}$**		
$[Ru(bpy)_3]^{2+}$	0.3	-1.3	5.4	-0.3	-2.3	6.1
5-Me	-0.4	7	7.7	-1.7	9.0	9.5
5,5′-Me	1.9	4.1	6.8	1.8	5	8.1
3,3′,5,5′-Me	27.4	-25.8	-27	38.0	-38.3	-39.6
6-Me	12.0	4.4	5.9	12.2	2.9	5.6
6,6′-Me	17.5	17.6	27.5	17.1	17.1	26.6
4,4′,6,6′-Me	22.8	20.5	34.3	27.0	22.5	38.0

3.4.2 TD-DFT absorption spectrum

The relative energy of the lowest 50 singlet and 50 triplet excited states have been estimated with TD-DFT for all the optimized geometries comparing the different functionals listed in the **Table** 3.17. The absorption spectrum of $[Ru(bpy)_3]^{2+}$ in experiment is dominated by two peaks with their maximum around 2.7 eV (455 nm) and 4.3 eV (285 nm), respectively. The low energy peak is generally attributed to MLCT transitions, while the higher energy involves different excitations such as MC transitions and LL (bipyridine-ππ*) transitions. By analysing the character of the states that contribute to the absorption bands listed in the **Table** 3.17, the lower energy bands could indeed be confirmed to arise from MLCT transitions, and the higher energy band involves the ligand-π to ligand-π* electron transitions (LL), metal-centred electron transitions (MC) and also in some cases metal-to-ligand electron transitions (MLCT). The OPBE functional provided good results with the

Table 3.17 Functional dependence (gas phase) of the TD-DFT absorption band maxima and solvent effect (acetonitrile) by PBE0 functional [eV].

Absorption bands					
	Gas phase				acetonitrile
Complexes	**PBE0**	**TPSSh**	**B3LYP**	**OPBE**	**PBE0**
$[Ru(bpy)_3]^{2+}$	3.1/4.9	2.8/4.7	2.9/4.8	2.6/4.5	3.0/4.9
5-Me	3.1/4.8	2.9/4.6	3.0/4.7	2.7/4.4	3.1/4.8
5,5´-Me	3.2/4.7	2.9/4.5	3.0/4.6	2.7/4.3	3.1/4.7
3,3´,5,5´-Me	3.1/4.6	2.8/4.3	2.9/4.5	2.2/4.1	3.0/4.6
6-Me	3.1/4.7	2.8/4.5	2.9/4.6	2.3/4.2	3.1/4.7
6,6´-Me	3.1/4.7	2.8/4.3	2.9/4.5	2.3/4.2	3.1/4.7
4,4´,6,6´-Me	3.1/4.7	2.8/4.3	2.9/4.5	2.3/4.0	2.9/4.7

absorption maximum of the lower energy band around 2.6 eV and the higher energy band around 4.3 eV for $[Ru(bpy)_3]^{2+}$ in good agreement with experiment data. The PBE0 (3.1 eV/4.9 eV), TPSSh (2.8 eV/4.7 eV) and B3LYP (2.9 eV/4.8 eV) provided the energies that are higher than the experimental ones. In the case of PBE0 and B3LYP, the absorption band maxima are similar for all the substituted complexes both in the lower energy band and in the higher energy band. This apparently means that adding methyl groups does not significantly affect the relative energies of the MLCT states. We observe a rather similar behaviour for the TPSSh functional. The lower energy absorption band presented an energy close to 2.8 eV for all substitutions but the higher energy absorption band is slightly lower in the case of the 3,3´,5,5´-Me (4.3 eV), 6,6´-Me (4.3 eV) and 4,4´,6,6´-Me (4.3 eV) substitutions. The OPBE functional predicts smaller relative energies for the states in the lower energy band for the 3,3´,5,5´-Me (2.2 eV), 6-Me (2.3 eV), 6,6´-Me (2.3 eV) and

4,4´,6,6´-Me (2.3 eV) substitutions, which shows that at least some of the MLCT excited state became lower by the effect of the methyl groups.

Considering that the best geometry is obtained by PBE0, this functional is used to estimate the solvent effects in acetonitrile with the conductor-like polarizable continuum model (CPCM model) for all the complexes. Comparing gas phase and CPCM results, we do not observe relevant changes in the band maxima.

3.4.3 TD-DFT lowest excited state

The discussion of the absorption spectrum in the previous section only provides a contour for the excitation transition, especially the higher energy absorption band is composed of multiple transitions, which make it difficult to exactly determine the evolution of the lowest MC and MLCT states in the different substituted complexes. For a more detailed inspection of the excited states that play a role in the photochemistry of the Ru polypyridyl complexes, we will now focus on the relative energies of the lowest singlet and triplet states of the MLCT and MC character and compare them for different compounds with different functionals. **Table** 3.18 lists the TD-DFT estimates of the lowest transition energies with the PBE0, TPSSh, B3LYP, OPBE and calculated by CASPT2 (in parentheses, taken from ref[17]). It is clear that the electronic transitions from the GS into the MLCT states are not affected by the substitutions on the bipyridine(s) although different functionals provided different excitation energies for same complex. As can be seen in **Table** 3.18, the OPBE functional produced lower energies for MLCT excitation and higher energies for MC excitation comparing with other three functionals and the CASPT2 results.

Because the addition of methyl groups on 6, 6,6´ and 4,4´,6,6´positions causes an enlargement of the Ru-N bond distance, a significant lowering of the MC excitation energies is observed induced by the weaker ligand field, making it less unfavourable

to transfer electrons from the non-bonding t_{2g} to anti-bonding e_g Ru-4d. In the 4, 4´-6, 6´-Me substituted complex the lowest ^{1}MC state appears heavily mixed with a collection of ^{1}MLCT. Instead of one clearly recognisable ^{1}MC state there is a whole

Table 3.18 TD-DFT and CASPT2 (in parentheses) excitation energies [eV] of the lowest MC and MLCT states.

	TD-DFT (PBE0/TPSSh/B3LYP/OPBE)			
	^{1}MC	**^{3}MC**	**^{1}MLCT**	**^{3}MLCT**
$[Ru(bpy)_3]^{2+}$	4.37/4.41/ 4.05/4.73/ (4.32)	3.59/3.78/ 3.48/4.18/ (3.76)	2.73/2.33/ 2.56/1.92/ (2.82)	2.56/2.23/ 2.42/1.85/ (2.92)
5-Me	4.40/4.44/ 4.06/4.72/ (4.30)	3.58/3.78/ 3.48/4.18/ (3.76)	2.69/2.35/ 2.54/1.93/ (2.81)	2.51/2.23/ 2.39/1.86/ (2.91)
5,5´-Me	4.39/4.42/ 4.10/4.72/ (4.36)	3.55/3.79/ 3.48/4.19/ (3.80)	2.70/2.35/ 2.54/1.94/ (2.82)	2.51/2.23/ 2.38/1.87/ (2.92)
3,3´5,5´-Me	4.81/4.33/ 4.16/4.90/ (4.29)	3.73/4.01/ 3.66/4.22/ (3.85)	2.67/2.29/ 2.50/1.89/ (2.67)	2.45/2.14/ 2.32/1.79/ (2.62)
6-Me	3.73/4.11/ 3.69/4.31/ (4.07)	3.12/3.82/ 3.02/3.91/ (3.48)	2.67/2.29/ 2.50/1.87/ (2.88)	2.45/2.13/ 2.32/1.79/ (2.85)
6,6´-Me	3.63/4.04/ 3.45/3.95/ (3.61)	3.37/3.53/ 3.06/3.61/ (2.54)	2.73/2.38/ 2.56/1.81/ (2.59)	2.49/2.23/ 2.38/1.75/ (2.89)
4,4´,6,6´-Me	4.82/3.96/ 3.27/3.91/ (3.51)	3.51/3.69/ 2.99/3.58/ (2.42)	2.66/2.26/ 2.51/1.81/ (2.47)	2.38/2.17/ 2.26/1.75/ (2.74)

series of states with contributions from the t_{2g}-e_g transitions lying in an interval between 3.64 and 3.98 eV, which is in the same energy region as the lowest ^{1}MC states in the 6-Me and 6,6´-Me substituted complexes. The distorted geometry of the bipyridine groups in the 3, 3´, 5, 5´-Me complex leads to small changes in the relative energies of all excited states. Despite the lowering of the relative energies of the MC states by approximately 0.4-0.7 eV, when the bipyridine is substituted at the 6, 6´-position, there is no inversion in the relative stability of the MLCT and MC states, the lowest excited states are still of MLCT character. However this picture changes for CASPT2 which have shown more stable ^{3}MC states when the substitution takes place at the 6, 6´ position and 4, 4´, 6, 6´ position, where the ^{3}MLCT state lies 0.4 eV higher than the ^{3}MC states. Again, we also performed the calculations using a solvent CPCM model for acetonitrile (ε= 36.6). From the comparison (only done with the PBE0 functional, see **Table** 3.19), we see that solvent effect hardly affected the relative energies for all the lowest excited states.

Table 3.19 TD-DFT excitation energies [eV] of the lowest MC and MLCT states in gas phase and solvent.

gas phase and acetonitrile TD-DFT (PBE0/def2-TZVP)				
	^{1}MC	**^{3}MC**	**^{1}MLCT**	**^{3}MLCT**
$[Ru(bpy)_3]^{2+}$	4.37 (4.29)	3.59 (3.64)	2.73 (2.58)	2.56 (2.54)
5-Me	4.40 (4.28)	3.58 (3.62)	2.69 (2.59)	2.51 (2.49)
5,5´-Me	4.39 (4.44)	3.55 (3.63)	2.70 (2.61)	2.51 (2.48)
3,3´,5,5´-Me	4.81 (4.84)	3.73 (3.91)	2.67 (2.63)	2.45 (2.44)
6-Me	3.73 (3.88)	3.12 (3.16)	2.67 (2.55)	2.45 (2.45)
6,6´-Me	3.63 (3.64)	3.37 (3.39)	2.73 (2.67)	2.49 (2.50)
4,4´,6,6´-Me	3.64-3.98 (3.46-3.61)	3.51 (3.47)	2.66 (2.61)	2.38 (2.39)

3.5 Conclusions

The present chapter provides a detailed theoretical studies of ligand modification in Fe(II) and Ru(II) complexes. The first part of this work mainly focused on the modifications of the FeN_6 core system based on the parent $[Fe(bpy)_3]^{2+}$ complex. We have introduced stronger σ-donating ligands to make the ^{3}MC states unstable relative to the ^{3}MLCT state. The comparison of vertical energies was used to have a fast first impression of the relative stability of the two states and led to the conclusion that replacing N coordinating ligands with P-coordinating ligands does not give the desired effect of destabilization of the MC states. On the contrary, CN^- replacements do definitely provide a stronger ligand field pushing the MC state up in energy to become higher than the MLCT state in the ground state geometry. However, the calculation of the adiabatic energies showed that the ^{3}MC state is still the lowest triplet state in $[Fe(bpy)_2(CN)_2]$, but it became ^{3}MLCT state in $[Fe(bpy)(CN)_4]^{2-}$, which indicates that the four CN^- ligands provide a strong enough ligand-field to push the ^{3}MC to a higher energy, resulting in a more stable ^{3}MLCT state. The comparison of the Fe-N distance by different functional showed that the TPSSh and PBE0 can produce the results in good agreement with experiment. The vertical absorption spectrum has been computed with TD-DFT for two complexes $[Fe(bpy)_2(CN)_2]$ and $[Fe(bpy)(CN)_4]^{2-}$ in gas phase and also in solvent, a significant blue-shift appeared in the solvent calculation bringing calculation and experiment in good agreement. The lifetime calculation for the $[Fe(bpy)_2(CN)_2]$ complex indicates that the ^{5}MC state is populated in approximately 18 ps after the transition from the GS to the ^{1}MLCT state, while there is experimental evidence that this process takes place on a sub-picosecond time scale (~200fs). Several reasons can be given for this mismatch, among which the DFT adiabatic energies and the approximate nature of Fermi´s golden rule to describe excited state dynamics are the most important, $[Fe(bpy)(CN)_4]^{2-}$ results matched the experiment better: after the initial excitation the

system gets trapped in the ^{3}MLCT and there is no possibility for further decay into the ^{5}MC state. The reduction potential calculation states that the electron transfer to acceptor molecules is favoured in ^{3}MLCT state as we expected for $[Fe(bpy)_2(CN)_2]$ complex but unfortunately, our calculations indicate that also the ground state of $[Fe(bpy)(CN)_4]^{2-}$ is unstable against oxidation when solvent effects are taken into account.

The second part of this work mainly paid attention to the study of the structure and excited states properties of adding methyl groups on the outside of the $[Ru(bpy)_3]^{2+}$ complex ligands in different positions with various methyl groups. Different functionals were used to optimize the geometries of a series of substituted complexes and the results close to experiment were obtained with the TPSSh and PBE0 functionals. The calculation of the TD-DFT vertical absorption spectrum showed that the lower absorption band is due to MLCT transitions. And that the higher energy band is composed of transitions of multiple character. The comparison of the lowest MC and MLCT states was performed by TD-DFT and CASPT2 methods and showed that the energy of the lowest MLCT state is not affected by the methyl substitutions, whereas the lowest MC state is significantly stabilized in the 6-Me, 6, 6´-Me, substituted complexes and becomes strongly mixed with MLCT states in the 4, 4´,6, 6´-Me complex. The TD-DFT calculation have not provided any clear proof that the relative stability of MLCT and MC states is inversed, but the CASPT2 calculations showed that the lowest MC is more stable than the lowest MLCT state in the 6, 6-Me and 4, 4´, 6, 6´-Me complexes.

3.6 Future work

The present chapter provides theoretical evidence for the influence of ligand modification on the relative energies of the excited states of three Fe(II) complexes. The strategies used in this work one is to replace the bipyridine ligand by a stronger

σ-donating ligand, which can push the Fe-3d(e_g) orbitals higher in energy and invert the relative stability of MLCT and MC states; another one is to lower the energy of the MLCT states directly by applying larger π-conjugation systems which also included in this work. Both strategies are effective to change the relative energies of the ^{3}MC and ^{3}MLCT states. But in neither approach the effect is strong enough to completely convert the ^{3}MC and ^{3}MLCT states and hence, it seems an interesting option to combine the two effects and use a ligand with a large π system and coordinating to Fe via a less electronegative atom than N. So far, all the adiabatic energies calculation were performed in gas phase by DFT and TD-DFT method, this totally neglected the distortions due to thermal motion and the effect caused by the environment. The calculation of the ISC rates with Fermi´s golden rule lacks non-adiabatic effects and can provide approximate results only. For further improvement of the theoretical description of the excited state, dynamics, a more precise computational method have to been used for the calculation of the adiabatic energies. CASPT2 energies with a partial reoptimization of the geometry at this level seems to be the most optimal way in terms of the efficiency versus accuracy. The description of the excited state dynamics in itself can be improved by a time evolution of the nuclei through molecular dynamics combined with surface hopping in which the electronic state is allowed to change under the influence of the nuclear movement. Otherwise, a full quantum treatment can be obtained by the multiconfigurational time dependent Hartree (MCTDH) method, which is currently under study in our group.

References

[1] W. Zhang, R. A. Mori, U. Bergmann, C. Bressler, M. Chollet, A. Galler, W. Gawelda, R. G. Hadt, R. W. Hartsock, T. Kroll, K. S.Kjær, K. Kubicek, H. T. Lemke, H. Liang, D. A. Meyer, M. M. Nielsen, C. Purser, J. S. Robinson, E. I. Solomon, Z. Sun, D. Sokaras, T. B. van Driel, G. Vankó, T. Weng, D. Zhu and K. J. Gaffney, *nature* **2014**, *509*, 345–348.

[2] a) C. Sousa, C. de Graaf, A. Rudavskyi, R. Broer, J. Tatchen, M. Etinski and C. M. Marian, *Chem. Eur. J.* **2013**, *19*, 17541 – 17551; b) C. Sousa, A. Domingo and C. de Graaf, *Chem. Eur. J.* **2017**, *23*, 1-8; c) C. Sousa, M. Alías, A. Domingo and C. de Graaf, *Chem. Eur. J.* **2019**, *25*, 1152 – 1164.

[3] a) G. M. Brown, B. S. Brunschwig, C. Creutz, J. F. Endicott and N. Sutin, *J. Am. Chem. Soc.* **1979**, *101*, 1298–1300; b) H. B. Gray and A. W. Maverick, *Science* **1981**, *214*, 1201–1205; c) C. Creutz, M. Chou, T. L. Netzel, M. Okumura and N. Sutin, *J. Am. Chem. Soc.* **1980**, *102*, 1309–1319; d) M. Chergui, *Dalton Trans.* **2012**, *41*, 13022–13029.

[4] a) J. R. Winkler, C. Creutz and N. Sutin, *J. Am. Chem. Soc.* **1987**, *109*, 3470–3471; b) J. R. Winkler and N. Sutin, *Inorg. Chem.* **1987**, *26*, 220–221.

[5] Y. Jean in *Molecular Orbitals of Transition Metal Complexes*, *Vol.* (Ed. OUP Oxford), Oxford University Press, **2005**, p. 288.

[6] W. Zhang, K. S. Kjær, R. Alonso-Mori, U Bergmann, M. Chollet, L. A. Fredin, R. G. Hadt, R. W. Hartsock, T. Harlang, T. Kroll, K. Kubicek, H. T. Lemke, H. Liang, Y. Liu, M. M. Nielsen, P. Persson, J. S. Robinson, E. I. Solomon, Z. Sun, D. Sokaras, T. B. van Driel, T. Weng, D. Zhu, K. Wärnmark, V. Sundström and K. J. Gaffney, *Chem. Sci.* **2017**, *8*, 515-523.

[7] a) P. Guionneau, M. Marchivie, G. Bravic, J. Létard and D. Chasseau in *Structural Aspects of Spin Crossover. Example of the [FeIIILn(NCS)2] Complexes.*, *Vol. 234* Springer, Berlin, Heidelberg, Berlin, Heidelberg, **2004**, pp. 97-128; b) W. Gawelda, V.-T. Pham, R. M. van der Veen, D. Grolimund, R. Abela, M.Chergui and C. Bressler, *J.Chem.Phys.*

References

2009, *130*, 9.

[8] W. Gawelda, V.-T. Pham, M. Benfatto, Y. Zaushitsyn, M. Kaiser, D.Grolimund, S. L. Johnson, R. Abela, A. Hauser, C. Bressler and M. Chergui., *Phys. Rev. Lett.* **2007**, *98*, 057401.

[9] a) J.Cirera, M. Via-Nadal and E. Ruiz, *Inorg. Chem.* **2018**, *57*, 14097–14105; b) K.P. Jensen and J. Cirera, *J. Phys. Chem. A* **2009**, *113*, 10033–10039; c) K.P. Kepp, *Coord. Chem. Rev.* **2013**, *257*, 196–209.

[10] V. Barone and M. Cossi, *J. Phys. Chem. A* **1998**, *102*, 1995-2001.

[11] K. S. Kjær, W. Zhang, R. A. Mori, U. Bergmann, M. Chollet, R. G. Hadt, R. W. Hartsock, T. Harlang, T. Kroll, K. Kubiček, H. T. Lemke, H. Liang, Y. Liu, M. M. Nielsen, J. S. Robinson, E. I. Solomon, D. Sokaras, T. B. van Driel, T. Weng, D. Zhu, P. Persson, K. Wärnmark, V. Sundström and K. J. Gaffney, *Struct. Dyn.* **2017**, *4*, 044030.

[12] C. de Graaf and C. Sousa, *Chem. Eur. J.* **2010**, *16*, 4550 – 4556.

[13] J.tatchen, N.Gilka and C.M.Marian, *Phys. Chem. Chem. Phys.* **2007**, *9*, 5209-5221

[14] H. Reiss and A. Heller, *J. Phys. Chem.* **1985**, *89*, 4207-4213.

[15] G. A. Fortuny in *Spin-Crossover beyond the traditional Fe(II) complexes: ab initio study of spin state stability in complexes with Mn, Ni and Ru*, *Vol. PhD* UNIVERSITAT ROVIRA I VIRGILI, **2016**.

[16] C. R. Bock, T. J. Meyer and D. G. Whitten, *J. Am. Chem. Soc.* **1975**, *97*, 2909-2911.

[17] G. Fortuny, J. Wu, R. Caballol and C. de Graaf, *J. Phys. Chem. A* **2018**, *122*, 1114-1123

"Believe you can and you´re halfway there."

--Theodore Roosevelt

Chapter 4

Benchmarks for HS-LS energy difference: NEVPT2, CASPT2 and DLPNO-CCSD(T) *vs.* TPSSh

4.1 Introduction

The theoretical modelling of the relative energy difference between spin states such as high-spin (HS) and low-spin (LS) in transition metal complexes express a challenging problem in computational chemistry. It is critical for predicting the chemical and physical properties of the complexes such as spin crossover and the reactivity in catalysis. The relative energy analysis is also a convenient way to assess the ground state properties of the TM complex, for example, classify the complex as a weak or strong ligand field complex. The choice of an appropriate method to accurately describe the spin state energetic is highly challenging from a theoretical

point of view. Density-functional theory (DFT) is a common method that can give good results but severely depends on the exchange-correlation functional. As for SCO, it has been shown that the hybrid GGA B3LYP* and the meta-GGA functional TPSSh which contain 15% and 10% Hartree-Fock exchange respectively, can produce quite accurate relative energies between spin states in many transition metal complexes studies.[1] However, in comparison to pure GGA functionals, these two hybrids are computationally more expensive and analytical gradients for the meta-GGA functional are not implemented in all standard quantum chemistry programs. Swart put forward the pure GGA functional OPBE as alternative[2] can give a good prediction of the spin ground state in number of complexes with small spin gaps. The reparametrization by Gruden and Swart[3] to reproduce also other properties of the TM complexes lead to a new GGA functional known as S12g, which is claimed to be an efficient and reliable functional to study the spin state energetics and the reactivity of these complexes. Among the wave function based approaches, second-order perturbation theory based on a complete active space self-consistent field (CASSCF) reference wave function (CASPT2) has been reported to provide reasonably accurate energy differences[4] but it has the limitation that it can only be routinely applied for small- to medium-sized systems and also in several cases the results have been found to bias to high-spin state when the standard value of the IPEA shift ϵ is used in the definition of $\hat{H}_0$. Results of the alternative NEVPT2 (NEV= n-electron valence) method which is based on an improved zeroth-order Hamiltonian, has been rarely reported.[5] The so-called "golden standard" method CCSD(T) is among the most accurate methods for calculating electronic energies provided that multi-configurational effects are small. In the case of Fe(II) SCO complexes, the LS and HS states can in principle be thought of as single configurational wave functions: the LS as a closed-shell 3d-(t_{2g}^6) configuration and the HS as an restricted open-shell HF determinant with a 3d-($t_{2g}^4e_g^2$) configuration. Therefore, we have also made an attempt to calculate the HS-LS energy difference

with coupled cluster. It is well known that the computational cost of CCSD(T) raises very fast with the size of the system (N^8 scaling), and therefore, we have opted for the DLPNO-CCSD(T) variant for all the complexes but the smallest models, where we do compare the two implementations of CCSD(T).

The main goal of this work is to evaluate the performance of different methods for the calculation of the $\Delta E_{HL} = E_{HS} - E_{LS}$ in a systematic manner. A set of mononuclear complexes including seven iron(II) SCO complexes and one cobalt(II) complex has been considered. ΔE_{HL} is the dominating quantity in enthalpy differences ΔH, the zero-point vibrational energy difference ΔZPVE is a minor term which always shows a negative value, thus bias the HS state.

4.2 Computational Details

All the structures are mononuclear transition metal complexes. The series includes the following molecules: (S1) $[Fe(NH_3)_6]^{2+}$, (S2) $[Fe(bpy)_3]^{2+}$, (S3) $[Fe(terpy)_2]^{2+}$, (S4) $[Fe(bpp)_2]^{2+}$, (S5) $[Fe(phen)_2(NCS)_2]$, (S6) $[Fe(tppn)]^{2+}$, (S7) [cis-Fe(m-MBPT)$_2$(NCS)$_2$] and (S8) $[Co(terpy)_2]^{2+}$ (See **Fig**. 4.1). Here, bpy stands for 2,2´-bipyridine, terpy stands for 2,2,6´,2´´-terpyridine, bpp stands for 2,6-[1H-pyrazol-3-yl]pyridine; phen stands for 1,10- phenanthroline; tppn stands for N,N,N´,N´-tetrakis(2-pyridylmethyl)-1,2-propylenediamine; m-MBPT stands for 4-m-methylphenyl-3, 5-bis (pyridine 2-yl)-1, 2, 4-triazole.

All calculations were performed with the ORCA 4.0 program package. The geometries of all the complexes were optimized both in HS and LS state using DFT with the gradient-corrected (GGA) exchange-correlation functional OPBE, def2-tzvpp basis set was used for all the atoms, but $[Fe(bpy)_3]^{2+}$, $[Fe(terpy)_2]^{2+}$ and $[Fe(bpp)_2]^{2+}$ for which we applied the def2-tzvp basis set.

Benchmarks for HS-LS energy difference

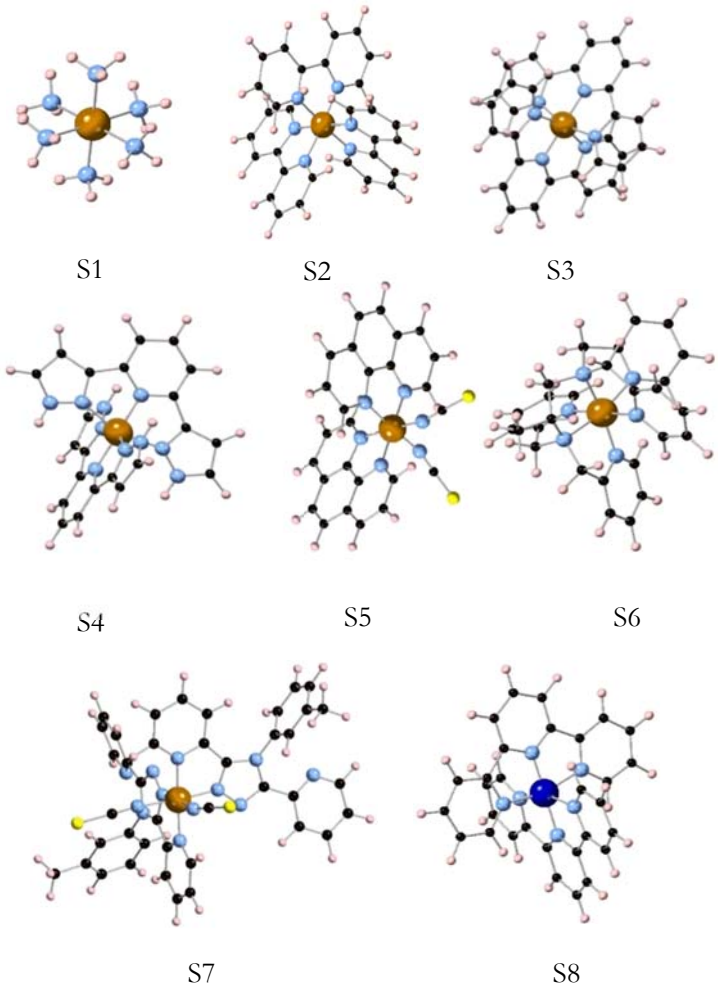

Figure 4.1 *Complexes studied in this work to benchmark different computational approaches for the calculation of* ΔE_{HL}.

The energy of the lowest HS and LS states for all the complexes were determined with the TPSSh functional using the OPBE optimized geometries. The resulting ΔE_{HL} has been compared to the outcomes of some wave function-based methods including CASSCF, CASPT2, NEVPT2 and CCSD(T). The calculations for the wave function-based method were carried out with various basis sets (see **Table** 4.1). The calculation of the zero-point vibrational energy (ZPVE) was performed by frequency

calculations using OPBE functional in ORCA 4.0 program. Since the Hessian for $[Fe(phen)_2(NCS)_2]$ and $[cis\text{-}Fe(m\text{-}MBPT)_2(NCS)_2]$ contained several (small) negative eigenvalues, which could not be removed by increasing the precision of the calculation (tighter thresholds and finer grids), we carried out the frequency calculations with the B3LYP functional and def2-tzvp basis set using the TURBOMOLE 6.6 program. No symmetry restrictions were imposed in any of the calculations. CASSCF/CASPT2 calculations have been done with MOLCAS v8.2 using the Cholesky decomposition technique to represent the two-electron integrals and reduce the computational cost. CASSCF/NEVPT2 and CCSD(T) calculations were done with ORCA 4.0. To speed up the calculations, we used the RI-JK representation of the two-electron integrals for NEVPT2 and the more 'aggressive' reduction implemented in the RIJCOSX approach for CCSD(T). All the basis sets were designed to include scalar relativistic effects by taking into account the Douglas-Kroll-Hess (DKH) method.

The basis sets defined in this work list in **Table** 4.1, basis A and B are Karlsruhe group basis sets, the difference between them lies in the Fe(II)/Co(II) basis: [10s6p4d1f] for basis A and [14s10p5d4f2g] for basis B. The contracted basis functions for the ligand atoms are [6s3p2d1f] for N and C, [3s1p] for H and [8s4p2d1f] for S. The other basis sets are atomic natural orbital basis sets, the basis C, C1, C2 have the same contracted basis functions for ligand atoms: [3s2p1d] for N, C, H and [4s3p1d] for S, but increasing metal centred contracted basis functions: [5s4p2d1f] for basis C, [7s6p5d3f2g1h] for basis C1 and [7s6p5d4f3g2h] for basis C2. The three D basis sets have the same basis functions for Fe and Co as the C basis sets, but increase the quality on the ligands to [4s3p2d1f] for N and C, [4s3p2d] for H and [5s4p2d1f] for S. The basis E has been used previously for the ligands in CASPT2 calculations of ΔE_{HL},[6] it has the same contracted basis functions as C1, D1 for metal centre, and the ligand atoms [4s3p1d] for N, [3s2p] for C, [2s] for H and [4s3p] for S.

Table 4.1. Summary of basis sets used in this work, the corresponding number of contracted functions for the metal centre and ligand atoms.

name		Fe(II)/Co(II)	N	C	H	S
A	def2-tzvp	10s6p4d1f	6s3p2d1f	6s3p2d1f	3s1p	8s4p2d1f
B	def2-qzvpp	14s10p5d4f2g	6s3p2d1f	6s3p2d1f	3s1p	8s4p2d1f
C	ANO-I	5s4p2d1f	3s2p1d	3s2p1d	3s2p1d	4s3p1d
C1	ANO-II	7s6p5d3f2g1h	3s2p1d	3s2p1d	3s2p1d	4s3p1d
C2	ANO-III	7s6p5d4f3g2h	3s2p1d	3s2p1d	3s2p1d	4s3p1d
D	ANO-IV	6s5p3d2f1g	4s3p2d1f	4s3p2d1f	4s3p2d	5s4p2d1f
D1	ANO-V	7s6p5d3f2g1h	4s3p2d1f	4s3p2d1f	4s3p2d	5s4p2d1f
D2	ANO-VI	7s6p5d4f3g2h	4s3p2d1f	4s3p2d1f	4s3p2d	5s4p2d1f
E	ANO-VII	7s6p5d3f2g1h	4s3p1d	3s2p	2s	4s3p

4.3 Results and Discussion

4.3.1 Geometry optimizations and the relative energies by DFT

The geometries of the HS and LS state have been optimized in DFT level using the OPBE functional, implemented in the ORCA 4.0 program package. The def2-tzvpp basis set has been used for all the atoms in the optimization of complexes S1, S5, S6, S7, S8; the basis set def2-tzvp applied for complexes S2, S3, S4. The lowest energy of HS and LS state were carried out by TPSSh functional correspond to the same basis set for their geometry optimization. The calculation of frequencies to obtain the zero-point vibrational energy. The results of average Fe-N distances for both states, and the ZPVE difference, the adiabatic energy difference between HS and LS state, with and without ZPVE correction listed in **Table** 4.2, also including the

available experimental data.

Experiment tells us that complexes S1 and S7 have HS ground states, while other ones have a LS ground state at low temperature. The calculated average metal-N distances at the ground state of the different complexes matched well with the available experimental data. For example, the average distance for S2 is 1.96 Å, close to the experimental 1.97-1.98 Å both in solid[7] state and in solution;[8] the 1.93 Å average distance for S3 is only a little shorter than the experimental 1.95 Å;[9] for S4, we obtained the same distance (1.93Å) as obtained from experiment;[10] the single-crystal X-ray investigation for S5 at room temperature corresponding the HS state shows the average distance around 2.16 Å[11] a little longer than the result we obtained 2.13 Å; for S6, we got a slightly shorter average distance 1.98 Å than experiment 1.99 Å[12] consistent with the low spin Fe(II); the experimental Fe-NCS distance in S7 is 2.05 Å while the N atoms of the triazole and pyridyl groups lie at 2.25Å and 2.22 Å from Fe, the corresponding calculated values are 2.01 Å, 2.25 Å and 2.23 Å, respectively, in good agreement with the experimental data; the calculated average distance of 2.02 Å for S8 coincides with the experimental estimate[17] at room temperature. As expected, the ZPVE energy is larger in the LS than in the HS. For the Fe(II) complexes, the HS state is stabilized by about 800-1000 cm^{-1}, while the effect is significantly smaller in the Co complex, where the ZPVE only contributes 300 cm^{-1} to the ΔH_{HL}. **Table** 4.2 shows that adding ΔZPVE to the electronic energy difference (ΔE_{HL}) to obtain ΔH_{HL} brings the calculated relative stability of LS and HS in better agreement with experiment, except for S5, where the HS state is even further stabilized, while experiment indicates this also to be a LS molecule.

Table 4.2 OPBE optimized average Fe-N distances [Å] and the relative HS-LS zero point energy contribution ΔZPVE [cm^{-1}], TPSSh calculated relative energies [cm^{-1}] ΔE_{HL} and ΔH_{HL} compared to the available experimental values.

	Fe-N distance		**Relative energies(HS-LS)**			
	LS	HS	ΔZPVE	ΔE_{HL}	$\Delta H_{HL}^{(*)}$	ΔH_{exp}
S1	2.049	2.306	-1494	-918	-2412	HS
S2	1.960	2.201	-893	5912	5019	~6000[8]
S3	1.933	2.170	-899	6439	5540	5200-6400[13]
S4	1.926	2.177	-863	2969	2106	2073
S5	1.856	2.130	-814	-529	-1344	719[14]
S6	1.983	2.260	-783	3532	2749	2090-2510[15]
S7	1.917	2.160	-784	2573	1789	
S8	2.016	2.119	-212	1610	1399	750-1340[16]
**Thermal corrections to the enthalpy are neglected*						

4.3.2 Basis set dependence of the relative energies

In this investigation, we report the results got for the HS-LS energy differences in the $3d^6$ iron(II) HS ground state complexes S1, S7 and LS ground state complexes S2, S3, S4, S5, S6 (LS is a singlet state and HS is a quintet state) and $3d^7$ cobalt(II) S8 complex (LS is a doublet state and HS is a quadruple state). Their spin-state energy differences have been calculated with CASSCF, CASPT2, NEVPT2 and DLPNO-CCSD(T) methods with various basis sets (see **Table** 4.1), since the size of the basis set may have a much larger effect on the accuracy for transition metal complexes.[18] The total number of the contracted basis functions for all the complexes are summarized in **Table** 4.3 and the comparison represented by **Fig.** 4.2.

The results of spin state energy by NEVPT2 and CASPT2 obtained from the

calculations that include eight electrons from the metal 3s and 3p orbitals in the second-order perturbation treatment, called "full correlation". Which described has effect bias toward high-spin states for CASPT2 calculation.[5] The active space used in the multi-configurational perturbation theory calculations are the same for NEVPT2 and CASPT2 in all cases and are built according to the standard rules for transition metal complexes. It consisted of 10 electrons correlated in 12 orbitals on the Fe(II) and 11 electrons correlated 12 orbitals on Co(II) complex which including six or seven electrons in the five Fe(3d) or Co(3d) orbitals, a second 3d' shell to account for the double-shell effect which usually the dynamic part of the molecules, and two doubly occupied metal-ligand σ-bonding orbitals to account for non-dynamic correlation effects associated with the covalent metal-ligand interactions. All calculations denoted as CASPT2 use the default IPEA shifts 0.25 Hartree for the zeroth-order Hamiltonian $\hat{H}_0$ and a small level shift 0.20 Hartree was used for $[Fe(phen)_2(CN)_2]$ and $[Fe(bpy)_3]^{2+}$ to exclude possible intruder states. The larger system $[cis\text{-}Fe(m\text{-}MBPT)_2(NCS)_2]$ lacks the CASPT2 result because the size of system needs more memory in the machine.

NEVPT2 calculations were performed by the SC-NEVPT2 (strongly contracted n-electron valence state perturbation theory) formalism with RIJK approximation to speed-up the calculation and state-average (s.a.) CASSCF, averaging over four singlets and five quintets for the Fe(II) complexes and two doublets and three quartets for the Co(II) complex. We also performed NEVPT2 calculations with the PC-NEVPT2 (partially contracted n-electron valence state perturbation theory) formalism, to investigate the influence of the contraction scheme; and also with several other factors such as using a state-specific (s.s.) reference wave function, and replacing RIJK by the RIJCOSX approximation.

Benchmarks for HS-LS energy difference

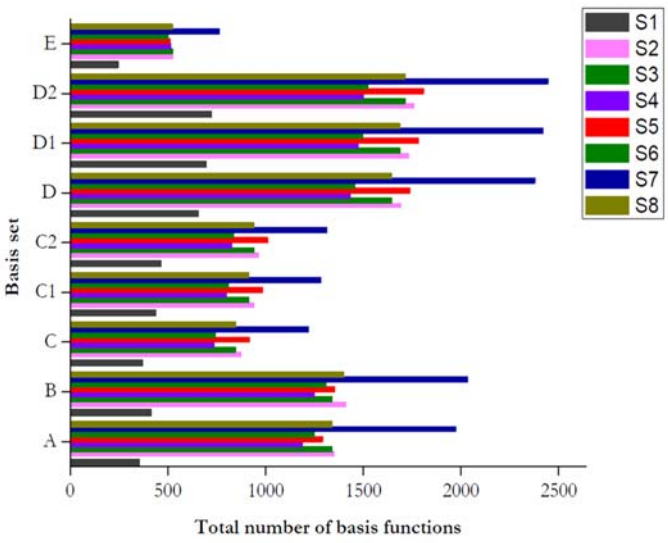

Figure. 4.2 *The comparison of the total number of contracted basis functions for the complexes studied in this work corresponding to the various basis sets. The different colors stand for different complexes.*

Table 4.3 The total number of basis functions corresponding to different basis sets for 8 complexes, respectively.

	S1	**S2**	**S3**	**S4**	**S5**	**S6**	**S7**	**S8**
A	355	1351	1339	1187	1249	1291	1973	1339
B	415	1411	1339	1247	1309	1351	2033	1399
C	370	874	846	734	742	916	1218	846
C1	436	940	912	800	808	982	1284	912
C2	463	967	939	827	835	1009	1311	939
D	653	1691	1645	1433	1455	1739	2377	1645
D1	694	1732	1686	1474	1496	1780	2418	1686
D2	721	1759	1713	1501	1523	1807	2445	1713
E	244	526	522	514	500	511	762	522

The coupled cluster estimates of the relative energies of the HS-LS states have been estimated using the domain-based local pair-natural orbital (DLPNO) approach developed by Neese et al.[19] They have been run with scalar relativistic (SR) effects through the use of the Douglas-Kroll-Hess (DKH) method as implemented in ORCA 4.0. All DLPNO-CCSD(T) calculations either closed-shell or open-shell species are supported through a UHF treatment with default NormalPNO. TightPNO as a test for further comparison. In this approach, the canonical Hartree-Fock orbitals are localized by some standard procedure like Pipek-Mezey or Boys localization and a low-level correlation calculation (typically MP2) is performed only considering the orbitals inside a certain domain. Next a set of natural orbitals is constructed from this low-level calculation, which in turn are used for the CCSD(T) calculation, selecting those natural orbitals with largest deviations from 2 and 0 in their natural occupation numbers. The number of natural orbitals used to correlate an electron pair is controlled by the PNO parameter, for which ORCA has two predetermined values known as normalPNO and tightPNO.

The calculated relative energies with the four methods CASSCF, CASPT2, NEVPT2 and DLPNO-CCSD(T) are collected in **Table** 4.4. The CASSCF calculations always produce high-spin ground states, and this negative ΔE_{HL} does not change much with various basis sets for each complex. The deviations are of the order of 100 cm^{-1} except for basis E for which deviations up to 800 cm^{-1} are observed, probably due to the fact that the basis set is somewhat unbalanced between metal and ligand. As the CASPT2 calculation are rather time-consuming for the larger systems here we only calculated the smallest system S1 for all the basis sets. For the other complexes we only applied the smallest basis E for CASPT2 calculation.

We take complex S1 as a model system to start the discussion. As discussed in section 4.2, basis A and B are Karlsruhe type (segmented) basis sets, the (general contracted) ANO-RCC basis C, C1, C2 have the same contracted basis functions for the ligand

atoms but gradually increase the quality of the metal basis set. Basis D, D1, D2 increase the contracted basis functions for the ligand atoms, while only metal D is increased compared to the C set to avoid an unbalanced basis set (see **Table** 4.1). Comparing the CASPT2 value of the ΔE_{HL} for basis A with the one calculated with basis B shows that the extension of the basis set on the metal stabilizes the LS state by about 2000 cm^{-1}. A similar increase of ΔE_{HL} is observed when the outcome of basis C is compared to the other ANO-RCC basis sets. Next, it also becomes clear that the size of the basis set on the ligand is less critical: C1 and D1, and C2 and D2 give practically the same energy difference. Basis set E gives again (slightly) different results, favouring even more the LS state. The negative ΔE_{HL} for all the basis sets is in line with the experimental HS grounds state for S1. In fact, the CASPT2 results with basis E give an accurate prediction of the LS ground state for all complexes except S8, for which a near degeneracy is predicted. Somewhat surprisingly, CASPT2 with basis A predicts a HS ground state for $[Fe(bpp)_2]^{2+}$ which is in contradiction with the experimental LS ground state. Since basis E gives consistently correct results (also in previous studies with very similar basis sets to basis E[6]). It can be concluded that, despite the unbalance between metal and ligand, this basis set works very well for the CASPT2 calculation. One should however keep in mind that this is probably (at least partially) due to a cancellation of errors.

Table 4.4 Basis set dependence of ΔE_{HL} [cm^{-1}] calculated for all the complexes in this work by different methods NEVPT2, CASPT2 and DLPNO-CCSD(T). With state-average (s.a.) and strongly contracted NEVPT2 (SC-NEVPT2) with RIJK approximation.

complex	BASIS SETS	CASSCF	CASPT2	NEVPT2	DLPNO-CCSD(T)
$[Fe(NH_3)_6]^{2+}$	A	-16809	-9003	-7853	-9771
	B	-16549	-6823	-5091	--
	C	-16360	-9274	-7806	--
	C1	-16580	-6749	-4813	-7694
	C2	-16596	-6052	-4142	--
	D	-16654	-6462	-4597	--
	D1	-16646	-6607	-4460	--
	D2	-16637	-6239	-4076	-7380
	E	-15868	-5757	-3802	-6265
$[Fe(bipy)_3]^{2+}$	A	-16509	--	-4721	-4422
	B	-16283	--	-2158	--
	C	-16540	--	-6994	--
	C1	-16426	--	-1660	-1855
	C2	-16405	--	-605	--
	D	-16373	--	-2516	--
	D1	-16328	--	-1974	--
	D2	-16321	--	-1512	-2142
	E	-15687	3563	-1550	-1998
$[Fe(terpy)_2]^{2+}$	A	-16462	--	-5087	-4892
	B	-16297	--	-2425	--

Benchmarks for HS-LS energy difference

	C	-16691	--	-8178	--
	C1	-16518	--	-2570	-2683
	C2	-16480	--	-1480	--
	D	-16431	--	-3426	--
	D1	-16379	--	-2790	--
	D2	-16370	--	-2300	-2730
	E	-15809	4757	-1930	-2132
$[Fe(bpp)_2]^{2+}$	A	-19127	-752	-7331	-7994
	B	-18968	--	-5473	--
	C	-19346	--	-12016	--
	C1	-19222	--	-6263	-5741
	C2	-19181	--	-5432	--
	D	-19184	--	-7360	--
	D1	-19106	--	-6853	--
	D2	-19098	--	-6411	-5800
	E	-18816	861	-5972	-5255
$[Fe(phen)_2(NCS)_2]$	A	-24064	--	-10582	-11581
	B	-23836	--	-7888	--
	C	-24619	--	-14674	--
	C1	-24206	--	-7809	-9274
	C2	-24151	--	-6711	--
	D	-23980	--	-8264	--
	D1	-23844	--	-7623	--
	D2	-23824	--	-7109	-8840
	E	-23197	78	-6862	-8814

$[Fe(tppn)]^{2+}$	A	-16580	--	-3805	-5000
	B	-16363	--	-1479	--
	C	-16420	--	-5516	--
	C1	-16305	--	-786	-2626
	C2	-16305	--	173	--
	D	-16439	--	-1451	--
	D1	-16418	--	-1310	--
	D2	-16413	--	-876	-2750
	E	-15533	1815	-376	-2236
cis-$[Fe(mMBPT)_2(NCS)_2]$	A	-18586	--	-10280	-8721
	B	-18358	--	-7697	--
	C	-18863	--	-12888	--
	C1	-18633	--	-7522	-6494
	C2	-18591	--	-6506	--
	D	-18509	--	-8311	--
	D1	-18404	--	-7618	--
	D2	-18392	--	-7170	-6602
	E	-17939	--	-6889	-5983
$[Co(terpy)_2]^{2+}$	A	-10668	--	-5622	-3967
	B	-10581	--	-4114	--
	C	-10585	--	-7170	--
	C1	-10759	--	-3710	-2544
	C2	-10698	--	-3086	--
	D	-10281	--	-4719	--
	D1	-10628	--	-3933	--

	D2	-10609	--	-3637	-2662
	E	-10568	-474	-3574	-2411

The same tendency have been observed when the SC-NEVPT2 method was applied with various basis sets for S1 complex as obtained by CASPT2 calculation. The difference of the ΔE_{HL} between basis A and basis B around 2800 cm^{-1} which metal effect even more stabilize the LS state than CASPT2 method. The mount of ANO-RCC basis sets gave the increased ΔE_{HL} same as CASPT2 presented respect to basis C. The basis C1 and D1, C2 and D2 with increased ligand atoms basis functions produced the energy difference is 353 cm^{-1} and 66 cm^{-1}, respectively. Indicating that the less effect from the ligand atoms. The unbalanced basis E also produced the largest value as applied in CASPT2 calculation comparing with other basis sets which favouring more the LS state but all gave the negative values, obviously not correct for the LS ground state complexes calculation. Overall all the results, we found that NEVPT2 not as our expected produce more accurate results as the theoretical description comparing with CASPT2 method (at least can produce the accurate ground state). Actually, the wrong values were obtained for all the LS ground state complexes. Our study proved that NEVPT2 method for TM complexes relative energies calculation gives disappointed results as Pierloot et al. have reported.[5]

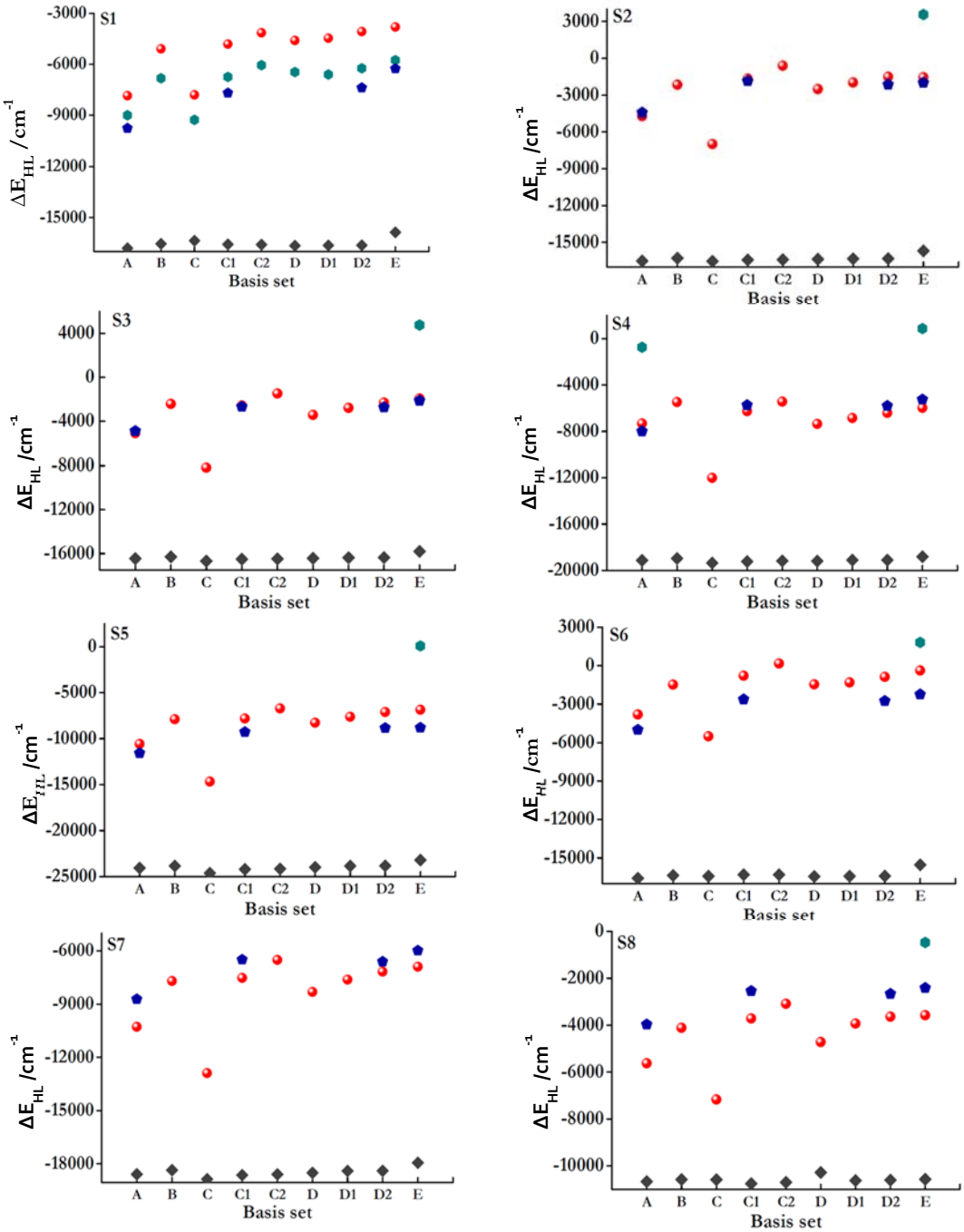

Figure. 4.3 *Computed relative energy difference [cm-1] between HS and LS states with various basis sets, using CASSCF (dark grey), CASPT2(green), NEVPT2 (red) and DLPNO-CCSD(T)(blue) methods for all the studied complexes.*

Benchmarks for HS-LS energy difference

The DLPNO-CCSD(T) method was performed by four different basis sets A, C1, D2 and E. We did not give an overall comparison with various basis sets, but we propose that this method can produce the same tendency as CASPT2 and SC-NEVPT2 presented based on the results we have analysed with these four basis sets. As noticed at **Table** 4.4, the slightly smaller values got for HS ground state complex S1 compared with the values got by CASPT2 and NEVPT2 methods correspond to the four basis sets which we used, respectively. However, for LS ground state complexes, DLPNO-CCSD(T) matched well with NEVPT2 results for S2 and S3, the difference only around 100-600 cm^{-1}. And slightly increased value for S4, the difference around 500-1000 cm^{-1}. The largely increased value for S7, S8, the difference around 1000-1500 cm^{-1} except for basis D2 for S7 at 500 cm^{-1}. And largely decreased value for S5 and S6, the difference decreased by 1000-2000 cm^{-1}. All the comparisons were respect to NVEPT2 calculations. These basis sets are illustrative for the whole series and provides us sufficient information to draw conclusions on the ability of the standard implementation of the DLPNO-CCSD(T) method in ORCA to predict the energy difference between HS and LS of the eight complexes. First and foremost, we observe that also DLPNO-CCSD(T) is not capable of correctly predicting the LS ground state of the complexes S2-S8. Note that the value listed in **Table** 4.4 do not include the ZPVE correction, making the failure to predict a LS ground state even more serious. The second conclusion that we can draw from the DLPNO-CCSD(T) values is that they are in six out of eight cases in remarkable agreement with the NEVPT2 results. The discrepancy for S1 may be caused by the small size of the complex making that a domain-based treatment of the electronic structure is somewhat forced. Test calculations shows a much better agreement between NEVPT2 and the canonical CCSD(T), -5409 cm^{-1} versus -5990 cm^{-1}. We have no logical explanation for the large discrepancy between NEVPT2 and DLPNO-CCSD(T) for S6.

4.3.3 Influence on relative energy of the RI approximation, the first-order interaction space and the orbital optimization

In the previous section we have found that only CASPT2 with a slightly unbalanced basis set is capable of correctly predicting the relative stability of the spin states in the series of complexes presented in **Fig**.4.3. Both NEVPT2 and DLPNO-CCSD(T) give rather disappointing results. In order to remove any doubts on the performance we have also studied the influence on the results of some computational details other than the basis set. In the first place, we have analysed how the orbital optimization affects the NEVPT2 values of the spin gap. In the calculations discussed in the previous paragraph, the orbitals of the HS state were optimized for an average of the five lowest quintets, corresponding to the $^5T_{2g}$ and ^5E_g states in an octahedral complex. This ensures a smooth convergence of the CAS (10, 12) as the average natural occupation numbers are different from 0 to 2 for all active orbitals. Similar reasoning makes that a state average optimization of the orbitals for the LS state is also advantageous. Typically one uses a four state average including not only the GS ($^1A_{1g}$ in O_h) but also the first three excited singlets ($^1T_{1g}$ in O_h). Actually, state averaging is even more practical for the LS than for the HS state as the electronic structure of the LS state is dominated by the Fe-3d (t_{2g}^6) configuration with doubly occupied t_{2g} and empty e_g orbitals. This could easily lead to convergence problems in the CASSCF calculation if one does not take sufficient precautions. Instead when the orbital optimization is extended to the lowest four singlets, average occupation numbers are again all different from zero and two and smooth convergence is ensured. Hence, state-average (s.a.) is computationally very convenient, but a single state (s.s) optimization is of course preferred if one can assure the correct character of all the active orbitals in both the LS and the HS state calculation. Starting from the s.a. orbitals, it is not too difficult to get the s.s. CASSCF wave function and we could study the influence on ΔE_{HL} of the orbital optimization. This was done for

complex S1, S2 and S3 for the full basis set series, results are collected in **Table** 4.5 and graphically represented for S1 and S2 in **Fig**. 4.4. A small correction was found for the CASSCF energy differences, the HS state becomes approximately 400 cm^{-1} more stable than in the s.a. procedure. This trend is inverted for NEVPT2, where we do see a significant stabilization of the LS state for S2 and S3 of 1000 to 2000 cm^{-1}, depending on the basis set. It is worth remarking that the NEVPT2 result for basis C2 now favours the LS state, although it still rather far from the experimental estimate of ~6000 cm^{-1}. A similar, but smaller effect, is observed for S1.

Table 4.5 Comparison of the calculated CASSCF and NEVPT2 with the state-average(s.a.) and state-specific(s.s.) results with RIJK approximation, Δ(a.s.)=s.a.-s.s. Units [cm^{-1}].

		Δ(a.s.)=s.a.-s.s.								
method	name	A	B	C	C1	C2	D	D1	D2	E
CASSCF	S1	410	422	231	457	457	426	445	449	450
	S2	429	462	238	492	490	47	493	495	493
	S3	399	458	208	484	485	--	--	--	486
SC-NEVPT2	S1	-649	-516	-407	-629	-636	-453	-385	-360	-617
	S2	-1977	-1853	-1308	-1769	-1744	-2377	-1925	-1916	-1528
	S3	-1858	-1499	-834	-1253	-1253	--	--	--	-1072

The next factor that can influence the energy difference is the choice of the first-order interacting space (FOIS). NEVPT2 has two variants, the strongly contracted (SC) and the partially contracted (PC) FOIS. The latter choice uses a similar way of constructing the perturber wave functions (configuration not included in the CAS) as in CASPT2 by applying single and double excitation operators on the CASSCF wave function as a whole. In SC-NEVPT2, the FOIS only contains 8 perturber wave

functions, one for each class of excitation (excitation classes are defined based on the number of holes and particles created in the inactive and virtual orbitals, see **Table** 4.6). This perturber is a fixed sum of all the perturbers of each class in the PC variant, which makes the SC variant faster and free of the orthogonality problems and linear dependencies as present in CASPT2 (and PC-NEVPT2). It has, however, less degrees of freedom and hence the results could be affected by the strong contraction of the FOIS.

As in most other quantum chemistry codes, ORCA has the possibility to speed-up the evaluation of the matrix elements by applying the resolution of the identity (RI) approximation. By introducing an auxiliary basis set to represent the density

$$\rho_{\nu\mu}(r) = \nu(r)\mu(r) \approx \tilde{\rho}_{\nu\mu}(r) = \sum_{c_{\nu\mu,P}} P(r)$$

4.1

the four-centre integrals can be written as a product of two three-centre integrals

$$(\mu\nu|\kappa\lambda) \approx \sum_{P,Q} (\nu\mu|P)(P|Q)^{-1}(Q|\kappa\lambda)$$

4.2

Which drastically reduces the computational cost. This is the basis for the RIJK approximation in ORCA, but for additional speed-up in methods with exact exchange (DFT with hybrid functionals and wave function based methods), Neese and co-workers defined the RIJCOSX procedure in which the locality of the exchange interaction is exploited.[20] The RIJCOSX is significantly faster than the standard RI methods but could also introduce additional loss of accuracy.

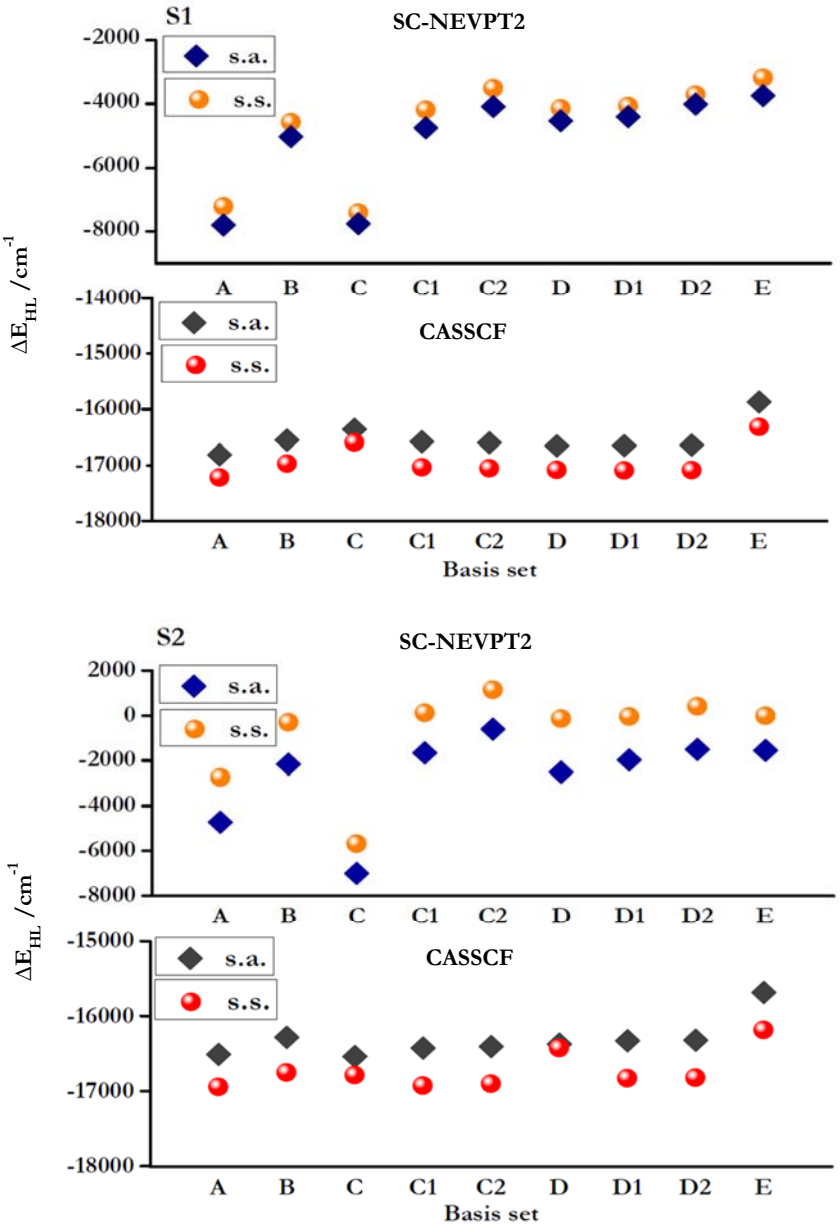

Figure 4.4 *The calculated state-average (s.a.) and state-specific (s.s.) for both HS ground state complex S1 (upper) and LS ground state complex S2 (bottom) by CASSCF and SC-NEVPT2.*

Table 4.6 Classification of the singly and doubly excited determinants by the number of holes/particles creased in the inactive (h, h´)/virtual (p, p´) orbitals.

Excitation operator(s)	CASPT2		NEVPT2
$\hat{E}_{ha}$; $\hat{E}_{ha}\,\hat{E}_{bc}$	Internal	VJTU	$\hat{V}_{h}^{+1}$
$\hat{E}_{ha}\,\hat{E}_{h'b}$	VJTI		$\hat{V}_{hh'}^{+2}$
$\hat{E}_{ap}$; $\hat{E}_{ap}\,\hat{E}_{bc}$	Semi-internal	ATVX	$\hat{V}_{p}^{-1}$
$\hat{E}_{hp}$; $\hat{E}_{hp}\,\hat{E}_{ab}$	AIVX		$\hat{V}_{h,p}^{0}$
$\hat{E}_{hp}\,\hat{E}_{h'a}$	VIAJ		$\hat{V}_{hh',p}^{+1}$
$\hat{E}_{ap}\,\hat{E}_{bp'}$	External	BVAT	$\hat{V}_{pp'}^{-2}$
$\hat{E}_{hp}\,\hat{E}_{ap'}$	BJAI		$\hat{V}_{h,pp'}^{-1}$
$\hat{E}_{hp}\,\hat{E}_{h'p'}$	BJAI		$\hat{V}_{hh',pp'}^{0}$

The a, b and c labels in the excitation operators refer to active orbitals, the four-letter code in the CASPT2 column refers to the classification used in Molcas with t, u, v and x as active orbitals, i and j are inactive orbitals and a and b virtual orbitals

Based on above discussion, here we listed the detailed comparison for all the complexes by these factors in **Table** 4.7 and a graphical representation of the tendencies is given in **Fig**. 4.5. Here we took the values obtained from the basis C1 with the strongly contracted (SC) FOIS and state-average CASSCF, using the RIJK approximation as a reference. The effect of changing the RIJK approximation with the faster RIJCOSX approach has in most complexes a negligible effect, although S4 and S7 are exceptions, for which we observe a stabilization of the LS (S4) or HS (S7) by almost 1000 cm^{-1}. It is difficult to rationalize this opposite tendency and probably a larger test set could clarify this apparent contradiction.

Table 4.7. Influence on ΔE_{HL} of the RI approximation (RIJK *vs.* RIJCOSX), the nature of the first-order wave function (strongly contracted (SC) *vs.* partially contracted (PC), and the state-average in the reference wave function optimization (State-average (s.a.) *vs.* State-specific (s.s.)). NEVPT2 values with basis C1.

(S1) $[Fe(NH_3)_6]^{2+}$					
Basis sets	RI approx.	First-order wf	Reference wf	ΔE_{HL}	difference
C1	RI-JK	SC	SA	-4813	--
	RIJCOSX	SC	SA	-4830	-17
	RI-JK	PC	SA	-4252	560
	RI-JK	SC	SS	-4184	629
	RI-JK	PC	SS	-3596	1217
(S2) $[Fe(bipy)_3]^{2+}$					
C1	RI-JK	SC	SA	-1660	--
	RIJCOSX	SC	SA	-1577	83
	RI-JK	PC	SA	-722	938
	RI-JK	SC	SS	109	1769
	RI-JK	PC	SS	1166	2826
(S3) $[Fe(terpy)_2]^{2+}$					
C1	RI-JK	SC	SA	-2570	--
	RIJCOSX	SC	SA	-2518	52
	RI-JK	PC	SA	-1717	853
	RI-JK	SC	SS	-1317	1253
	RI-JK	PC	SS	-270	2300
(S4) $[Fe(bpp)_2]^{2+}$					
C1	RI-JK	SC	SA	-6263	--
	RIJCOSX	SC	SA	-5291	972
	RI-JK	PC	SA	-5397	866
	RI-JK	SC	SS	-5351	912

	RI-JK	PC	SS	-4316	1947
(S5) $[Fe(phen)_2(NCS)_2]$					
C1	RI-JK	SC	SA	-7809	--
	RIJCOSX	SC	SA	-7380	429
	RI-JK	PC	SA	-6522	1287
	RI-JK	SC	SS	-3439	4370
	RI-JK	PC	SS	-2080	5729
(S6) $[Fe(tppn)]^{2+}$					
C1	RI-JK	SC	SA	-786	--
	RIJCOSX	SC	SA	-823	-37
	RI-JK	PC	SA	135	921
	RI-JK	SC	SS	455	1241
	RI-JK	PC	SS	1426	2212
(S7) $[cis\text{-}Fe(m\text{-}MBPT)_2(NCS)_2]$					
C1	RI-JK	SC	SA	-7522	--
	RIJCOSX	SC	SA	-8355	-833
	RI-JK	PC	SA	-6343	1179
	RI-JK	SC	SS	-4151	3371
	RI-JK	PC	SS	-3089	4433
(S8) $[Co(terpy)_2]^{2+}$					
C1	RI-JK	SC	SA	-3710	--
	RIJCOSX	SC	SA	-3701	9
	RI-JK	PC	SA	-6683	-2972
	RI-JK	SC	SS	-4218	-508
	RI-JK	PC	SS	-5861	-2151

Benchmarks for HS-LS energy difference

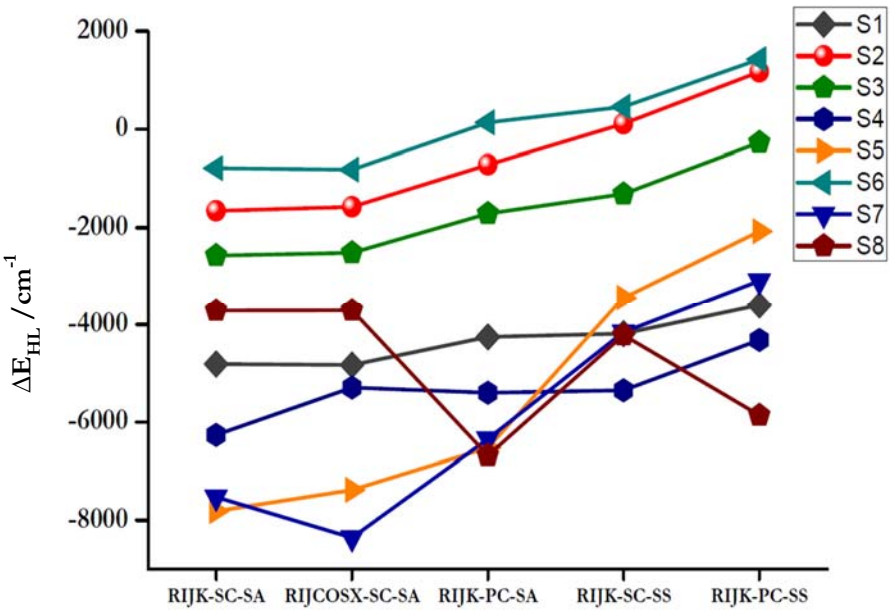

Figure 4.5 *Calculated relative energies by NEVPT2 with different factors with basis C1 (strongly contracted (SC) and partially contracted (PC) effect, state-average (s.a.) and state-specific (s.s.), RI approximation (RIJK, RIJCOSX). The different colors represent each complex.*

Next, we focus on the effect of decontracting the FOIS comparing the SC-NEVPT2 results with those obtained with the PC FOIS. All Fe(II) complexes show a stabilization of the LS state of approximately 1000 cm^{-1} (a little smaller in the model complex S1), whereas the Co(II) complex shows a large opposite effect; an almost 3000 cm^{-1} lower HS energy. Changing the SA CASSCF orbital optimization to a SS approach has a similar effect on ΔE_{HL}. It stabilizes the LS state in the Fe(II) complexes and the HS in the Co(II) complex. The LS stabilization is especially large in the two complexes with NCS ligands (S5 and S7). The last row for the complexes in **Table** 4.7 combines the application of the PC FOIS and the SS orbital optimization and one can clearly see that the two effects are approximately additive. In consequence, we conclude that the standard computational setting for calculating is largely improved by using the partially contracted variant of NEVPT2 and a single state optimization of the orbitals. Although this is a significant step in the right direction, NEVPT2 is still incapable of correctly predicting the ΔE_{HL} in most of the

complexes studied here. Certainly, in some of them we do get a LS ground state (e.g.$[Fe(bpy)_3]^{2+}$), but the calculated energy difference is still too small when compared to experimental estimates. For example, the ΔE_{HL} calculated for $[Fe(bpy)_3]^{2+}$ is ~1200 cm^{-1}, whereas experiments point at an energy difference around 6000 cm^{-1}.

4.3.4 Effect of the perturbative triple excitations in CC calculation

As the results of the DLPNO-CCSD(T) were not fully satisfactory, we also checked some computational settings for these calculations. In the first place we have checked the effect of the perturbative estimate of the triple excitations by comparing the CCSD results to the CCSD(T) ones. **Fig.**4.6 compares the calculated ΔE_{HL} for different basis sets and **Table** 4.8 lists the change in the energy difference by adding the triples correction. For this it is readily seen that

$$\Delta E_{HL}|CCSD < \Delta E_{HL}|CCSD(T) < 0$$

meaning that the triples correction stabilizes the LS state by ~1000 cm^{-1} for the smaller systems and gradually increases to ~2500 cm^{-1} for the larger ones.

Table 4.8 DLPNO-CCSD/CCSD(T) calculation based on the four different basis sets and the perturbation effect for the difference of the relative energy [cm^{-1}].

Δ(ΔE(T))	complexes							
Basis sets	S1	S2	S3	S4	S5	S6	S7	S8
A	1593	2185	2246	2187	2325	2054	2041	1029
C1	1973	2608	2686	2636	2806	2367	2458	1259
D2	1998	2582	2656	2614	2782	2420	2473	1281
E	1997	2515	2740	2690	2827	2334	2462	1275

Benchmarks for HS-LS energy difference

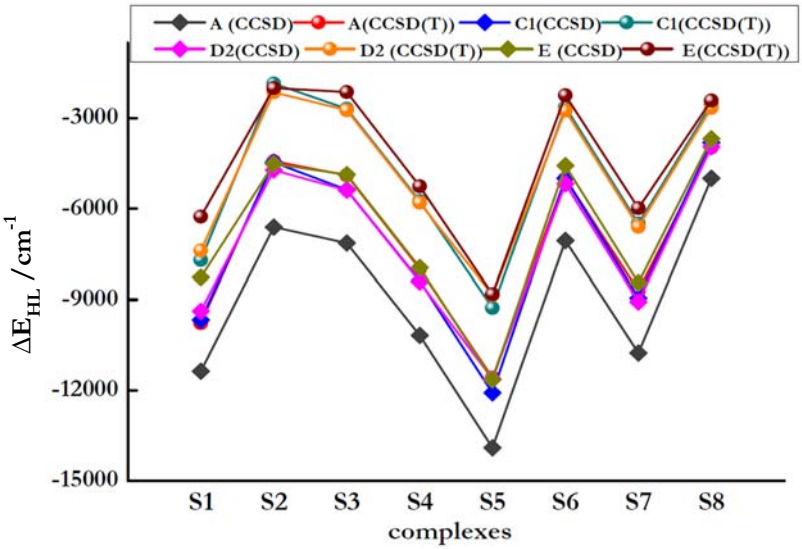

Figure 4.6 *Calculated relative energies of DLPNO-CCSD and DLPNO-CCSD(T) with basis A, C1, D2 and E for all the complexes.*

To further investigate the accuracy of DLPNO-CCSD(T) method, we also did some test calculation at two different levels (termed as 'NormalPNO' and 'TightPNO') according to the truncation thresholds that define to what extent electron pairs are correlated in space and the number of natural orbitals used in the CCSD(T) calculation. (see **Table** 4.9 below for further details). NormalPNO is the default thresholds set in ORCA4.0 and it is the accurate choice for most computational applications, such as general thermochemistry and thermochemical kinetics, and the TightPNO set is considered as the level of choice for very accurate calculations. **Table** 4.10 summarizes the relative energies calculated for $[Fe(NH_3)_6]^{2+}$ HS ground state complex using the different PNO settings for DLPNO-CCSD(T), TightPNO improves the relative energies by 613 cm^{-1} respect to NormalPNO at basis A, 847 cm^{-1} at basis C1, 767 cm^{-1} at basis D2 and 527 cm^{-1} at basis E. Illustrating that the TightPNO setting favours the LS state, which could bring the CCSD(T) results for the larger complexes in better agreement with the experimental observations of the LS ground states.

Table 4.9 Values [E_h] for the different thresholds of the DLPNO-CCSD(T) method employed in this work.

setting	NormalPNO	TightPNO
TCutPairs	10^{-4}	10^{-5}
TCutPNO	$3.33 \cdot 10^{-7}$	$1.00 \cdot 10^{-7}$

Table 4.10 Relative energies ΔE_{HL} [cm^{-1}] calculated for the S1 complex at NormalPNO and TightPNO level using DLPNO-CCSD(T) method.

$[Fe(NH_3)_6]^{2+}$	$\Delta E_{NormalPNO}$	$\Delta E_{TightPNO}$	$\Delta_{N-T}(\Delta E)$
A	-9771	-9158	-613
C1	-7694	-6847	-847
D2	-7380	-6613	-767
E	-6265	-5738	-527

4.4 Conclusions

We have presented different methods for accurately estimating the HS-LS energy difference ΔE_{HL} for HS ground state complex S1 and S7, LS ground state complexes S2, S3, S4, S5, S6, S8 by DFT, CASSCF, CASPT2, NEVPT2 and DLPNO-CCSD(T) methods. In our benchmark study, we found that among the different density functionals the TPSSh functional produced the most accurate relative energies compared with the available experimental values. The comparison of wave function-based methods CASPT2, SC-NEVPT2 and DLPNO-CCSD(T) were carried out with different basis sets. The results show that CASPT2 gives more realistic estimates of ΔE_{HL} than NEVPT2 and DLPNO-CCSD(T). The basis sets dependency have been observed that the change of the metal centre basis functions have significant effect on the studied systems, less effect is observed from the extension of the basis on the ligand atoms. Basis E with the smallest total number of contracted functions

but produced more accurately values respect to other large basis sets such as C1 and D2. Replacing the large basis set by basis E can largely reduce the cost of the computation. Other factors such as strongly-contracted (SC) and partially-contracted (PC) NEVPT2 have been studied with state-average (s.a.) and state-specific (s.s.) with different speed-up approximation RIJK or RIJCOSX combined with basis sets C1. The results obtained show that state-specific orbital optimization favors the LS state as does the partial decontraction of the FOIS in PC-NEVPT2. Comparing the RI approximations RIJK and RIJCOSX did not show large differences (except for two complexes) and is probably not critical to the calculated ΔE_{HL}, although it may be useful to test the effect in more complexes. We also did test calculation for DLPNO-CCSD(T) with 'NormalPNO' and 'TightPNO'. The parameter setting of 'TightPNO' changes the relative energies by about 1000 cm^{-1} for S1. As we observed that wave function method CASPT2 is still, from a pragmatic point of view, the best method to predict the HS-LS relative energies. Unfortunately, NEVPT2 method for TM complexes calculation does not produce good results although from a theoretical point of view it is more accurate than CASPT2. DLPNO-CCSD(T) does not provide accurate results with the tested basis sets either. A possible origin of the shortcoming of the CC-based calculations could be the fact that it uses a single reference wave function. As rationalized in ref[21] this is probably a less valid approximation for the LS state is SCO complexes with sizeable sigma donation. Certainly, more work in this field will be required in the future to establish an accurate yet computationally feasible method for predicting the energetic of spin states. For instance, the MC-PDFT method has been proposed as an alternative for CASPT2 and can be a good candidate for further investigations of the spin-state energetics.

References

[1] a) M. Pápai, G. Vankó, C. de Graaf and T. Rozgonyi., *J. Chem. Theory Comput.* **2013**, *9*, 509-519; b) S. Saureu and C. de Graaf, *Phys. Chem. Chem. Phys.* **2016**, *18*, 1233-1244; c) O. S. Siig and K. P. Kepp, *J. Phys.Chem. A* **2018**, *122*, 4208–4217; d) K. P. Kepp, *Coord. Chem. Rev.* **2013**, *257*, 196–209.

[2] M. Swart, A. R. Groenhof, A. W. Ehlers and K. Lammertsma., *J. Phys. Chem. A* **2004**, *108*, 5479-5483.

[3] M. Gruden, S. Stepanović and M. Swart, J. Serb. *Chem. Soc.* **2015**, *80*, 1399–1410.

[4] a) K. Pierloot and S. Vancoillie, *J. Chem. Phys.* **2006**, *125*, 124303; b) K. Pierloot and S. Vancoillie, *J. Chem. Phys.* **2008**, *128*, 034104; c) A. Rudavskyi, C. Sousa, C. de Graaf, R. W. A. Havenith and R. Broer, *J. Chem. Phys.* **2014**, *140*, 184318.

[5] K. Pierloot, Q. M. Phung and A. Domingo, *J. Chem. Theory Comput.* **2017**, *13*, 537-553.

[6] C. Sousa, C. de Graaf, A. Rudavskyi, R. Broer, J. Tatchen, M. Etinski and C. M. Marian, *Chem. Eur. J.* **2013**, *19*, 17541 – 17551.

[7] S. Dick and Z. Kristallogr., *New Cryst.Struct.* **1998**, *213*, 370–370.

[8] W. Gawelda, V.-T. Pham, M. Benfatto, Y. Zaushitsyn, M. Kaiser, D. Grolimund, S. L. Johnson, R. Abela, A. Hauser, C. Bressler and M. Chergui, *Phys. Rev. Lett.* **2007**, *98*, 057401.

[9] H. Oshio, H. Spiering, V. Ksenofontov, F. Renz and P. Gütlich, *Inorg. Chem.* **2001**, *40*, 1143-1150.

[10] J. M. Holland, J. A. McAllister, Z. Lu, C. A. Kilner, M. Thornton-Pett and M. A. Halcrow., *Chem. Commun.* **2001**, *2001*, 577-578.

[11] B. Gallois, J. A. Real, C. Hauw and J. Zarembowitch, *Inorg. Chem.* **1990**, *29*, 1152–1158.

[12] J. K. McCusker, A. L. Rheingold and D. N. Hendrickson, *Inorg. Chem.* **1996**, *35*, 2100-2112.

References

[13] A. Hauser, C. Enachescu, M. L. Daku, A. Vargas and N. Amstutz, *Coord. Chem. Rev.* **2006**, *250*, 1642-1652.

[14] M. Sorai, *Bull. Chem. Soc. Jpn.* **2001**, *74*, 2223-2253.

[15] J. J. McGarvey, I. Lawthers, K. Heremans and H. Toftlund, *Inorg.Chem.* **1990**, *29*, 252-256.

[16] J. K. Beattie, R. A. Binstead, M. T. Kelso, P. Del Favero, T. G. Dewey and D. H. Turner, *Inorg. Chim. Acta* **1995**, *235*, 245-251.

[17] B. N. Figgis, E. S. Kucharski and A. H. White, *Aust. J. Chem.* **1983**, *36*, 1527–1535.

[18] A. Kazaryan and E. J. Baerends., *J.Comput. Chem.* **2013**, *34*, 870-878.

[19] a) C. Riplinger and F. Neese, *J. Chem. Phys.* **2013**, *138*, 034106; b) C. Riplinger, B. Sandhoefer, A. Hansen and F. Neese, *J. Chem. Phys.* **2013**, *139*, 134101

[20] S. Kossmann and F. Neese., *Chem. Phys. Lett.* **2009**, *481*, 240-243.

[21] A. Domingo, M. A. Carvajal and C. de Graaf, *Int. J. Quantum Chem.* **2010**, *110*, 331-337.

"Thermodynamics, science of the relationship between heat, work, temperature, and energy."

Chapter 5

The role of vibrational anharmonicity in the computational study of thermal spin crossover

5.1 Introduction

Traditionally, the thermal spin crossover process has been schematically depicted as a one-dimensional potential energy diagram where the LS and HS states are represented within the harmonic approximation and the reaction coordinate corresponds to the totally symmetric normal mode. A key parameter for the characterization of SCO systems is the zero-point corrected energy difference between the HS and LS states, ΔH_{HL}^{ZPE}. However, this property is in many cases difficult to access by experimental techniques. In turn, the transition temperature, $T_{1/2}$, can be determined experimentally by magnetic susceptibility measurements, Mössbauer spectroscopy, or calorimetric experiments.[1] Under thermodynamic equilibrium conditions, where the variation of Gibbs energy equals zero, the

transition temperature can be written as:

$$T_{1/2} = \frac{\Delta H_{HL}^{ZPE}}{\Delta S_{HL}(T_{1/2})}$$

5.1

where the enthalpy difference between the HS and LS states is assumed to be temperature independent and $\Delta S_{HL}(T_{1/2})$ is the variation of entropy between the HS and LS states at the corresponding transition temperature.

The entropy increases on going from the LS to the HS state, and its value significantly changes with the temperature. Hence, the LS to HS conversion is considered an entropy-driven spin transition. For octahedral Fe(II) complexes with N-ligands, the ΔS_{HL} values normally range within 35-80 $JK^{-1}mol^{-1}$. By a great amount, the vibrational contribution is the largest portion of ΔS_{HL}; the electronic contribution arising from the change of spin multiplicity being a constant value of 13.38 JK^{-1} mol^{-1} and the rotational contribution notably minor. Moreover, previous studies based on Raman and IR spectroscopy[2] and by a combination of these techniques with density functional theory (DFT) calculations[3] demonstrated that the vibrational part of ΔS_{HL} is recovered by the low-energy vibrational modes, approximately 20% of the vibrations. Among these, the 15 modes involving the FeN_6 core account for about 75% of ΔS_{HL}.

The previous discussion stresses the importance of the vibrational contribution in both the value of the energy difference between the LS and HS states, ΔH_{HL}, through the vibrational zero point energy (ZPE) correction, and in the entropy change accompanying the spin transition, ΔS_{HL}. From the theoretical point of view, both properties, ΔH_{HL} and ΔS_{HL}, can be computed in a straightforward manner, and therefore, the transition temperature, $T_{1/2}$, can be estimated following Eq. 5.1.

All the computational studies performed to estimate the entropy variation, ΔS_{HL}, and the transition temperature, $T_{1/2}$, were based on the harmonic model to describe the molecular vibrations. Here, we aim to explore the effect of the anharmonic terms on

the SCO process and, in particular, the effect on the energy difference between the LS and HS states, the change of entropy accompanying the spin transition, and on the final transition temperature.

As has become apparent from the above discussion, molecular vibrations are essential to the understanding of SCO, but there are more research areas where molecular vibrations and the degree of anharmonicity are at the centre of interest. IR, Raman,[4] and even UV-Vis[5] spectra cannot always be fully explained without the inclusion of anharmonic corrections. Second-order vibrational perturbation theory[6] provides researchers with an efficient tool to study in great detail the underlying mechanisms that give rise to the richness of features in the experimental spectra. The description of the spin-vibration coupling has recently been extended with the inclusion of anharmonic terms, which turn out to be essential to explain the relaxation mechanism at higher temperatures.[7] To quantify the importance of anharmonicity in the context of SCO, several iron compounds have been considered, and for all of them, displacements along all the normal vibrational modes of the complex have been explored. By fitting the energy variation of the system along the vibrational coordinate of each normal mode to the fourth-order polynomial:

$$E(Q_i) = aQ_i^2 + bQ_i^3 + cQ_i^4 \qquad 5.2$$

anharmonic corrections can be extracted, and as a result, the influence on the ZPE, ΔS_{HL} and $T_{1/2}$ can be estimated.

5.2 Computational Details

Eleven different iron complexes and one cobalt complex have been studied, which are shown in **Fig.**5.1. These encompass the two oxidation states of iron, Fe(II) and Fe(III), and one oxidation state of cobalt Co(II), and various arrangements of the Fe first-neighbor coordination. First, the model system $[Fe(NCS)_2(NCH)_4]$ was studied as a test case.[8] Thereafter, we considered a set of six Fe(II) complexes with an octahedral FeN_6 coordination, which was studied in a previous work.[9] These

include two complexes with monodentate ligands, $[Fe(mtz)_6]^{2+}$ and $[Fe(iso)_6]^{2+}$ (with mtz = 1-methyltetrazole and iso = isoxazole), three bidentate ligand complexes, $[Fe(phen)_2(NCS)_2]$, $[Fe(pic)_3]^{2+}$, and $[Fe(bpy)_3]^{2+}$ (where phen = 1,10-phenanthroline, pic = 2-picolylamine, and bpy = 2,2´-bipyridine), and a tridentate ligand Fe(II) complex, $[Fe(terpy)_2]^{2+}$, with terpy = 2,2´:6´,2´´-terpyridine. The first four complexes of this set are susceptible to undergoing SCO, whereas the $[Fe(bpy)_3]^{2+}$ and $[Fe(terpy)_2]^{2+}$ systems are LS compounds where SCO is only possible by irradiation of light. In particular, the $[Fe(phen)_2(NCS)_2]$ system has been extensively studied both experimentally[2, 10] and by theoretical calculations[3b, 11] as a representative example of a Fe(II) SCO complex with an octahedral FeN_6 coordination. For this system, thermal spin conversion occurs at 176 K, and the SCO enthalpy is estimated to be 8.60 ± 0.14 kJ mol^{-1}. Next, two six-coordinated Fe(II) complexes where the central iron is bonded to sulfur-contained ligands were considered. In such a way, the effect in the anharmonic vibrations of third-row atoms as first-nearest neighbors can be explored and compared to the usual second-row C, N, or O atoms. Specifically, the $[Fe(CO)(N_HS_4)]$ and $[Fe(NH_3)(N_HS_4)]$ complexes, with $N_HS_4^{2-}$ = 2,2´-bis(2-mercaptophenylthiol)diethylamine dianion, have been studied.[12] Subsequently, a Fe(II) heptacoordinated complex has been considered, the dicyano[2, 13-dimethyl-6, 9-dioxa-3, 12, 18-triazabicyclo [12.3.1] octadeca-1 (18), 2, 12, 14, 16-pentaene] iron(II) monohydrate compound, $[FeL(CN)_2]\cdot H_2O$.[13] In this system, SCO is concomitant with a structural change from a hepta-coordination for the HS to a hexa- coordination in the LS. Thermal spin crossover by cooling is observed at 155 K. A compound containing Fe(III) in a six-coordinated surrounding was included in this study, the $[Fe(acac)_2trien]^+$ complex with acac = acetylacetonate-triethylenetetramine.[14] This complex has a sextet HS and a doublet LS, and the HS-LS enthalpy was determined for various solvents, with values in the range 700–1172 cm^{-1}.[14b] Finally, the widely studied $[Co(terpy)_2]^{2+}$ complex has been included, for which the transition occurs from the doublet low-spin to the quartet high-spin state,

the SCO enthalpy is estimated to be 9-16 kJ mol^{-1}.[15]

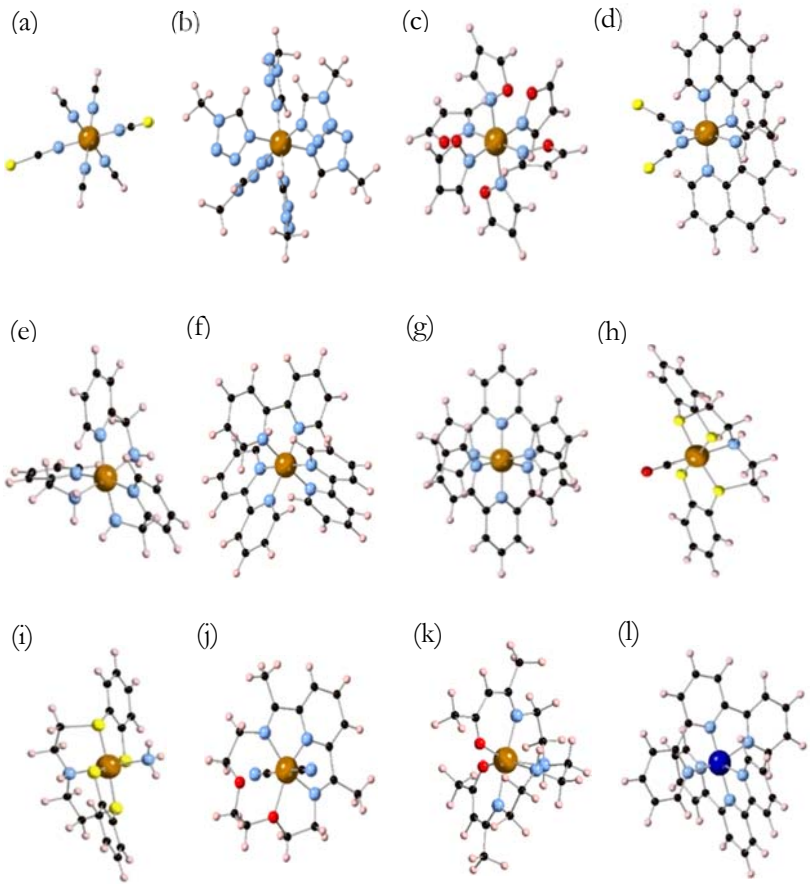

Figure 5.1 *Molecular complexes investigated in this study: $[Fe(NCS)_2(NCH)_4]$ (a), $[Fe(mtz)_6]^{2+}$ (b), $[Fe(iso)_6]^{2+}$ (c), $[Fe(phen)_2(NCS)_2]$ (d), $[Fe(pic)_3]^{2+}$ (e), $[Fe(bpy)_3]^{2+}$ (f), $[Fe(terpy)_2]^{2+}$ (g), $[Fe(CO)(N_HS_4)]$ (h), $[Fe(NH_3)(N_HS_4)]$ (i), $[FeL(CN)_2]\cdot H2O$ (j), and $[Fe(acac)_2trien]^+$ (k), $[Co(terpy)_2]^{2+}$ (l), Fe, Co is in the centre of the complexes, represented by a light brown and dark blue sphere. Black spheres represent C; blue is N; red is O; yellow is S; and pink is H.*

All DFT calculations were performed with the ORCA 4.1.1 code.[16] Geometry optimizations and frequency calculations were done with the TPSSh density functional and the Gaussian type basis sets of Weigend and Ahlrichs of the triple-ζ

+ polarization (def2-TZVP) quality for all atoms, but iron, for which we applied a basis set of quadruple-ζ +double polarization quality (def2-QZVPP).[17] The calculation of the exact Fock contribution was accelerated by applying the RIJCOSX approximation developed by Neese and co-workers.[18] Tight convergence criteria and a fine grid for the numerical integration (grid5) were chosen to avoid numerical noise in the calculation of the vibrational frequencies, which has to be done by numerical differentiation. In a study of the anharmonic effects in a series of metallocenes by Latouche et al., it was shown that the choice of basis set and density functional is not of critical importance; all the different combinations studied gave basically the same anharmonic corrections.[19] The complete active space second-order perturbation theory (CASPT2) calculations of the adiabatic high-spin/low-spin energy difference were performed with Molcas 8.2.[20] Following the conclusions of earlier studies,[21] we applied ANO-RCC basis sets with a (7s, 6p, 5d, 4f, 3g, 2h) contraction for Fe, triple-ζ + polarization for the atoms in first coordination sphere, and double-ζ for the other atoms. The active space contained 12 orbitals (5 Fe-3d, a second d-shell, and the two ligand-σ orbitals) and 10 or 9 electrons for Fe(II) and Fe(III), respectively. This is the standard active space for (quasi-)octahedral third-row transition metal complexes with 5 or more electrons in the d-shell.[22] The standard zeroth-order Hamiltonian (IPEA = 0.25) was used and an imaginary level shift of 0.15 E_h added to the denominators to avoid the appearance of intruder states. All electrons were included in the treatment of the dynamic correlation except the deep-core electrons ($1s^2$, $2s^2$, $2p^6$ for Fe and S and $1s^2$ for C, N and O). Since a full CASPT2 geometry optimization is out of reach for these molecules, we optimized the Fe-L distances by single-point calculations on a series of structures that interpolate between the DFT HS and LS state minima. Each point in this series was generated by a DFT geometry optimization in which only the Fe-L distances were fixed.

The effect of anharmonicity on the vibrational entropy and the zero point

vibrational energy was estimated by the following procedure. After the calculation of the (harmonic) vibrational frequencies ω_i and the corresponding normal modes Q_i (the eigenvectors of the Hessian), we generated 40 geometries along all normal modes (%mtrkeyword of ORCA) for the LS and HS states with a step size δQ_i that depended on ω_i. For the normal modes with ω smaller than 200 cm^{-1}, we applied a step size of $0.06 \cdot Q_i$, for $\omega > 2500$ cm^{-1} (C-H and N-H stretching vibrations), $\delta Q_i = 0.1 \cdot Q_i$, and for all the intermediate vibrations, we used a step size of $0.25 \cdot Q_i$. The changes in the step size were applied to ensure a realistic interval of atom displacements in all vibrational modes avoiding too large energy increases at the largest Q_i. Next, DFT calculations were performed on these geometries, and the results were fitted with the polynomial of Eq.5.2 using the least squares fitting procedure of the SciPy library of Python. This analytical function defines $\hat{V}$ in the Hamiltonian $\hat{H} = \hat{T} + \hat{V}$, with $\hat{T}$ the kinetic energy operator. The Schrödinger equation was solved for the 15 eigenvalues for each vibrational mode using the eigenvalue solver linalg.eigsh from SciPy. Even at the highest temperature considered, the population of the 15th level was low enough to have a negligible effect on the thermodynamic properties. The 15 eigenvalues were used to calculate the partition function Z_i and, subsequently, the total vibrational partition function Z as $\prod_i Z_i$, from which the entropy followed as $\Delta S = E/T + k_B \ln Z$. The sum of the lowest eigenvalue of all the vibrational modes defined the ZPE with anharmonic corrections.

5.3 Results and Discussion

5.3.1 Anharmonic corrections on the harmonic potential energy curve

To start the discussion, first we want to give a completely interpretation for the effect of anharmonic correction on the harmonic potential curve. **Fig.**5.2 illustrates the

effect of the cubic (b) and quartic (c) corrections on the harmonic curve $E(Q) = aQ^2$ with a=1, displayed in red. The first two panels of the upper row show that the cubic correction introduces asymmetry in the potential energy curve, tightening the curve on the right (left) and widening it on the left (right) for b larger (smaller) than zero. The next two panels show how the introduction of a quartic correction maintains the symmetry, but narrows (loosens) the curve for c larger (smaller) than zero. In the lower row, the combined effect of the two corrections is shown. We have taken the limiting case where the two corrections are similar in magnitude; in other cases, the upper row applies. When b and c have the same sign, their effect is largely cancelled on one side of the curve, while it rises more steeply on the other side. For opposite signs, the effect is again cancelled on one side, but the curve is now opened on the other side, resulting in a potential energy curve that resembles to some extent a Morse potential.

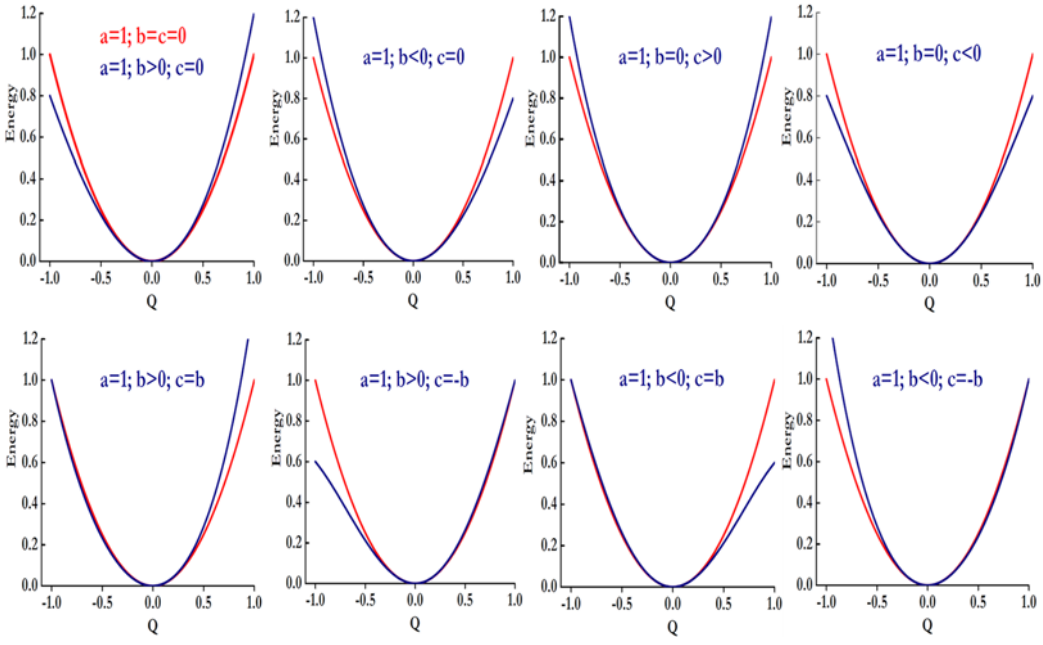

Figure 5.2 *Influence of the cubic (b) and quartic (c) corrections (in blue) on the harmonic potential energy curve (in red).* $|b|$ *and* $|c|$ *are 0.2 when non-zero.*

5.3.2 Anharmonic corrections on model system $[Fe(NCS)_2(NCH)_4]$

We first focus on the model complex $[Fe(NCS)_2(NCH)_4]$ to illustrate the differences between harmonic potential energy curves (given by Eq. 5.2 with b = c = 0 and a = $0.5\omega_i$, the harmonic vibrational frequency of mode *i*) and those that are obtained by fitting the calculated data to the quartic expression of Eq. 5.2. The normal mode of the LS state corresponding to the in-plane movement of the NCH ligands has a harmonic frequency of 147.3 cm^{-1}. Close to the equilibrium geometry, the NCH groups have very little interaction, but when they approach each other, the repulsion increases and the energy rises faster than predicted by the harmonic approximation, as can be seen on the right part of **Fig.** 5.3 Due to the symmetry in the plane, this faster rising is equal for positive and negative displacements defined by the coordinate Q. Hence, a sizeable quartic contribution (c=2.13) arises when the computed energies are fitted, while the cubic contribution stays very close to zero. The quadratic term (the anharmonic frequency) becomes 148.6 cm^{-1}, slightly larger than the harmonic frequency. Therefore, the ZPE is increased, and the shape of the fitted curve also makes the strict regular spacing between the vibrational levels be lost, although the effect is not dramatic. The energy difference between υ_0 and υ_1 is 148.7 cm^{-1}, and $\Delta E\upsilon_{14}$-υ_{15} equals 150.4 cm^{1}.

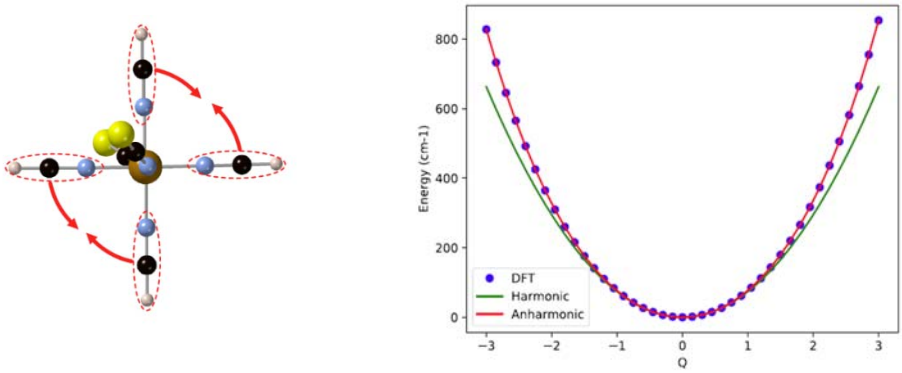

Figure 5.3 *left: In-plane NCH bending mode of the low-spin (LS) state of [Fe(NCS)$_2$(NCH)$_4$]. Right: Comparison of the harmonic potential energy curve (in green) and the calculated energies (blue dots) fitted with a quartic expression (red line).*

As an example of cubic corrections to the harmonic approximation, we mention the vibrational mode mainly characterized by the off-centre movement of Fe as shown on the left of **Fig.**5.4. When the iron moves away from the NCS groups (in the direction of the red arrow), the energy rises less rapidly than when it moves towards these groups. The harmonic frequency of this mode is 343.7 cm^{-1}, and the fitting of the DFT energies introduces a cubic term of -13.6 and an anharmonic frequency of 347.8 cm^{-1}. The quartic term is small in this case. The ZPE is again larger, but now, the spacing between the vibrational levels of the anharmonic curve remains constant within 0.1 cm^{-1}.

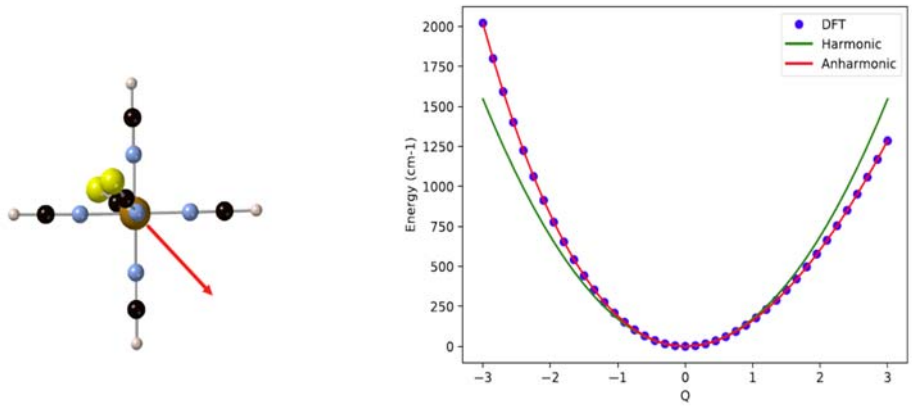

Figure 5.4 *left: Off-center Fe displacement vibrational mode of the LS state of [Fe(NCS)$_2$(NCH)$_4$]. Right: Comparison of the harmonic potential energy curve (in green) and the calculated energies (blue dots) fitted with a quartic expression (red line).*

The anharmonic correction to the ZPE is small in all 56 normal modes of the LS state of the model complex, but positive in almost all cases and finally adds up to a significant contribution of 159.7 cm^{-1}. The vibrational entropy term TΔS at T = 298 K within the harmonic approximation is 85.5 kJ mol^{-1}, decreasing to 79.0 kJ mol^{-1} when the anharmonic terms are taken into account, which is in line with the general tendency of larger ZPE for the anharmonic curves.

5.3.3 Effect of anharmonicity on zero point vibrational energy

Table 5.1 summarizes how the ZPE is affected by the anharmonicity of the potential energy curves for the eleven other complexes. Positive values indicate an increased ZPE (overall hardening of the vibrational modes), while negative numbers indicate that the ZPE has been lowered by the introduction of the anharmonic terms, that is a net softening of the modes. The third column shows the effect on the HS-LS ZPE difference to be added to the electronic energy difference between the two states. Except for [FeL(CN)$_2$]·H$_2$O, the effect on the HS-LS energy difference is limited to a correction smaller than 200 cm^{-1}. Ordering the complexes with a Fe(II)N$_6$ core by

Table 5.1 Contribution of the anharmonicity to the zero point energy with respect to the harmonic value [cm^{-1}]. HS, high-spin; LS, low-spin.

system	LS	HS	HS-LS
$[Fe(mtz)_6]^{2+}$	690	645	-46
$[Fe(iso)_6]^{2+}$	-312	-160	152
$[Fe(phen)_2(NCS)]$	298	177	-122
$[Fe(pic)_3]^{2+}$	97	142	45
$[Fe(bpy)_3]^{2+}$	31	-143	-174
$[Fe(terpy)_2]^{2+}$	123	-69	-192
$[Fe(CO)(N_HS_4)]$	1014	1166	153
$[Fe(NH_3)(N_HS_4)]$	213	247	35
$[FeL(CN)_2]\cdot H_2O$	667	-191	-857
$[Fe(acac)_2trien]^+$	511	446	-65
$[Co(terpy)_2]^{2+}$	141	38	-103

increasing contribution of the anharmonicity to the ZPE difference between HS and LS, it becomes apparent that the coordination mode of the ligand is likely to play a role in the importance of the anharmonicity. $[Fe(terpy)_2]^{2+}$, with two tridentate ligands, has the largest negative contribution, followed by $[Fe(bpy)_3]^{2+}$, three bidentate ligands, and $[Fe(phen)_2(NCS)_2]$ with two bidentate ligands. $[Fe(pic)_3]^{2+}$ has also bidentate ligands, but these are much less rigid than the phenanthroline or bipyridine ligands of the other two complexes. The two monodentate complexes, $[Fe(mtz)_6]^{2+}$ and $[Fe(iso)_6]^{2+}$, have a small negative contribution and a moderate positive one, respectively. This difference may be related to the size of the ligands; 1-methyl-tetrazole has significantly more atoms than isoxazole. Inserting the other complexes in trend is more difficult. $[FeL(CN)_2]\cdot H_2O$ increases the coordination of Fe from six to seven upon the LS to HS transition, which induces large changes in

the vibrational modes. $[Fe(acac)_2trien]^+$ contains a Fe(III) ion, and the two complexes with the N_HS_4 ligand have four sulfur atoms in the first coordination sphere of Fe. These two compounds differ by the axial ligand. With CO (a π acceptor ligand), the system is LS, and with NH_3, a σ-donor, the ground state of the complex is an HS state. $[Co(terpy)_2]^{2+}$ with two tridentate ligands, has a doublet ground state which makes the comparison with the other complexes more intricate.

5.3.4 Effect of anharmonicity on vibrational entropy

The second property that is affected by the anharmonic contributions to the potential energy curves is the vibrational entropy. **Table** 5.2 lists the most important results to illustrate the effect of anharmonicity on the energetics of the complexes studied here. In addition to the ZPE and the entropy, we also list the electronic energy difference between HS and LS (ΔH_{HL}) and the ZPE corrected energy (ΔH_{HL}^{ZPE}). As mentioned in the introduction, precise estimates of the latter quantity are difficult to calculate. CASPT2 has been shown in several studies to provide reasonable estimates, but this comes at the cost of having to reoptimize the first coordination sphere of the metal ion. Optimal CASPT2 Fe-Ligand distances are systematically shorter than those obtained with DFT, the difference being typically between 0.05 Å and 0.08 Å. This geometrical reorganization has a marked effect on ΔH_{HL}, and if one wants to stick to the standard definition of the zeroth-order CASPT2 Hamiltonian, the optimization of the first coordination sphere is mandatory; ΔH_{HL} calculated on the DFT geometries does not in general give the best estimates. Alternatively, one could increase the so-called IPEA parameter in $\hat{H}^{(0)}$, but this introduces a certain arbitrariness into the calculation that should ideally be avoided. For the compounds that were studied previously in [21a], all with a $Fe\text{-}N_6$ coordination, we list the CASPT2 values for ΔH_{HL}. For the new complexes, we limited ourselves to the TPSSh estimates, because the optimization of the first coordination sphere becomes very laborious for these complexes since the scan along the symmetric stretching frequency (as done in the previously studied

complexes) is not adequate for determining the optimal Fe-ligand distances. The coordination sphere is too asymmetric for this, and one would have to perform a two- or even three-dimensional exploration of the potential energy surface, which goes well beyond the scope of this study; the electronic energy difference ΔH_{HL} is not directly influenced by the anharmonicity. TPSSh gives the correct spin multiplicity for all complexes but one. $[Fe(NH_3)(N_HS_4)]$ is reported to be a high-spin molecule, but the TPSSh energies indicate an LS ground state. A series of single point CASPT2 calculations along the one-dimensional interpolation path between HS and LS optimized geometries resulted in an HS ground state (ΔH_{HL}= -1165 cm^{-1}). However, note that this is only a starting point and that a definite CASPT2 estimate requires the independent optimization of the Fe-S, Fe-NH_3, and the Fe-NR_2 distances in this particular case.

Moving to the next column of **Table** 5.2, we see that the ZPE in the harmonic approximation adds another 500–1000 cm^{-1} to the HS-LS energy difference in favor of the HS state. The larger Fe-ligand distance leads to wider potential energy curves in the HS and hence to smaller ZPEs, reducing the HS-LS gap for LS molecules. The anharmonic effects introduce changes to the ΔZPE_{HL} on the order of 50–200 cm^{-1}, except for the much larger variation in $[FeL(CN)_2]\cdot H2O$ caused by the change in coordination number, as discussed before. Adding the ZPE correction to the HS-LS energy difference greatly reduces the gap and results in small ΔH_{HL}^{ZPE} values for those complexes that are susceptible to SCO. The only missing aspect to complete the picture is the entropy contribution. To give an impression of how anharmonicity affects the entropy, the last two columns of **Table** 5.2 list the calculated variation of entropy at T =298 K for the series of complexes in the HS and LS states. Apart from the vibrational term, ΔS_{HL} also includes the electronic contribution to the entropy, a temperature independent term that only depends on the spin multiplicity of the HS and LS states. This term is equal to 13.38 JK^{-1} mol^{-1} for the Fe(II) complexes and 9.13 JK^{-1} mol^{-1} for the Fe(III) complex. For the first

Table 5.2 TPSSh values of the HS-LS energy difference, ΔH_{HL}, zero point energy (ZPE) contribution, ΔZPE_{HL}, zero point corrected HS-LS energy difference, ΔH_{HL}^{ZPE}, and entropy variation at 298K, ΔS_{HL}, computed using the harmonic and anharmonic approximations. Energies in cm^{-1} and entropy variation in JK^{-1} mol^{-1}.

system	ΔH_{HL}	ΔZPE_{HL}		ΔH_{HL}^{ZPE}		ΔS_{HL} (298K)	
		harm	anharm	harm	anharm	harm	anharm
$[Fe(mtz)_6]^{2+}$	1051[a]	-966	-1012	85	39	88.5	83.8
$[Fe(iso)_6]^{2+}$	1062[a]	-920	-768	142	294	87.9	147.1
$[Fe(phen)_2(NCS)]$	1362[a]	-754	-875	608	487	60.8	23.1
$[Fe(pic)_3]^{2+}$	1320[a]	-981	-937	339	383	68.4	66.8
$[Fe(bpy)_3]^{2+}$	5807[a]	-515	-689	5292	5118	54.6	88.2
$[Fe(terpy)_2]^{2+}$	7919[a]	-501	-692	7418	7227	59.5	84.2
$[Fe(CO)(N_HS_4)]$	9154	-867	-714	8287	8440	63.3	38.9
$[Fe(NH_3)(N_HS_4)]$	2595	-818	-783	1776	1811	78	65
$[FeL(CN)_2]\cdot H_2O$	3998	-847	-1704	3151	2293	41.4	42.2
$[Fe(acac)_2trien]^+$	3642	-811	-877	2831	2766	38.8	36.8
$[Co(terpy)_2]^{2+}$	1610	-212	-315	1399	1295	13.6	21.4

a: complete active space second-order perturbation theory (CASPT2) values taken from[21a].

four molecules, the effect of anharmonicity on the ZPE is also reflected in the entropy at 298 K. When anharmonicity reduces ΔH_{HL}^{ZPE}, that is when the anharmonicity raises more (or lowers less) the ZPE in the HS than in the LS state, the entropy at 298 K increases more (or decreases less) in the HS state with respect to the LS state. This may at first sight lead to the conclusion that the entropy changes are fully governed by the ZPE, but the results for the other complexes show that the picture is more complicated and that the non-uniform level spacing also plays a role in the way in which anharmonicity affects the entropy. This effect is more complicated to analyze since it changes from vibration to vibration. As the entropy has contributions from all vibrational modes, we have not been able to find a simple

reasoning to explain the tendency in the changes of the entropy upon the inclusion of anharmonic effects.

5.3.5 $T_{1/2}$ beyond the harmonic approximation

With the entropy and ZPE corrected for anharmonic effects, we are now ready to study its influence on the critical temperature for spin transition, $T_{1/2}$, for those complexes that show SCO behavior. Before discussing the results listed in **Table** 5.3, it is important to note that we do not pretend to give a precise number for the transition temperature. Although we account reasonably well for most of the factors related to the electronic structure of the complexes (ZPE, entropy, relativistic effects, etc.), the gas phase material model applied here is not sufficient to obtain a realistic estimate of $T_{1/2}$. However, this is not the aim of the study. Instead, the numbers listed in **Table** 5.3 do give some hints on how the anharmonicity affects the transition temperature. Following Eq. 5.1, we have determined the critical temperature for SCO with and without anharmonic corrections by looking for the temperature at which TΔS(T) is equal to ΔH_{HL}^{ZPE}. **Table** 5.3 lists the resulting $T_{1/2}$ and the variation in the entropy at that temperature.

The temperatures within the harmonic approximation are practically the same as in the previous study[21a] despite the different functional (B3LYP versus TPSSh) and the larger basis for Fe (TZVP versus QZVPP). The inclusion of the anharmonicity introduces small changes in the critical temperature in four cases and affects quite significantly the transition temperature of the $[Fe(phen)_2(NCS)_2]$ complex. However, the presence of very low frequency vibrational modes in the latter molecule makes the comparison between harmonic and anharmonic somewhat delicate, since small changes in the interval used for fitting the DFT energies lead to substantial changes in the anharmonic parameters. The fitting procedure is much more robust for vibrations with higher frequencies, and the size of the interval does not have great influence on the other complexes.

Table 5.3 Computed values of the zero point corrected HS-LS energy difference, ΔH_{HL}^{ZPE}, entropy variation at $T_{1/2}$, $\Delta S_{HL}(T_{1/2})$, and transition temperature, $T_{1/2}$. Energies in cm^{-1}, temperature in K, and entropy variation in J K^{-1} mol^{-1}.

system	ΔH_{HL}^{ZPE}		ΔS_{HL} ($T_{1/2}$)		$T_{1/2}$		Exp.	
	h.	anh.	h.	anh.	h.	anh.	ΔH_{HL}	$T_{1/2}$
$[Fe(mtz)_6]^{2+}$	85	39	34.8	26.5	30	19	120[23]	78[24]
$[Fe(iso)_6]^{2+}$	142	294	38.2	70.7	44	49	-	91[25]
$[Fe(phen)_2(NCS)_2]$	608	487	54.4	22.0	134	264	719[10a]	176[10b]
$[Fe(pic)_3]^{2+}$	339	383	49.6	46.8	82	98	744[26]	114-121[27]
$[Fe(acac)_2trien]^{+}$	827	761	37.8	35.6	262	256	700-1200[14b]	-
h. (harmonic); anh.(anharmonic)								

5.4 Conclusions

After carefully analyzing the effect of the anharmonicity on the molecular vibrational model by explicitly calculating the DFT energies along all normal modes of a collection of Fe complexes, we can conclude the following. Firstly, the change in the ZPE upon the addition of the anharmonic effect was loosely related to the stiffness of the ligands coordinating the Fe ion. The HS-LS ZPE difference decreased most for the tridentate and bidentate ligands, whereas it increased slightly for the complex with the smallest monodentate ligand. Secondly, a tendency in the variation of the entropy was more difficult to reveal; both the ZPE and the spacing between the vibrational levels played a role in the final value of the entropy, and the effect was a subtle balance between these two ingredients. Finally, we observed that the overall effect of the anharmonic correction was in general small enough to rely on the much

simpler harmonic model, which gave direct estimates of the ZPE and ΔS without having to perform energy scans along the normal modes of the system under study. To proceed towards a computational strategy that is capable of reliably predicting transition temperatures for thermal spin crossover, it is more important to focus on a more sophisticated material model; environmental effects[28] and cooperativity[29] are expected to have a much larger influence than the anharmonic corrections.

References

[1] a) M. A. Halcrow, *Polyhedron* **2007**, *26*, 3523-3576; b) M. M. Dîrtu, A. Rotaru, D. Gillard, J. Linares, E. Codjovi, B. Tinant and Y. Garcia, *Inorg. Chem.* **2009**, *48*, 7838-7852; c) M. Yamada, H. Hagiwara, H. Torigoe, N. Matsumoto, M. Kojima, F. Dahan, J. P. Tuchagues, N. Re and S. Iijima, *Chem. Eur. J.* **2006**, *12*; d) J. A. Rodríguez-Velamazan, C. Carbonera, M. Castro, E. Palacios, T. Kitazawa, J. F. Létard and R. Burriel, *Chem. Eur. J.* **2010**, *16*, 8785–8796.

[2] A. Bousseksou, J. J. McGarvey, F. Varret, J. A. Real, J. P. Tuchagues, A. C. Dennis and M. L. Boillot., *Chem. Phys. Lett.* **2000**, *318*, 409–416.

[3] a) J. A. Wolny, H. Paulsen, A. X. Trautwein and V. Schünemann, *Coord. Chem. Rev.* **2009**, *253*, 2423–2431; b) G. Brehm, M. Reiher and S. Schneider., *J. Phys. Chem. A* **2002**, *106*, 12024–12034; c) K. L. Ronayne, H. Paulsen, A. Höfer, A. C. Dennis, J. A. Wolny, A. I. Chumakov, V. Schünemann, H. Winkler, H. Spiering, A. Bousseksou, P. Gütlich, A. X. Trautwein and J. J. McGarvey, *Phys. Chem. Chem. Phys.* **2006**, *8*, 4685–4693.

[4] V. Barone, M. Biczysko and J. Bloino, *Phys. Chem. Chem. Phys.* **2014**, *16*, 1759–1787.

[5]V. Barone, M. Biczysko, M. Borkowska-Panek and J. Bloino, *Chem.Phys.Chem* **2014**, *15*, 3355–3364.

[6] V. Barone, *J. Chem. Phys.* **2005**, *122*, 014108.

[7] A. Lunghi, F. Totti, R. Sessoli and S. Sanvito, *Nat. Commun.* **2017**, *8*, 14620.

[8] A. Domingo, M. A. Carvajal and C. de Graaf, *Int. J. Quantum Chem.* **2010**, *110*, 331–337.

[9] A. Rudavskyi, C. Sousa, C. de Graaf, R. W. A. Havenith and R. Broer, *J. Chem. Phys.* **2014**, *140*, 184318.

[10] a) M. Sorai, *Bull. Chem. Soc. Jpn.* **2001**, *74*, 2223-2253; b) B. Gallois, J. A. Real, C. Hauw and J. Zarembowitch, *Inorg. Chem.* **1990**, *29*, 1152–1158.

References

[11] a) M. Reiher, O. Salomon and A. Hess, *Theor. Chem. Acc.* **2001**, *107*, 48–55; b) M. Reiher, *Inorg. Chem.* **2002**, *41*, 6928–6935.

[12] a) S. Ye and F. Neese, *Inorg. Chem.* **2010**, *49*, 772–774; b) D. Sellmann, W. Soglowek, F. Knoch, G. Ritter and J. Dengler, *Inorg. Chem.* **1992**, *31*, 3711–3717; c) M. Gruden, S. Stepanović and M. Swart, J. Serb. *Chem. Soc.* **2015**, *80*, 1399–1410.

[13] P. Guionneau, F. Le Gac, A. Kaiba, J. Sánchez Costa, D. Chasseau and J. F. Létard, *Chem. Commun.* **2007**, 3723-3725

[14] a) O. S. Siig and K. P. Kepp, *J. Phys.Chem. A* **2018**, *122*, 4208–4217; b) E. V. Dose, K. M. M. Murphy and L. J. Wilson, *Inorg. Chem.* **1976**, *15*, 2622–2630.

[15] J. K. Beattie, R. A. Binstead, M. T. Kelso, P. Del Favero, T. G. Dewey and D. H.Turner, *Inorg. Chim. Acta* **1995**, *235*, 245–251.

[16] F. Neese, *WIREs Comput. Mol. Sci.* **2018**, *8*.

[17] F. Weigend and R. Ahlrichs., *Phys. Chem. Chem. Phys.* **2005**, *7*, 3297-3305.

[18] a) F.Neese, F. Wennmohs, A. Hansen and U. Becker, *Chem. Phys.* **2009**, *356*, 98-109; b) T. Petrenko, S. Kossmann and F. Neese, *J. Chem. Phys.* **2011**, *134*, 054116.

[19] C. Latouche, F. Palazzetti, D. Skouteris and V. Barone, *J. Chem. Theory Comput.* **2014**, *10*, 4565–4573.

[20] F. Aquilante, J. Autschbach, R. K. Carlson, L. F. Chibotaru, M. G. Delcey, L. De Vico, I. F. Galván, N. Ferré, L. M. Frutos, L. Gagliardi, M. Garavelli, A. Giussani, C. E. Hoyer, G. L. Manni, H. Lischka, D. Ma, P. Å. Malmqvist, T. Müller, A. Nenov, M.Olivucci, T. B. Pedersen, D. Peng, F. Plasser, B. Pritchard, M. Reiher, I. Rivalta, I. Schapiro, J.Segarra-Martí, M. Stenrup, D. G. Truhlar, L. Ungur, A.Valentini, S. Vancoillie, V. Veryazov, V. P. Vysotskiy, O. Weingart, F. Zapata and R. Lindh, *J. Comput. Chem.* **2016**, *37*, 506-541.

[21] a) A. Rudavskyi, C. Sousa, C. de Graaf, R. W. A. Havenith and R. Broer, *J. Chem. Phys.* **2014**, *140*, 184318; b) B. Ordejón, C. de Graaf and C. Sousa, *J. Am. Chem. Soc.* **2008**, *130*, 13961–13968.

[22] a) K. Pierloot and S. Vancoillie, *J. Chem. Phys.* **2006**, *125*, 124303; b) K. Pierloot and S. Vancoillie, *J. Chem. Phys.* **2008**, *128*, 034104.

[23] R. Hinek, P. Gütlich and A. Hauser, *Inorg. Chem.* **1994**, *33*, 567–572.

[24] J. Kusz, H.S piering and P. Gütlich, *J. Appl. Crystallogr* **2001**, *34*, 229–238.

[25] W. Hibbs, P. J. van Koningsbruggen, A. M. Arif, W. W. Shum and J. S. Miller, *Inorg. Chem.* **2003**, *42*, 5645.

[26] T. Nakamoto, Z. C. Tan and M. Sorai, *Inorg. Chem.* **2001**, *40*, 3805–3809.

[27] H. Köppen, E. W. Müller, C. P. Köhler, H. Spiering, E. Meissner and P. Gütlich, *Chem. Phys. Lett.* **1982**, *91*, 348–352.

[28] a) S. Vela, M. Fumanal, J. Ribas-Ariño and V. Robert, *Phys. Chem. Chem. Phys.* **2015**, *17*, 16306–16314; b) M. Fumanal, F. Jiménez-Grávalos, J. Ribas-Ariño and S. Vela, *Inorg. Chem.* **2017**, *56*, 4474–4483.

[29] a) L. Kreutzberg, C. G. Hübner and H. Paulsen, *Materials* **2017**, *10*, 172; b) R. Bertoni, E. Collet, H. Cailleau, M. L. Boillot, A. Tissot, J. Laisney, C. Enachescu and M. Lorenc, *Phys. Chem. Chem. Phys.* **2019**, *21*, 6606–6612.

Theoretical study of the excited state lifetime by ligand modifications and the vibrational anharmonicity for Fe(II) and Ru(II) complexes

Jianfang Wu

"Never underestimate your power to change yourself!"

Chapter 6

General Conclusions

In this chapter, we want to give an overall conclusion about the whole work we have done and summarize the most important achievements. All the results described in this work are based on the ab initio calculation method to study the SCO transition metal complexes. Focusing on the description of the SCO properties such as geometries, frequencies, vertical absorption spectrum, excited state lifetime and transition temperature we have gained insight into the complexes that we have studied and the theoretical methods that we used.

We have tested and investigated the performance of a series of functionals for the calculation of different properties of the transition metal complexes. Although it is difficult to generalize, we found that TPSSh and PBE0 are best suited for the purpose of this thesis, therefore these functionals have been used in every chapter to do the geometry optimization, vibrational frequencies, absorption spectrum and the relative energies calculations.

In the study of the chapter 3, we changed the prototype $Fe^{II}N_6$ system by ligand modifications to investigate the lifetime of the ^{3}MLCT excited state. Two strategies have been used to achieve this goal. In the first place, we have used stronger sigma

donating ligands to create a stronger ligand on the metal and in the second place, we have enlarged the π conjugated system on the ligand to lower the orbital energy of the empty π* orbitals. We found that replacing one (two) bpy ligand(s) with two (four) CN^- ligands inverts the relative energies of the ^{3}MLCT and ^{3}MC states. In $[Fe(bpy)_2(CN)_2]$, the ^{3}MLCT state is only slightly more stable than the ^{3}MC but in $[Fe(bpy)(CN)_4]^{2-}$ the ^{3}MLCT is well separated from the ^{3}MC and in fact lies not too far in energy from the singlet ground state. A significantly increased lifetime has been observed in the ^{3}MLCT state based on the Fermi´s golden rule in both complexes. Although in $[Fe(bpy)_2(CN)_2]$ the excited state still has the possibility to undergo a SCO to the MC quintet state and in $[Fe(bpy)(CN)_4]^{2-}$ the relaxation process back to the initial non-magnetic singlet state is rather efficient. The calculation of the redox potentials show that both modified complexes are easily oxidized when they are in the excited ^{3}MLCT state. However, a warning is in place here, since the energy of the oxidized $[Fe(bpy)(CN)_4]^{2-}$ complex is lower than the ground state energy of the complex as synthesized. It is well known that the calculation of the negatively charged molecules is non-trivial and further study is required to firmly establish the relative stability of the $[Fe(bpy)(CN)_4]^{2-}$ complex with respect to the oxidized form. So far, our outcomes can provide a theoretical background for the ligand modifications study of the controlling the lifetime of the excited state, but we cannot confirm neither $[Fe(bpy)_2(CN)_2]$ nor $[Fe(bpy)(CN)_4]^{2-}$ as ideal candidates to replace $[Ru(bpy)_3]^{2+}$ as photoactive electron donor.

In the study of chapter 4, we benchmarked the calculation of the HS-LS energies difference of eleven complexes by different methods. Among the different density functionals we observed that TPSSh can produce rather accurate relative energies with or without zero-point vibrational energies. Concerning the Wave-function based methods, CASPT2 turns out to be the most adequate method to calculate $\Delta E_{HL,}$ despite its more approximate nature in comparison to the other methods that we have tested, NEVPT2 and CCSD(T). This is most likely due to an efficient

cancellation of errors by CASPT2. The choice of the basis sets do have significant effect for the methods we used. Large basis sets on the metal are required and preferably one should maintain a certain balance in the basis set size of metal and ligand. The results indicated that no matter how we combined different effect factor such as PC-, SC-, state average and state specific orbital optimization, NEVPT2 cannot produce accurate results for the relative energies calculation. The performance of the "golden standard" CCSD(T) method was also somewhat disappointing. The poor predictions of ΔE_{HL} is most probably related to a combination of an incomplete basis set and the approximation of taking a single determinantal reference wave function.

Finally, we have studied the effect of vibrational anharmonicity for several complexes on the thermal SCO transition temperature. Although we have found certain correlations between the effect of the anharmonicity of the ZPVE and the coordination mode of the Fe(II) ion, the overall conclusion of this study is that the anharmonic effects on the transition temperature are small and other factors such as environment are more relevant to include in the determination of $T_{1/2}$.

Turning back to the objectives formulated at the end of the introduction of this thesis, we can conclude that

(i) Ligand modifications can lead to an inversion of the stability of the MLCT and MC states leading to longer lifetimes of the ^{3}MLCT state, mimicking to some extent the situation of the Ru-polypyridyl complexes with the much more abundant Fe ion.

(ii) The calculation of the HS-LS energy difference continues to be a complicated task for quantum chemistry. Neither NEVPT2 nor DLPNO-CCSD(T) provide satisfactory results, while CASPT2 most probably gives the right answer for the wrong reason.

(iii) The effect of anharmonicity in the molecular vibrations is computationally

detectable but only has a small effect on the properties relevant to spin crossover. Other effects missing in the calculations should be taken care of before one has to start worrying about the anharmonicity.

Theoretical study of the excited state lifetime by ligand modifications and the vibrational anharmonicity for Fe(II) and Ru(II) complexes

Jianfang Wu

Theoretical study of the excited state lifetime by ligand modifications and the vibrational anharmonicity for Fe(II) and Ru(II) complexes

Jianfang Wu

Theoretical study of the excited state lifetime by ligand modifications and the vibrational anharmonicity for Fe(II) and Ru(II) complexes

Jianfang Wu

Theoretical study of the excited state lifetime by ligand modifications and the vibrational anharmonicity for Fe(II) and Ru(II) complexes

Jianfang Wu

UNIVERSITAT
ROVIRA i VIRGILI